OPTICA ACTA

Vol. 3. N° 4 December 1956

Etude des propriétés optiques des couches minces transparentes en liaison avec leur structure

P. Bousquet
Laboratoire de Physique Générale de la Faculté des Sciences de Marseille

Sommaire. — *On expose les résultats fournis par l'étude expérimentale d'un certain nombre de propriétés optiques des couches minces transparentes déposées par évaporation thermique, et on montre comment on peut utiliser ces résultats pour déterminer la structure de ces couches. Les mesures effectuées ont surtout été des mesures spectrophotométriques en incidence normale et en incidence oblique ; on a étudié de façon approfondie les phénomènes qui se produisent pour des incidences situées dans la zone de réflexion totale.*

Tous les résultats obtenus concourent à prouver que les couches minces étudiées ont une structure beaucoup plus complexe que celle qu'on leur attribue généralement. Ces couches ne sont pas continues ; leur structure granulaire est mise en évidence par le fait qu'elles diffusent une partie de la lumière qu'elles reçoivent, ce qui peut donner lieu à un très brillant système de franges de diffusion dans la zone de réflexion totale ; elles ne sont pas homogènes, c'est-à-dire présentent des gradients d'indice et des couches de passage ; enfin, elles sont quelquefois anisotropes.

Zusammenfassung. — *Die optischen Eigenschaften aufgedampfter dünner durchsichtiger Schichten werden experimentell untersucht. Die Ergebnisse erlauben die Struktur solcher Schichten zu bestimmen. Dabei werden spektrophotometrische Methoden bei senkrechtem und schiefem Lichteinfall benutzt. Besonders eingehend untersucht sind die Erscheinungen nahe der Grenze der Totalreflexion.*

Alle Ergebnisse deuten darauf hin, dass die untersuchten dünnen Schichten eine sehr viel verwickeltere Struktur haben als man gemeinhin glaubt. Sie sind nicht homogen ; ihre körnige Struktur geht daraus hervor, dass sie einen Teil des einfallenden Lichtes streuen. An der Grenze der Totalreflexion können sie zu sehr hellen Diffusionsstreifen Anlass geben. Sie zeigen neben ungestörten Durchgängen örtliche Veränderungen des Brechwertes, also Anisotropie.

Summary. — *An experimental study has been made of some optical properties of thin transparent films formed by evaporation, and it is shown that these results can be used to determine the structure of the films. Spectrophotometric measurements have been made at normal and oblique incidence, with particular attention to the region of total reflection.*

The results show that the thin films studied have a much more complex structure than has generally been supposed. These films are not continuous, their granular structure giving rise to diffusion of some of the incident light, which can give rise to a brilliant system of diffusion fringes in the region of total reflection ; they are inhomogenous, showing refractive index gradients and " couches de passage " ; finally they are sometimes anisotropic.

Introduction. — On admet le plus souvent qu'une couche mince transparente déposée par évaporation sous vide est assimilable du point de vue optique à une simple lame à faces planes et parallèles, complètement définie par son indice et son épaisseur. C'est évidemment l'hypothèse la plus simple. Elle permet de prévoir facilement, par des calculs d'interférences classiques, les diverses propriétés optiques des couches, et, inversement, d'imaginer de nombreuses méthodes pour déterminer les deux paramètres caractéristiques à partir de données expérimentales. Beaucoup d'auteurs ont travaillé dans cette voie.

Malheureusement, il n'a jamais été fait, à ma connaissance, de vérification expérimentale précise de cette hypothèse fondamentale. Or, il faut bien se rendre compte que lorsqu'on admet que la couche est parfaitement définie par son indice et son épaisseur, on suppose implicitement qu'au moins les conditions suivantes sont remplies :

1° la couche est *continue*, puisqu'on néglige la lumière diffusée qui pourrait être due à une structure granulaire ;

2° elle est *homogène*, c'est-à-dire d'indice constant dans toute l'épaisseur ;

3° chaque surface de séparation, côté air et côté support, correspond à une discontinuité parfaite de l'indice, sans existence de couches de passage ou zones de transition d'aucune sorte ;

4° la couche est *isotrope*.

Or, rien ne prouve à priori que les couches minces obtenues par évaporation thermique possèdent toutes ces propriétés. Etant donné le mécanisme de leur préparation, cela semblerait même assez étonnant. Nous nous sommes par suite proposés les buts suivants [1] :

1° déterminer d'abord, avec la plus grande précision possible, les propriétés optiques d'un certain nombre de corps transparents en couches minces ;

2° comparer les résultats obtenus avec ceux qu'on peut calculer en appliquant la théorie simplifiée de la lame continue, homogène et isotrope ;

3° montrer enfin comment les différences observées parfois très importantes, peuvent s'expliquer si on abandonne les hypothèses simplificatrices habituelles, en déduire des indications sur la structure véritable des couches et prouver, à l'occasion, comment les méthodes classiques de détermination de l'indice et de l'épaisseur des lames peuvent conduire à des résultats erronés.

Nous diviserons cet exposé en deux parties principales. La première sera consacrée aux résultats fournis par les mesures spectrophotométriques effectuées en incidence normale ou en incidence oblique. Dans la deuxième partie nous mettrons en évidence les nombreux résultats que fournit l'étude des couches minces transparentes dans la zone de réflexion totale.

I. **Mesures spectrophotométriques.** — L'appareil avec lequel ces mesures ont été effectuées [1] a été conçu pour répondre à un certain nombre d'exigences : il permet les mesures de facteurs de réflexion et de transmission sous toutes les incidences depuis l'incidence normale jusqu'au voisinage de l'incidence rasante ; le faisceau lumineux monochromatique est polarisé rectilignement avant de tomber sur la couche mince ; enfin, l'incertitude sur les mesures de facteurs de réflexion et de transmission ne dépasse pas deux à trois millièmes en *valeur relative*, dans le cas général.

1. *Mesures en incidence normale.* — Dans le cas idéal de la lame continue, homogène, à faces planes et parallèles, d'indice n_2 et d'épaisseur d_2 bien définis, le calcul montre facilement que les facteurs de réflexion R et de transmission T, doivent subir, en fonction de la longueur d'onde de la lumière incidente, des variations d'allure sinusoïdale. C'est là un résultat classique, sur lequel est basée une méthode, classique également, de détermination des quantités n_2 et d_2. Si l'indice n_2 de la couche a une valeur comprise entre les indices n_1 et n_3 des milieux environnants, on montre que les *maxima des courbes donnant le facteur de réflexion R* en fonction de la longueur d'onde ont pour expression :

$$R_M = \left[\frac{n_1 - n_3}{n_1 + n_3}\right]^2,$$

c'est-à-dire sont égaux au facteur de réflexion du support nu.

Nous avons mesuré, en fonction de la longueur d'onde, les facteurs de réflexion sous incidence normale d'un grand nombre de couches minces transparentes, d'épaisseurs variées, obtenues par évaporation thermique de diverses substances, telles que le fluorure de calcium, la cryolithe, le fluorure de magnésium. Les résultats que nous avons obtenus ne s'accordent jamais avec ceux que laissent prévoir les calculs basés sur l'hypothèse de la lame continue et homogène. *En particulier les maxima du facteur de réflexion de la couche ne sont jamais égaux au facteur de réflexion du support.*

Les exemples les plus typiques sont fournis par les couches de fluorure de calcium pour lesquelles les maxima de R sont très inférieurs au facteur de réflexion du support. De plus, ces maxima ont une valeur qui varie avec la longueur d'onde (fig. 1 et 2).

Sur la figure 2 on a reporté également la courbe représentant, en fonction de la longueur d'onde, le facteur de transmission T de la couche. On peut vérifier, qu'à la précision de nos mesures photométriques (2 à 3 millièmes en valeur relative), R et T sont parfaitement complémentaires ; il n'y a donc pas d'absorption ni de diffusion mesurables pour de telles couches, en incidence normale. Ceci a une conséquence pratique

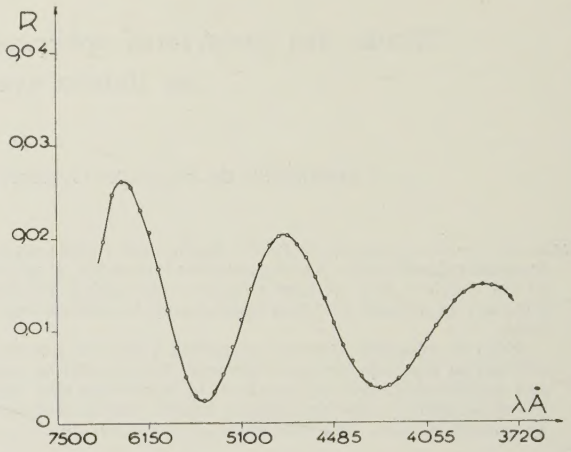

Fig. 1. — Facteurs de réflexion en fonction de la longueur d'onde d'une couche de fluorure de calcium, d'épaisseur optique voisine de 9 600 Å, déposée sur verre.

importante : par suite de la faible valeur des maxima de R et de l'absence d'absorption, les minima de T sont plus grands, de 2/100 environ, que ne le laisse croire la théorie classique. *L'effet « antireflet » de ces couches de*

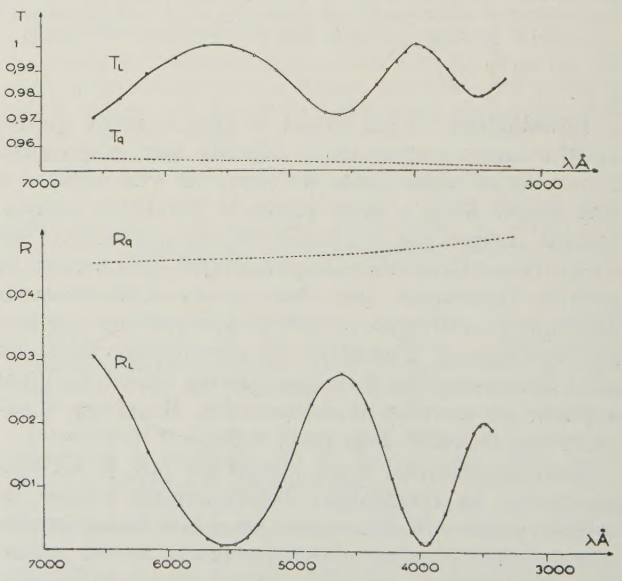

Fig. 2. — Facteurs de réflexion et facteurs de transmission, en fonction de la longueur d'onde, d'une couche de fluorure de calcium, d'épaisseur optique voisine de 6 900 Å, déposée sur quartz. En pointillé : facteurs de réflexion R_q et de transmission T_q du support.

fluorure de calcium est donc bien meilleur qu'on ne le croit habituellement. La figure 3 représente, en fonction de la longueur d'onde, les variations du facteur de

réflexion d'une couche de cryolithe et la figure 4 celles du facteur de réflexion d'une couche de fluorure de magnésium. On constatera que les maxima de R sont,

FIG. 3. — Rapport du facteur de réflexion de la couche mince à celui du support, en fonction de la longueur d'onde, pour une couche de cryolithe, d'épaisseur optique voisine de 8 000 Å, déposée sur quartz.

là encore, différents du facteur de réflexion du support nu ; mais, contrairement au cas du fluorure de calcium, ils lui sont ici supérieurs. Il convient d'ailleurs de noter que, pour le fluorure de magnésium, l'écart entre

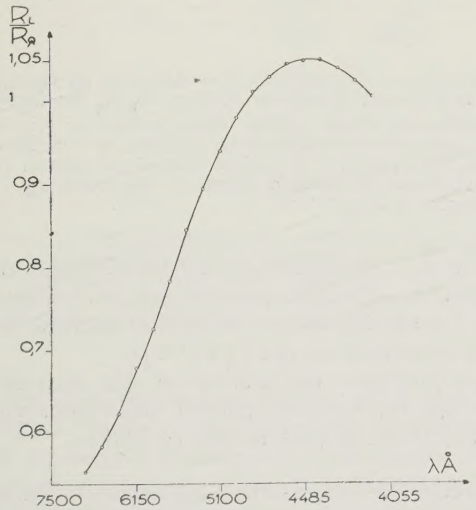

FIG. 4. — Rapport du facteur de réflexion de la couche mince à celui du support, en fonction de la longueur d'onde, pour une couche de fluorure de magnésium déposée sur verre.

es maxima du facteur de réflexion de la couche et celui du support est beaucoup plus faible que pour la cryolithe et le fluorure de calcium.

Les résultats expérimentaux que nous venons d'exposer sont inexplicables dans l'hypothèse d'une couche homogène d'indice n_2 constant. Ils peuvent par contre s'interpréter correctement si l'on abandonne cette hypothèse de l'homogénéité des couches minces.

L'existence d'un simple gradient d'indice, c'est-à-dire d'une variation régulière de n_2 d'une face à l'autre de la couche, pourrait suffire à expliquer le fait que les maxima du facteur de réflexion sont différents du facteur de réflexion du support. Mais cette hypothèse ne peut expliquer la variation de la grandeur de ces maxima en fonction de la longueur d'onde ; cette variation est pourtant très importante. L'ensemble des résultats expérimentaux rappelés ci-dessus peut par contre être expliqué complètement si l'on admet l'existence de couches de passage sur les surfaces de séparation de la couche mince avec les deux milieux qui l'entourent. Nous verrons d'ailleurs plus loin que les résultats des mesures spectrophotométriques en incidence oblique confirment, de façon plus directe et sans aucun doute possible, l'existence de ces couches de passage. On peut alors montrer que si $\rho' e^{i\varphi'}$ et $\rho'' e^{i\varphi''}$ désignent les coefficients de réflexion complexes de chacune des couches de passage, pris du côté de la couche principale, le facteur de réflexion de l'ensemble s'écrit :

$$(1) \quad R = 1 - \frac{(1 - \rho'^2)(1 - \rho''^2)}{(1 - \rho'\rho'')^2 + 4\,\rho'\rho''\sin^2\frac{\psi}{2}},$$

avec

$$\psi = \frac{4\pi n_2 d_2}{\lambda} - \varphi' - \varphi''.$$

Si les couches de passage n'ont pas une épaisseur très petite par rapport à la longueur d'onde, ρ' et ρ'' varient avec λ et il s'en suit que les maxima de R sont également fonction de λ.

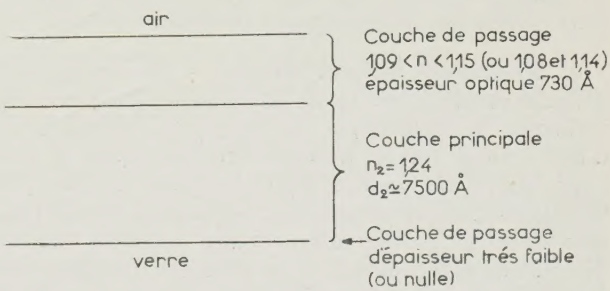

FIG. 5.

Il est possible, tout au moins si l'épaisseur de la couche est suffisante, de déduire de la détermination expérimentale des facteurs de réflexion des renseignements suffisamment précis sur les caractéristiques de la couche principale et des couches de passage. La figure 5 résume le résultat de ces déterminations pour la couche de fluorure de calcium dont les facteurs de réflexion sont représentés par la courbe de la figure 1.

On a là un exemple des résultats que l'on peut tirer de l'étude spectrophotométrique des couches minces

transparentes, en incidence normale. Il faut cependant remarquer que ces résultats ne sont pas complets, car nous avons supposé, pour faire la figure ci-dessus, que l'indice de la couche principale était constant ; or, rien ne prouve qu'il en est ainsi et il est fort possible que, comme la couche de passage, cette couche principale présente elle-même un gradient d'indice.

Remarquons, d'autre part, que nous sommes ici dans un cas relativement simple, puisque nous avons une seule couche de passage, sur l'interface air-fluorure. Sur l'interface fluorure-verre, la couche de passage, si elle existe, est d'épaisseur très petite et par suite, n'a pas d'influence sur la valeur des facteurs de réflexion. Il n'en est pas toujours ainsi et il arrive que les deux couches de passage existent et aient toutes deux une influence non négligeable.

A la lumière des résultats fournis par les mesures de facteurs de réflexion sous incidence normale, on voit que les couches se présentent généralement comme un ensemble complexe constitué par une couche principale, dont l'indice n'est pas obligatoirement constant, entouré d'une ou de deux couches de passage, elles-mêmes non homogènes.

Même dans le cas favorable de couches assez épaisses il est impossible de déduire du résultat de ces seules mesures tous les renseignements nécessaires sur la structure de ces couches. C'est que, par suite de la complexité de cette structure, le nombre de paramètres à déterminer devient important. Nous sommes loin de la simple lame homogène, parfaitement définie par deux grandeurs seulement, l'indice et l'épaisseur. Il s'en suit que l'application brutale à de telles couches des méthodes classiques de détermination des paramètres caractéristiques ne peut conduire qu'à des résultats erronés. Nous allons voir maintenant comment les résultats des mesures spectrophotométriques en incidence oblique viennent confirmer et compléter ceux fournis par les mesures en incidence normale.

2. *Mesures en incidence oblique.* — Comme en incidence normale, il est facile de montrer que pour une incidence θ_1 quelconque, le facteur de réflexion R d'une couche mince transparente, *homogène et isotrope*, subit, en fonction de la longueur d'onde, des variations d'allure sinusoïdale. Supposons encore l'indice n_2 de la couche intermédiaire entre les indices des milieux environnants. Si la vibration lumineuse est perpendiculaire au plan d'incidence, les maxima de R sont égaux au facteur de réflexion du support. Il en est de même dans le cas où la vibration est parallèle au plan d'incidence, si l'angle d'incidence θ_1 est inférieur à l'angle de Brewster θ_B sur la surface air-couche mince. Pour les incidences supérieures, ce sont les minima de $R_{\|}$ qui sont égaux au facteur de réflexion du support.

Les mesures spectrophotométriques en incidence oblique pourraient permettre l'étude de l'anisotropie d'une couche mince homogène. Nous avons en effet montré [1] qu'à partir du résultat de ces mesures de facteurs de réflexion, on peut calculer, pour n'importe quelle incidence, les indices de la couche relatifs à ses différents axes de symétrie électrique.

Malheureusement, une telle méthode n'est applicable que dans le cas d'une couche homogène. Nous savons déjà que, pratiquement, il n'en est généralement pas ainsi ; ici aussi l'interprétation des résultats n'est donc pas aussi immédiate que ne le laissent croire les formules.

Nous avons effectué des mesures de facteurs de réflexion en incidence oblique principalement sur des couches de cryolithe et de fluorure de calcium. De ces mesures nous pouvons tirer trois résultats principaux qui sont en contradiction avec l'hypothèse de la couche homogène et isotrope.

a) Comme en incidence normale, les maxima du facteur de réflexion R de la couche (ou les minima s'il s'agit de la vibration parallèle et d'incidences supérieures à θ_B), ne sont jamais égaux à leur valeur théorique qui est le facteur de réflexion du support.

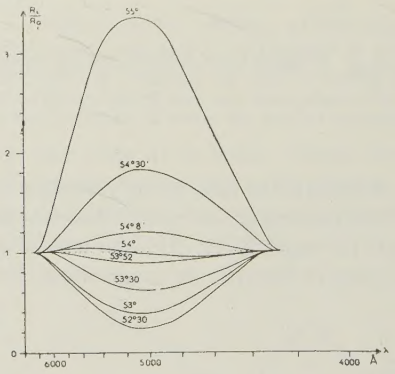

Fig. 6. — *Courbes théoriques* donnant, en fonction de la longueur d'onde, le rapport R_L/R_Q du facteur de réflexion d'une couche mince à celui du support nu, pour diverses incidences voisines de l'incidence brewstérienne sur la surface air-couche mince. Ces courbes ont été *calculées* dans le cas d'une couche *homogène* d'indice 1,375.

b) Il n'y a pas disparition des interférences dans la lame pour la vibration parallèle au plan d'incidence lorsque l'angle d'incidence est égal à l'angle de Brewster sur la surface air-lame [1] [2].

c) Les positions des maxima et des minima de R dans le spectre sont, en général, différentes pour les deux directions de polarisation [1] [3].

Le premier de ces résultats est normal ; il n'est que l'extension de ce que nous avons déjà vu en incidence normale.

Le deuxième résultat apparaît comme une preuve directe de l'existence d'une couche de passage sur la surface de séparation lame-air. Il est facile de montrer en effet que, dans le cas d'une couche homogène, les interférences dans la lame doivent disparaître lorsque θ_1 est égal à θ_B, le coefficient de réflexion sur l'interface lame-air étant nul pour la vibration parallèle. Dans ces conditions, le facteur de réflexion de la couche mince

$R_{\|}$, sous l'incidence θ_B, doit être égal au facteur de réflexion du support pour toutes les longueurs d'onde [5]. Les courbes de la figure 6 représentent les variations du rapport R_L/R_K du facteur de réflexion de la couche mince à celui du support, *calculées* pour quelques angles d'incidence au voisinage de θ_B, dans le cas d'une couche mince supposée homogène, d'indice 1,375 ($\theta_B = 54°$). On a tenu compte, dans le calcul, de la dispersion de la couche mince, ce qui explique les petits écarts entre la courbe relative à $\theta_I = 54°$ et la droite d'ordonnée 1. On voit que, dans le cas d'une lame parfaitement homogène, les oscillations du rapport $\frac{R_L}{R_Q}$ en fonction de la longueur d'onde doivent s'effacer sur place à mesure que θ_I croît jusqu'à θ_B, pour s'inverser lorsque θ_I est supérieur à θ_B.

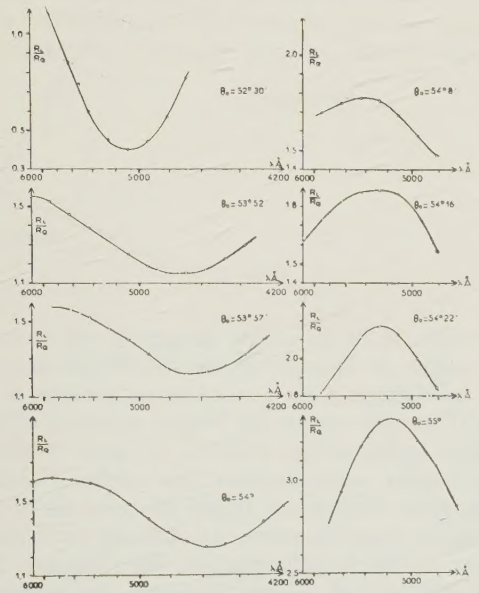

FIG. 7. — Rapport du facteur de réflexion d'une couche de cryolithe à celui du support nu, en fonction de la longueur d'onde, pour différentes incidences voisines de l'incidence brewstérienne sur la surface air-couche mince (courbes expérimentales).

Voyons ce qui se passe en réalité : sur la figure 7 on a tracé les courbes expérimentales représentant le rapport du facteur de réflexion de la couche mince à celui du support, en fonction de la longueur d'onde, pour différentes incidences voisines de l'incidence brewstérienne sur la surface air-couche mince. Le rapprochement de ces courbes expérimentales avec les courbes de la figure 6 montre que le passage par l'incidence θ_B se fait de façon tout à fait différente de celle attendue pour une couche homogène. Au lieu d'avoir passage d'un maximum à un minimum, ou inversement, par déformation sur place de la courbe, on a en réalité déplacement de l'ensemble de cette courbe vers les courtes longueurs d'onde. Les oscillations du rapport $\frac{R_L}{R_Q}$ ne disparaissent pour aucune valeur de l'angle d'incidence, mais restent, au contraire, toujours très marquées.

Ce résultat est sans doute la preuve la plus directe de l'existence d'une couche de passage sur l'interface lame-lair. Le fait que les oscillations du facteur de réflexion $R_{\|}$ ne disparaissent jamais prouve que le coefficient de FRESNEL sur l'interface air-lame n'est nul pour aucune incidence ; le déplacement progressif des maxima et des minima de $R_{\|}$ dans le spectre prouve que le changement de phase à la réflexion sur cet interface varie progressivement au lieu de présenter une discontinuité de π. Ce sont là des résultats caractéristiques de l'existence d'une couche de passage sur la surface de séparation considérée.

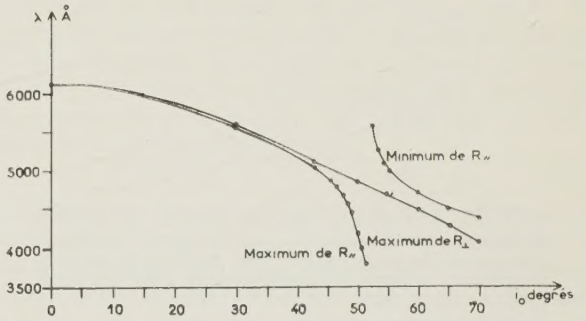

FIG. 8. — Positions dans le spectre, en fonction de l'angle d'incidence et pour les deux directions principales de polarisation, des maxima et minima du facteur de réflexion d'une couche mince de fluorure de calcium.

Cette existence est confirmée par notre troisième résultat expérimental : *les positions des maxima et minima du facteur de réflexion dans le spectre sont différentes pour les deux directions de polarisation.* Ceci est illustré par les courbes des figures 8 et 9. La première représente les positions dans le spectre, en fonction de l'angle d'incidence, des maxima et des minima du facteur de réflexion d'une couche mince de fluorure de calcium, pour les deux directions principales de polarisation. La figure 9 donne les mêmes résultats pour une couche de cryolithe. On retrouve sur ces courbes le phénomène déjà décrit du déplacement rapide dans le spectre des maxima et minima de $R_{\|}$ au passage par l'incidence θ_B. On y voit, de plus, qu'il existe en général pour toutes les incidences un écart $\Delta\lambda$ plus ou moins grand entre les positions des maxima et des minima relatifs aux deux directions principales de polarisation. Cet écart $\Delta\lambda$ est de signe différent suivant que l'angle d'incidence est inférieur ou supérieur à θ_B. Ce dernier résultat exclut toute possibilité d'interpréter ce résultat uniquement en faisant appel à une anisotropie possible des couches. Par contre, l'ensemble des résultats représentés par les courbes ci-dessus s'explique complètement à partir de l'exis-

tence d'une couche de passage sur l'interface couche-air. Les écarts $\Delta\lambda$ observés entre les positions des maxima et des minima relatifs aux deux directions de polarisation apparaissent alors dus aux différences entre les changements de phase à la réflexion sur la couche de passage relatifs aux deux composantes.

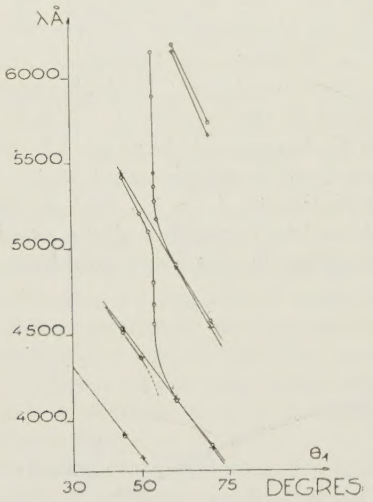

Fig. 9. — Positions dans le spectre, en fonction de l'angle d'incidence, et pour les deux directions principales de polarisation, des maxima et minima du facteur de réflexion d'une couche mince de cryolithe.

Les différents résultats que l'on peut tirer des mesures spectrophotométriques en incidence oblique confirment donc ceux que l'on avait déduit des mesures en incidence normale. Nous avons pu vérifier l'accord entre les valeurs numériques des paramètres caractéristiques des couches étudiées,qu'elles soient déduites du résultat de mesures en incidence normale ou en incidence oblique. Ces deux types de mesures peuvent se compléter mutuellement et nous permettre d'accroître nos connaissances sur la structure des couches minces transparentes.

Remarquons enfin que les mesures spectrophotométriques ou polarimétriques en incidence oblique sont à la base de plusieurs méthodes de détermination de l'indice et de l'épaisseur des lames minces transparentes. Toutes ces méthodes sont naturellement basées sur l'hypothèse que la couche étudiée est homogène et isotrope. A la lumière de ce que nous savons maintenant de la structure de ces couches, ces méthodes apparaissent d'application difficile ; elles peuvent souvent conduire à des erreurs.

II. **Etude des couches minces transparentes dans la zone de réflexion totale.** — Les couches minces n'ont été que très rarement étudiées sous des incidences supérieures à l'angle limite, sauf peut-être en ce qui concerne le cas de la réflexion totale « frustrée » qui a trouvé des applications dans les filtres interférentiels. Nous allons montrer que l'on peut pourtant tirer des résultats intéressants d'études faites dans cette région.

1. *Première Expérience : Franges par défaut de réflexion totale.* — Considérons l'expérience schématisée par la figure 10. Une couche de fluorure de calcium, d'épaisseur supérieure à 2 λ environ, est déposée sur la face hypoténuse d'un prisme rectangle isocèle. Un faisceau lumineux convergent, polarisé rectilignement, parallèlement ou perpendiculairement au plan d'incidence, se réfléchit sur cette face. Il est facile de montrer que, théoriquement, la présence d'une couche mince transparente sur l'hypoténuse du prisme ne doit en rien modifier le phénomène observé sur l'écran. La séparatrice délimitant la zone de réflexion totale de celle de réflexion partielle doit occuper la même place que dans le cas du prisme nu ; au delà de cette séparatrice la réflexion doit être totale.

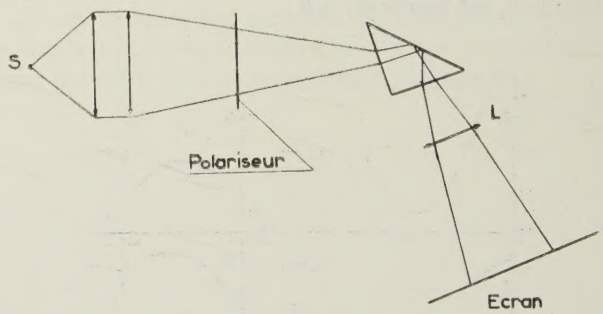

Fig. 10.

En réalité, si l'hypoténuse du prisme est recouverte d'une couche de fluorure de calcium d'épaisseur suffisante, la réflexion n'est pas totale au delà de la séparatrice. Tout une région de l'écran apparaît sillonnée de franges sombres bien visibles. On peut vérifier que c'est la région correspondant aux angles d'incidence compris entre l'incidence limite fluorure-air et l'incidence limite verre-fluorure. Au delà de cette dernière incidence limite, la réflexion est effectivement totale.

La figure 11 est la photographie du système de franges obtenu avec une couche de fluorure de calcium d'environ 10 λ d'épaisseur optique ($\lambda = 4358$ Å, vibration perpendiculaire au plan d'incidence). Des mesures de facteurs de réflexion que nous avons effectuées dans cette zone précisent quantitativement ce phénomène. Au lieu d'être égal à 1 pour toutes les incidences supérieures à l'incidence limite couche-air, le facteur de réflexion présente des minima très nets, d'autant plus nombreux et mieux marqués que l'épaisseur de la couche est plus grande.

Ce phénomène trouve son explication dans le fait que, par suite de leur structure granulaire, les couches minces, particulièrement celles de fluorure de calcium, diffusent une partie de la lumière qui les traverse. C'est à cette perte de lumière par diffusion qu'est dû le fait que le facteur de réflexion, au delà de l'angle limite, n'est pas égal à 1. Nous avons pu montrer que l'on retrouve par le calcul l'allure des courbes expérimentales donnant le facteur de réflexion au delà de l'angle limite si l'on affecte à la couche un indice

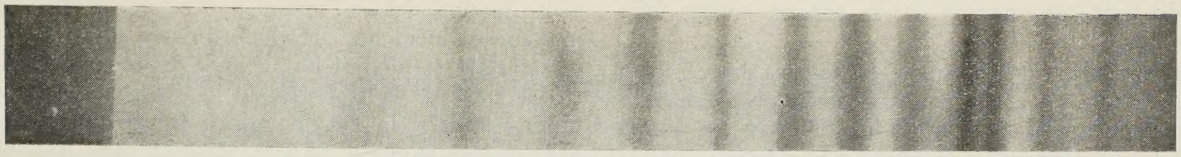

FIG. 11. — Franges sombres obtenues par réflexion sur une couche de fluorure de calcium, pour des incidences *supérieures à l'angle limite* (expérience de la figure 10).

d'extinction $\varkappa$ pour traduire la perte de lumière due à la diffusion. Cet indice d'extinction est toujours très faible (de l'ordre de 10^{-4} environ), ce qui explique qu'il ne produise aucun effet mesurable en incidence normale. Par contre, son importance devient prépondérante ici, du fait de l'inclinaison beaucoup plus grande des rayons dans la lame. C'est donc là l'exemple d'un phénomène que seules des mesures dans la zone de réflexion totale permettent d'étudier facilement.

La lumière diffusée par les couches minces de fluorure de calcium peut être mise en évidence de façon particulièrement brillante par une autre expérience,

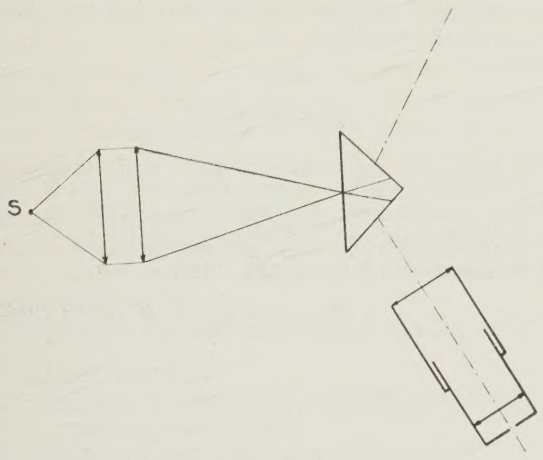

FIG. 12.

schématisée par la figure 12 [4]. La couche mince, toujours déposée sur la face hypoténuse du prisme, est éclairée par un faisceau lumineux d'ouverture et d'incidence quelconques. On s'arrange simplement pour qu'il ne puisse pas y avoir de rayon qui subisse la réflexion totale sur la face hypoténuse. Dans ces conditions, en l'absence de lumière diffusée, une lunette visant dans des directions situées dans la zone de réflexion totale, ne doit recevoir aucune lumière. En réalité, au lieu d'être obscur, le champ dans la lunette apparaît sillonné de franges brillantes, fines et très contrastées. On peut vérifier que ces franges brillantes de diffusion occupent exactement la place des franges sombres observées dans la lumière réfléchie lors de la première expérience. Ces franges de diffusion sont dues au fait que la lumière diffusée par chaque particule de matière subit des réflexions multiples dans la couche et se répartit par suite suivant un système de franges à l'infini. Observées en lumière blanche, ces franges présentent de vives colorations. La figure 13 représente les franges de diffusion produites par la couche de fluorure de calcium ayant fourni les franges par défaut de réflexion totale de la figure 11 ; la longueur d'onde et l'état de polarisation de la lumière sont également les mêmes. On peut vérifier facilement que les deux systèmes sont complémentaires.

2. *Deuxième Expérience. Anomalies au voisinage de l'angle limite verre-couche : Franges par polarisation.* — Les phénomènes que nous venons de décrire s'interprètent correctement, en tenant compte de la diffusion de la lumière à l'intérieur de la couche, sauf pour les incidences les plus grandes, c'est-à-dire au voisinage de l'angle limite verre-fluorure. Dans une zone d'un ou deux degrés avant cette incidence limite, on observe des irrégularités dans la position des franges, dont la distribution ne peut plus s'expliquer aussi simplement que nous l'avons fait jusqu'ici. Une nouvelle expérience va nous prouver l'existence de phénomènes plus complexes dans cette région.

Nous reprenons le montage de notre première expérience (fig. 10), mais nous plaçons maintenant deux polariseurs de part et d'autre du prisme, leur section principale étant à 45° du plan d'incidence. Le calcul laisse prévoir que nous obtiendrons sur l'écran un système de franges dû à des interférences en lumière polarisée. Mais ces franges ne devraient avoir qu'un contraste faible ; leur répartition dans le plan d'observation devrait d'autre part être régulière. Or, on observe en réalité un système de franges excessivement contrasté présentant des minima nuls et des maxima très intenses. En lumière blanche le phénomène est particulièrement brillant. De plus, au voisinage de l'angle limite verre-fluorure, la position de ces franges n'est

FIG. 13. — Franges de diffusion obtenues avec la même couche de fluorure de calcium que dans le casde la figure 11 (expérience de la figure 12).

pas du tout celle prévue par la théorie simple faite jusqu'ici.

La répartition de l'intensité lumineuse dans le plan d'observation au cours de l'expérience précédente est conditionnée par la valeur de la différence $\Delta r_\perp - \Delta r_\parallel$ entre les changements de phase par réflexion sur la couche mince relatifs aux deux directions principales de polarisation. Il semble donc que, dans la région voisine de l'incidence limite verre-fluorure, cette différence $\Delta r_\perp - \Delta r_\parallel$ subisse des variations anormales et beaucoup plus importantes que celles prévues par le calcul. Ceci a été confirmé par des mesures de la quantité $\Delta r_\perp - \Delta r_\parallel$ réalisées à l'aide d'un analyseur de Chaumont. Les mesures ont montré effectivement que lorsque l'épaisseur de la couche dépasse 1 ou 2 λ, il y a toujours au voisinage du 2e angle limite, un désaccord important entre les valeurs de $\Delta r_\perp - \Delta r_\parallel$ mesurées et celles que l'on peut calculer à partir des données que l'on possède sur la couche étudiée. Les courbes expérimentales présentent, en particulier, d'importantes oscillations que l'on ne retrouve jamais sur les courbes théoriques.

Rien de ce que nous avons appris jusqu'ici de la structure de nos couches ne nous permet d'expliquer ces anomalies. Il semble que seule l'hypothèse d'une anisotropie de la couche mince puisse fournir l'explication cherchée. Nous avons pu montrer en effet qu'il suffisait de supposer l'existence d'une très faible anisotropie de la couche (différence d'indices de 3 à 4 millièmes environ) pour retrouver, par le calcul, exactement la forme des courbes expérimentales représentant $\Delta r_\perp - \Delta r_\parallel$ en fonction de l'angle d'incidence.

Il en est donc de l'anisotropie comme de la diffusion ; inappréciables l'une et l'autre en incidence normale ou en incidence oblique ordinaire, elles prennent en réflexion totale une importance prépondérante.

Par suite de la très grande inclinaison des rayons lumineux dans la couche mince toute une série de phénomènes trop peu importants pour être décelables dans les conditions ordinaires prennent ici une importance considérable. C'est dire tout l'intérêt qui s'attache à des mesures effectuées dans cette zone.

Conclusion. — Les résultats de toutes les mesures que l'on peut effectuer sur les couches minces transparentes concourent à prouver que la structure de ces couches est bien plus complexe qu'on ne l'admet généralement. Elles ne sont pas homogènes, c'est-à-dire présentent des gradients d'indice et des couches de passage ; elles ne sont pas continues, leur structure granulaire étant mise en évidence par le fait qu'elles diffusent une partie de la lumière qu'elles reçoivent ; enfin, elles apparaissent quelquefois anisotropes. Par suite, le nombre de paramètres qui les caractérise est très grand ; les méthodes classiques de détermination des constantes optiques de ces couches sont alors le plus souvent en défaut.

RÉFÉRENCES

[1] P. Bousquet, Thèse Doct. Sc. Phys. Paris, 1956 (à paraître aux Annales de Physique).
[2] P. Bousquet, *C. R. A. S.*, **240**, 1955, p. 2502.
[3] P. Bousquet, *C. R. A. S.*, **241**, 1955, p. 478.
[4] P. Bousquet, *C. R. A. S.*, **237**, 1953, p. 516.
[5] F. Abelès, *C. R. A. S.*, **228**, 1949, p. 553.

Manuscrit reçu le 16 juillet 1956.

Total illumination in an aberration-free diffraction image

J. FOCKE
Mathematisches Institut, Leipzig

SUMMARY. — *Asymptotic expressions are derived for the total illumination in a defocused aberration-free diffraction image based on the asymptotic approximations of the diffraction integral due to* SCHWARZSCHILD *or to* VAN KAMPEN *respectively.*

SOMMAIRE. — *Des expressions asymptotiques basées sur les approximations de l'intégrale de diffraction de* SCHWARZSCHILD *ou de* VAN KAMPEN *sont données ici pour représenter l'énergie « encerclée » dans une image de diffraction, dépourvue d'aberrations, en présence d'un défaut de mise au point.*

ZUSAMMENFASSUNG. — *Es werden auf Grund der von* SCHWARZSCHILD *bzw.* VAN KAMPEN *angegebenen asymptotischen Näherungen des Beugungsintegrals asymptotische Ausdrücke für die Totalbeleuchtung in einem extrafokalen aberrationsfreien Beugungsbild hergeleitet.*

Beside the intensity distribution in an aberration-free diffraction image, which was studied in classical memoirs by AIRY (1835) and LOMMEL (1885) and more recently by ZERNIKE and NIJBOER, it is also of interest to know the total illumination in the various rings of the diffraction pattern. In modern times formulae were published by E. WOLF [1] which permit direct calculation of the total illumination. In the present paper approximations are derived for the total illumination, which represent the first term of asymptotic expansions with respect to small wavelength. These approximations therefore are intermediate between physical and geometrical optics. They asymptotically approach the exact results of wave theory and can often be used instead of them. The numerical computations are of a very simple kind, even at large distances from the focus.

Following [1] we introduce the following notation:

f focal length,
Δf distance between the receiving plane and the geometrical focus,
R radius of the opening of the aperture,
r, θ polar co-ordinates in the receiving plane,
λ wave-length,
u, φ normalized co-ordinates,

$$u = \frac{2\pi}{\lambda}\frac{R^2}{f^2}\Delta f\,, \quad \varphi = \frac{2\pi}{\lambda}\frac{R}{f}r, \quad (\theta = 0)$$

($u = \varphi$, boundary of the geometrical shadow),

$$\mathfrak{J}(u,\varphi) = \left|\frac{1}{\pi}\int_0^1\int_0^{2\pi} \mathbf{e}^{-\mathbf{i}(\varphi\rho\cos\varphi + u\rho^2/2)}\ \rho\,\mathrm{d}\rho\,\mathrm{d}\varphi\right|^2$$

light intensity, normalized to $\mathfrak{J}(0,0) = 1$;

$$(1) \qquad L(u,\varphi_0) = \frac{1}{2}\int_0^{\varphi_0}\mathfrak{J}(u,\varphi)\ \varphi\,\mathrm{d}\varphi$$

total illumination of a disk with radius φ_0 in the receiving plane $u = \text{const.}$, normalized to $L(u,\infty)=1$.

We start from the asymptotic expansions of the diffraction integral with respect to u and φ (implicitly containing $1/\lambda$) which were first published by N. G. VAN KAMPEN [2] and later on by the author [3] in a rigorous mathematical treatment. Under restriction to the first term we have

$$(2) \qquad \mathfrak{J}(u,\varphi) \sim \frac{4}{u^2} \qquad \text{for} \qquad 0 < \varphi < u$$

$$(3) \qquad \mathfrak{J}(u,\varphi) \sim \frac{2}{\pi\varphi}\left|\frac{\mathbf{i}\,\mathbf{e}^{-\mathbf{i}(\varphi-\pi/4)}}{\varphi+u} - \frac{\mathbf{i}\,\mathbf{e}^{\mathbf{i}(\varphi-\pi/4)}}{\varphi-u}\right|^2$$

$$\sim \frac{2}{\pi\varphi}\left[\frac{1}{(\varphi+u)^2} + \frac{1}{(\varphi-u)^2}\right] - \frac{4\sin 2\varphi}{\pi\varphi(\varphi^2-u^2)}$$

$$\text{for } 0 \leqslant u < \varphi.$$

These expressions in the error-free case are also given by SCHWARZSCHILD [4]. They fail to be valid in the neighbourhood of the edge of the geometrical shadow. According to [2] or to [4] in that region the intensity can be approximated by FRESNEL's integrals.

$$(4) \qquad \mathfrak{J}(u,\varphi) \sim \frac{2}{\pi\varphi}\left|\frac{\mathbf{i}\,\mathbf{e}^{-\mathbf{i}(\varphi-\pi/4)}}{\varphi+u} + B\mathbf{e}^{\mathbf{i}(\varphi-\pi/4)}\right|^2$$

$$\text{for } 0 < u \leqslant \varphi$$

where $B = \mathbf{e}^{\mathbf{i}\frac{(\varphi-u)^2}{2u}}\sqrt{\frac{\pi}{u}} \times$

$$\times\left[\left(\frac{1}{2} - C(t)\right) - \mathbf{i}\left(\frac{1}{2} - S(t)\right)\right]_{t=\frac{\varphi-u}{\sqrt{\pi u}}}$$

$$C(t) + \mathbf{i}\,S(t) = \int_0^t \mathbf{e}^{\mathbf{i}\pi\tau^2/2}\,\mathrm{d}\tau.$$

This formula not only is valid near the edge of the geometrical shadow but also in the whole shaded region, for by substituting

$$(5) \qquad \left[\left(\frac{1}{2} - C(t)\right) - \mathbf{i}\left(\frac{1}{2} - S(t)\right)\right] \sim$$

$$\sim \begin{cases} -\dfrac{\mathbf{i}}{\pi t}\,\mathbf{e}^{-\mathbf{i}t^2\pi/2} & \text{for } t > 0 \\ 1 - \mathbf{i} & \text{for } t < 0 \end{cases}$$

expression (4) passes into (3) when $\varphi \gg u$. Within the illuminated region we have similarly

(6)
$$\mathfrak{J}(u,\varrho)\sim\frac{2}{u^2}\left[\left(\frac{1}{2}-C(t)\right)^2+\left(\frac{1}{2}-S(t)\right)^2\right]_{t=\frac{\varrho-u}{\sqrt{\pi u}}}$$
for $0<\varrho\leqslant u$

and this expression is also valid at a large distance from the edge of the shadow ; for applying (5) formula (4) goes over into (2) when $\varrho\ll u$. On the boundary of the shadow the first term from (4) is of a smaller order of magnitude than the second term and can be neglected. Equations (4) and (6) are therefore in good agreement for $u=\varrho$. However all approximations constructed above fail to be true in the neighbourhood of the optical axis. Consequently we calculate the total illumination in the following form :

(7) $$L(u,\infty)-L(u,\varrho_0)=1-L(u,\varrho_0)=\frac{1}{2}\int_{\varrho_0}^{\infty}\mathfrak{J}(u,\varrho)\,\varrho\,\mathrm{d}\varrho.$$

The case $u<\varrho_0$. — Substituting from (3) into (7) we obtain

(8) $$1-L(u,\varrho_0)\sim\frac{1}{\pi}\left[\frac{1}{\varrho_0-u}+\frac{1}{\varrho_0+u}\right]-\frac{2}{\pi}\int_{\varrho_0}^{\infty}\frac{\sin 2\varrho}{\varrho^2-u^2}\,\mathrm{d}\varrho.$$

By partial integration

(9) $$\int_{\varrho_0}^{\infty}\frac{\sin 2\varrho}{\varrho^2-u^2}\,\mathrm{d}\varrho=\frac{1}{2}\frac{\cos 2\varrho_0}{\varrho_0^2-u^2}-\int_{\varrho_0}^{\infty}\frac{\cos 2\varrho}{(\varrho^2-u^2)^2}\,\varrho\,\mathrm{d}\varrho.$$

We find that the integral in (8) is of a smaller order of magnitude than the first term and can therefore be neglected. We finally obtain

(10) $$1-L(u,\varrho_0)\sim\frac{2}{\pi}\frac{\varrho_0}{\varrho_0^2-u^2}\qquad\text{for } 0\leqslant u<\varrho_0\ .$$

The case $u\leqslant v_0$, (v_0-u) *small.* — Substituting from (4) into integral (7) we obtain, to the first order,

(11) $$1-L(u,\varrho_0)\sim\frac{1}{\pi}\int_{\varrho_0}^{\infty}|B|^2\,\mathrm{d}\varrho=\sqrt{\frac{\pi}{u}}\left[H(t)\right]_{t=\frac{\varrho_0-u}{\sqrt{\pi u}}}$$
for $0<u\leqslant\varrho_0$, (ϱ_0-u) small,

where

$$H(t)=\int_t^{\infty}\left[\left(\frac{1}{2}-C(\tau)\right)^2+\left(\frac{1}{2}-S(\tau)\right)^2\right]\mathrm{d}\tau$$
$$=\frac{2}{\pi}\left(\frac{1}{2}-S(t)\right)\cos\frac{\pi}{2}t^2-\frac{2}{\pi}\left(\frac{1}{2}-C(t)\right)\sin\frac{\pi}{2}t^2-$$
$$-t\left[\left(\frac{1}{2}-C(t)\right)^2+\left(\frac{1}{2}-S(t)\right)^2\right],$$

$$H(0)=\frac{1}{\pi}\ ,\quad H(t)\sim\frac{1}{\pi^2}\frac{1}{t}\qquad\text{for } t>0,$$
$$H(t)\sim-2t\qquad\text{for } t<0.$$

Herein the expression for $H(t)$ is constructed by a double partial integration. In table 1 are given some numerical values of this function. On the boundary of the shadow we have

(12) $$1-L(u,u)\sim\sqrt{\frac{1}{\pi u}}\ .$$

The case $\varrho_0\leqslant u$. — In this case we split integral (7) into

(13) $$1-L(u,\varrho_0)=1-L(u,u)+\int_{\varrho_0}^{u}\mathfrak{J}(u,\varrho)\,\varrho\,\mathrm{d}\varrho.$$

Substituting from (6) into (13) we obtain

(14) $$1-L(u,\varrho_0)\sim\left[\sqrt{\frac{\pi}{u}}H(t)-\frac{\pi}{u}F(t)\right]_{t=\frac{\varrho_0-u}{\sqrt{\pi u}}}$$
for $0<\varrho_0\leqslant u$,

where

$$F(t)=\int_0^t\left[\left(\frac{1}{2}-C(\tau)\right)^2+\left(\frac{1}{2}-S(\tau)\right)^2\right]\tau\,\mathrm{d}\tau$$
$$F(t)\sim t^2\qquad\text{for } t<0.$$

Some numerical values of $F(t)$, calculated by numerical quadrature, are given in table 1.

Table 1

t	$H(t)$	$H(-t)$	$F(-t)$
0.0	0.32	0.32	0.00
2	24	44	01
4	18	62	07
6	14	88	20
8	12	1.24	45
1.0	0.10	1.70	0.87
2	08	2.24	1.46
4	07	2.77	2.15
6	06	3.24	2.85
8	06	3.60	3.46
2.0	0.05	3.91	4.06

The case $0\leqslant\varrho_0<u$, ϱ_0 *small.* — We have not derived the total illumination directly from (1), because the asymptotic approximations fail in the neighbourhood of the optical axis. But now $\mathfrak{J}$ is bounded near the axis, therefore $\mathfrak{J}\varrho$ tends to zero as ϱ vanishes. Hence we may expect that the neighbourhood of the axis will not contribute essentially to the value of the integral (1). Consequently it is permissible to substitute from (2) into (1) and we obtain, in agreement with geometrical optics,

(15) $$L(u,\varrho_0)\sim\left(\frac{\varrho_0}{u}\right)^2\qquad\text{for}\qquad 0\leqslant\varrho_0<u.$$

With the help of formulae (10), (11), (14) and (15) we can calculate the asymptotic values of the total illumination in every receiving plane $u=$ const., apart from the immediate neighbourhood of the focus. Naturally a distinction of several cases is necessary. Now we will show that the various expressions indeed pass into one another in the intermediary regions. Near the edge of the shadow for decreasing (ϱ_0-u)

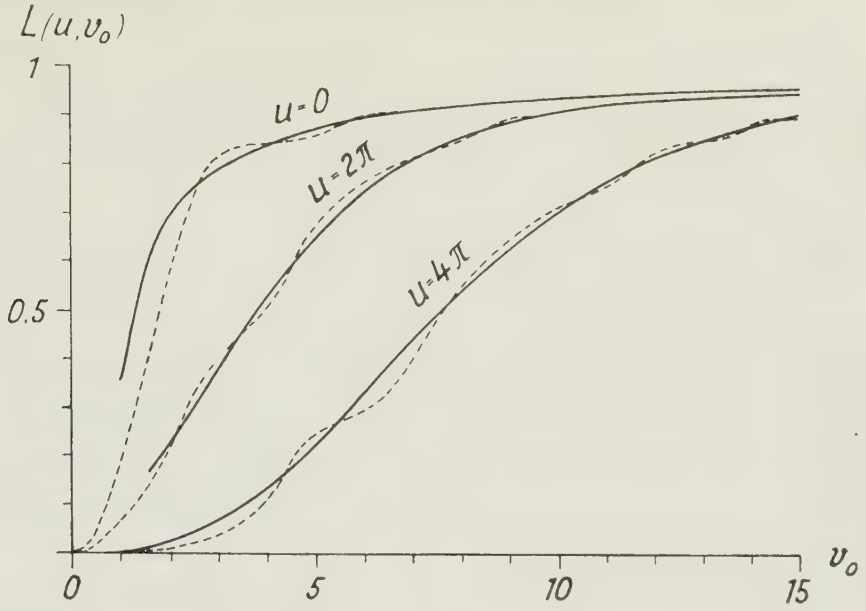

FIG. 1. — The total illumination $L\ (u,\ v_0)$ in the receiving planes $u = 0$, $u = 2\pi$, $u = 4\pi$. ---- exact behaviour (after E. WOLF [1], fig. 4a). ——— asymptoticb ehaviour.

the term $1/(v_0 - u)$ becomes large compared with $1/(v_0 + u)$, therefore formula (10) is approximately given by $1/\pi(v_0 - u)$. On the other hand for increasing $(v_0 - u)$ or t respectively we have

$$\sqrt{\frac{\pi}{u}}\,H(t) \sim \sqrt{\frac{\pi}{u}}\,\frac{1}{\pi^2 t} = \frac{1}{\pi}\,\frac{1}{v_0 - u}$$

and the expression (10) and (11) pass into each other. On the boundary of the shadow (11) and (14) are in exact agreement. Within the illuminated region for negative increasing $(v_0 - u)$ (14) passes into (15).

$$(16)\quad \sqrt{\frac{\pi}{u}}\,H(t) - \frac{\pi}{u}\,F(t) \sim \sqrt{\frac{\pi}{u}}\,(-2t) - \frac{\pi}{u}\,t^2 = -\,1 - \frac{v_0^2}{u^2}\,.$$

For numerical computation every expression is to be used until it passes into the following expression.

Now we will make two comparisons with WOLF's results. From [1], (2.30) it follows that exactly

$$(17)\quad L(u, v_0) = 1 - \sum_{s=0}^{\infty} \frac{(-1)^s}{2s+1}\left(\frac{u}{v_0}\right)^{2s} Q_{2s}(v_0) \qquad \text{for } u < v_0,$$

where $$Q_{2s}(v) = \sum_{\sigma=0}^{2s} (-1)^{\sigma}\left[\mathfrak{J}_{\sigma}(v)\,\mathfrak{J}_{2s-\sigma}(v) + \mathfrak{J}_{\sigma+1}(v)\,\mathfrak{J}_{2s-\sigma+1}(v)\right].$$

Substituting the asymptotic expansions of BESSEL functions into (17) we find that

$$(18)\qquad Q_{2s}(v) \sim (-1)^s\,\frac{2(2s+1)}{\pi v}\,.$$

Hence

$$(19)\quad L(u, v_0) \sim 1 - \sum_{s=0}^{\infty}\left(\frac{u}{v_0}\right)^{2s}\frac{2}{\pi v_0} = 1 - \frac{2}{\pi}\,\frac{v_0}{v_0^2 - u^2}$$

in agreement with (10). On the edge of the shadow WOLF's solution reduces to the simple form [1], (2.27),

$$(20)\quad L(u, u) = 1 - \mathfrak{J}_0(u)\cos u - \mathfrak{J}_1(u)\sin u \simeq -\sqrt{\frac{1}{\pi u}}$$

in asymptotic agreement with (12).

The asymptotic behaviour of the total illumination in the planes $u = 0, 2\pi$ and 4π in comparison with the exact behaviour due to E. WOLF is shown in figure 1.

The exact values approach closely the asymptotes in an oscillating manner ; the asymptotes reproduce therefore very well the behaviour of the total illumination and hence the distribution of light intensity. In many applications, for instance for the study of the intensity distribution in the image of an edge, the use of our smooth asymptotes is more convenient than the use of the exact values of the total illumination. In comparison with geometrical optics we have obtained a much better approximation to physical reality.

REFERENCES

[1] E. WOLF, *Proc. Roy. Soc.* **A.**, **204**, 1951, 533-548.
[2] N. G. VAN KAMPEN, *Physica*, **14**, 575-589.
[3] J. FOCKE, *Ber. Sachs. Ak. Wiss.*, **101**, Heft 3, 1954.
[4] K. SCHWARZSCHILD, *Münch, Ber.*, **28**, 1898, 271-294.

Manuscrit reçu le 18 juillet 1956

The third order aberrations in the interferometric measurement of concentration gradients

Harry Svensson
Laboratories of LKB-Produkter Fabriksaktiebolag, Stockholm, Sweden

Summary. — *The optical path difference between two coherent rays in the interferometric recording of a diffusion boundary is computed to the accuracy represented by terms of the third degree in the entrance angle and the refractive index difference across the boundary. It is found that even third-degree terms acquire a minimum value for that defocusing of the middle of the cell which in the second order theory was found to eliminate the Wiener skewness aberration. The third order aberrations are found to be highly dependent on the entrance angle, and there is a certain entrance angle that is more favourable than any other angle. The third-order aberrations are shown to decrease rapidly with time, and it is possible to define a critical initial time period of diffusion, after which the aberrations can no longer be observed. This critical time period is shown to be at a minimum for the optimum entrance angle. Exact equations for the optimum entrance angle and for the critical time period are given in terms of apparatus constants and the total number of fringes in the interferogram. The blurring of fringes due to a vertically extended light source in conjunction with a defocused cell is put in relation to the critical time period. It is possible to arrange an automatic guard against the evaluation of interferograms not yet free from aberrations by certain adjustments causing the blurring and the aberration to fade out to insignificance at the same time. Finally, the effect of uncollimated light is analysed, and exact conditions for the divergence or convergence of the light are presented.*

Sommaire. — *La différence de chemin optique entre deux rayons cohérents dans l'enregistrement interférométrique d'une frontière de diffusion est calculée avec la précision représentée par les termes du troisième degré par rapport à l'angle d'entrée et à la différence d'indice de réfraction au passage de la frontière. On trouve que les termes du troisième degré acquièrent une valeur minimum lorsque le défaut de mise au point au milieu de l'objet a la valeur trouvée dans la théorie du second ordre comme éliminant l'aberration d'obliquité de Wiener. On trouve que les aberrations du troisième ordre dépendent fortement de l'angle d'entrée, et qu'il existe un certain angle d'entrée qui est plus favorable que tout autre. On montre que l'interférogramme est pratiquement exempt d'aberration après le passage d'une certaine période de temps initiale. Si l'angle d'entrée le plus favorable est utilisé, cette période de temps est réduite au minimum. Des équations exactes pour l'angle d'entrée optimum et pour la période de temps critique sont données en fonction des constantes de l'appareil et du nombre total de franges de l'interférogramme. Le brouillage des franges dû à une source lumineuse étendue dans le sens vertical et à un défaut de mise au point est mis en relation avec la période de temps critique. Il est possible d'arranger une protection automatique contre l'emploi d'interférogrammes qui ne sont pas encore exempts d'aberrations, par certains dispositifs ayant pour effet que le brouillage et l'aberration deviennent négligeables en même temps. Finalement, on analyse l'effet d'un défaut de collimation de la lumière et on présente les conditions exactes de convergence ou divergence de la lumière.*

Zusammenfassung. — *Der optische Wegunterschied zwischen zwei kohärenten Strahlen bei der interferometrischen Registrierung einer Difusionszone wird bis zu einer Genauigkeit der dritten Ordnung für den Eintrittswinkel des Lichtes und für den gesamten Zuwachs des Brechungsindex in der Diffusionszone berechnet. Es ergibt sich, dass die Fehler dritter Ordnung einen Minimalwert für diejenige Defokusierung der Zellenmitte aufweisen, die schon die Theorie zweiter Ordnung forderte, um die Wienersche schiefe Lage der Gradientenkurve zu beseitigen. Die Fehler dritter Ordnung sind stark vom Eintrittswinkel abhängig und es gibt darunter einen bestimmten Winkel, der günstiger als alle anderen ist. Die Fehler dritter Ordnung klingen mit der Zeit rasch ab und man kann eine gewisse kritische Diffusionszeit angeben, nach der die Fehler nicht mehr beobachtet werden können. Diese kritische Zeit ist für den erwähnten optimalen Eintrittswinkel ein Minimum. Die mathematischen Ausdrücke für diesen Eintrittswinkel und diese kritische Zeit enthalten nur bekannte Apparatkonstanten und die Zahl der Interferenzstreifen. Die Unschärfe der Streifen, die von der Defokusierung der Zellenmitte und der vertikalen Ausdehnung der Lichtquelle herrührt, wird ebenfalls mit der kritischen Diffusionszeit in Zusammenhang gebracht. Man kann sich gegen eine Auswertung von noch nicht fehlerfreien Interferogrammen schützen. Das geschieht durch bestimmte Justierungen, durch die sowohl die Fehler als auch die Unschärfe der mittleren Streifen gleichzeitig zum Verschwinden gebracht werden. Schliesslich wird auch der Einfluss von nicht parallelem Licht untersucht und es werden die mathematischen Bedingungen für die zulässigen Beträge der Konvergenz und Divergenz des Lichtes aufgestellt.*

I. **Introduction.** — Interferometry has made it possible to measure diffusion coefficients with a formerly unknown precision. It is carried out by taking photographs of interferograms from twin cells, one compartment of which is filled with a solvent throughout, while the other one contains the same solvent stratified on top of a solution of the substance to be measured in such a way that the starting boundary is very sharp. The interferograms taken during the course of the free diffusion between solution and solvent are interpreted by the simple equation:

$$\Delta S = a\,[\,n(x) - m\,], \tag{1}$$

where ΔS denotes the difference in optical path length between the two coherent light beams, a the cell thickness, m the refractivity of the solvent, and $n(x)$ the variable refractivity across the diffusion boundary in the cell (x is the vertical cell coordinate).

As was pointed out in a previous article [1] on this subject, equation (1) is only a first approximation to the real path difference. The equation would be exact if the light passed horizontally through the diffusion and reference cells, but it does not. The light may enter the cell under a finite entrance angle, and, if collimated horizontal light is used, it will in any case be deflected in the medium of variable refractivity and describe a curved path, a trajectory, within the cell. A light pencil will thus sweep through a certain vertical region of the cell, within which the refractivity cannot possibly be regarded as constant,

especially with regard to the high accuracy obtainable by interferometric means. As soon as the refractivity along the trajectory varies more than corresponds to the accuracy of the interferometric method, the simple equation (1) can no longer be expected to be valid, and an exact path length difference can only be obtained by an integration over the length of the trajectory. There are also other reasons for deviations from the simple equation (1). For a more detailed discussion of this question, the reader is referred to the cited article.

It was shown in the said article that the expression for the exact path length difference is too complicated to be of any practical use, but that it is possible, by a proper use of mathematic approximations, to derive equations which are practically useful and more exact than equation (1). Thus it was found, by taking care of the terms next biggest to the main term in (1), that the optical path length difference can be described by the equation :

$$(2) \quad \Delta S = a\,[n(x) - m] + \frac{a^2\delta_0\,(1-2r)\,n'(x)}{2m} + \frac{a^3\,(2-3r)\,n'^2(x)}{6m},$$

where r is a parameter open to free choice in the adjustment of the optical system. It was also shown that both the above aberration terms could be brought to disappear by certain tricks in the adjustment of the optical system. The last term, which is most serious and responsible for the skewness of the gradient curve predicted by Wiener [2], can apparently be brought to disappear if r is chosen equal to 2/3. This corresponds physically to an optical adjustment making a plane 1/3 of the cell thickness from the exit wall optically conjugate to the photographic plate, *i. e.* to defocusing the middle of the cell 1/6 of the cell thickness. The first aberration term, on the other hand, can apparently be extinguished by making $\delta_0 = 0$, but this is not necessary. Even in oblique, collimated, and in uncollimated light, this aberration can be cancelled by another optical trick, *viz.* by a certain coordinate transformation, the physical correspondence of which consists in the experimental determination of the photographic enlargement factor by placing the object in the plane of the middle of the cell, although this is not optically conjugate to the plate. More details of this, and of other interesting properties of the two aberration terms are to be found in reference 1.

These results, which have been experimentally verified [3], are of course very favourable since they show that the simple equation (1) is worthy of a great deal more confidence than could be expected, if the tricks mentioned above are applied. On the other hand, they show that the second order theory is not sufficient to reveal the ultimate limit of interferometry in the measurement of strong refractivity gradients. It was mentioned already in reference 1 that the second order theory could not give any information of the critical relation between the thickness of the cell and that of the diffusion boundary. There must be such a relation, beyond which a light pencil traverses too great a portion of the diffusion boundary, causing the optical path length to assume an average value over this portion rather than the desired path length along a horizontal line. To get this information, a third order approximation of the path length difference is necessary. It will be the object of this investigation to derive the third order aberrations, among which we will find the terms responsible for this averaging effect.

II. **Notation and basic equations.** — The notation and the general scheme of the analysis will be explained with reference to figure 1, which shows the paths of two coherent light pencils through a diffusion cell and a reference cell. The z axis is the optic axis, and a monochromatic point source is situated at $z = -p+ra$, $x = q$. The distance p can then be regarded as a divergence parameter, $p = \infty$ corresponding to collimated light, while the ratio q/p can be regarded as an off-axis parameter. Both parameters are open to free choice in an experimental arrangement. The diffusion and reference cells are both situated between the planes $z = 0$ and $z = a$. The two coherent pencils are thus projected on to the same plane, although they may have any mutual orientation in reality. To begin with, the cell walls are imagined as infinitely thin. The diffusion cell has a variable refractivity, $n(x)$, assumed to be independent of z, while the constant refractive index of the reference cell is called m. In order to facilitate the calculation, this medium is first assumed to extend even outside the cells, through the whole part of the optical system that we have to deal with. This assumption will be omitted at the end of the analysis. The plane $z = ra$ is assumed to be the Gaussian image plane of the plate where the interferogram is formed, thus the parameter r may be called the cell-focusing parameter. It is also open to free choice in an experimental arrangement. The optical imagery from this plane to the photographic plate is, moreover, assumed to be completely aberration-free. There is then no optical path length difference between two light pencils passing from the same spot in the plane $z = ra$ to the same point on the photographic plate. This is the reason why our calculation of path length differences can be stopped at the plane $z = ra$.

One coherent pencil enters the diffusion cell at $x = x_0$ under the entrance angle δ_0, describes a curved path within the cell, leaves it at $x = x_a$ under the exit angle δ_a, and strikes the plane $z = ra$ at the level $x = x_{ra}$. The internal entrance and exit angles are called α_0 and α_a, respectively. The other coherent light pencil takes, due to our simplifying assumption, the direct rectilinear course from the light source to

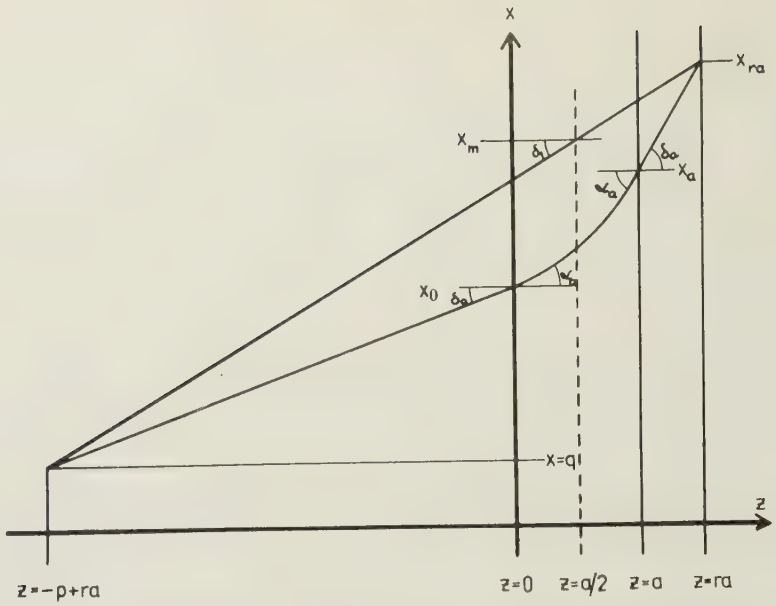

Fig. 1. — Light paths from light source to the left through reference and diffusion cells to the Gaussian image plane, $z = ra$, of the photographic plate. The cells are situated between the planes $z = 0$ and $z = a$. The light path through the reference cell is rectilinear, whereas that through the diffusion boundary is curved. The two pencils are coherent since they originate at the same spot of the light source. Moreover, they are capable of interference on the photographic plate, since they both arrive at the same spot of its optically conjugate image plane. The plane $z = a/2$ is used in the calibration of the cell (in the determination of the photographic enlargement). Therefore, the coordinate x_m, and not x_{ra}, is the coordinate read on the photographic plate.

the same point x_{ra} in the plane $z = ra$. This pencil strikes the plane through the middle of the cell at $x = x_m$.

It is now easy to formulate an exact expression for the optical path length difference between the two coherent rays. It is

$$(3) \qquad \Delta S = \frac{m\ (p—ra)}{\cos\ \delta_0} + \int_0^a \frac{n\ (x)\ \mathrm{d}z}{\cos\ \alpha} + \\ + \frac{ma\ (r—1)}{\cos\ \delta_a} - \frac{mp}{\cos\ \delta_1}.$$

As already pointed out, this expression is of no practical use since it contains an integral of a function that is not directly integrable, and since it also contains the angle δ_a, which is not known to an experimental worker. The work now to be performed consists in the computation of a sufficiently accurate approximate value of the integral, and in the elimination of δ_a and other unknown variables that may appear in the integral. Moreover, the whole expression has to be converted into a convenient form, suitable for drawing practical conclusions regarding the best choice of the free parameters.

Each term in equation (3) will be submitted to mathematical approximations, and since this article is called a third-order theory, we will then take into account all terms being one or two orders of magnitude smaller than the main term given by (1). The concept of order of magnitude then apparently requires some further explanation.

If equations (1) and (2) are divided through by a, we get equations for the relative difference in optical path length, and both sides of the equations become dimension-less. The first approximation of this relative difference is identical with the refractivity difference, $n(x)—m$, at the level x. As long as we are concerned with dilute solutions, and as long as we are using the solvent in the reference cell, this is a quantity that is small compared to unity. In general, it is not greater than 0.002, but we may allow it to rise to the order of magnitude of 0.01. By definition, we will regard a dimension-less quantity of this order of magnitude as a quantity of the first order or first degree. The total refractive index increase across the diffusion boundary will be denoted Δn and will be assumed to be of the same order of magnitude, *i. e.* also as a quantity of the first degree.

All angles, δ_0, δ_1, δ_a, α_0, and α_a, will be regarded as first-degree quantities on this scale, *i. e.* they will be assumed not to be appreciably larger than 0.01 radians.

The quantity $an'(x)$ is identical with the angular deflection of a light pencil in the refractive index gradient, and will thus also be regarded as a first degree quantity. Now, the first derivative can be written, for an ideal diffusion boundary :

$$(4) \qquad n'(x) = \frac{\Delta\ n}{b} f(y),\ y = x/b,$$

where $f(y)$ is the Gaussian error function, and b is half the distance between the two inflexion points

of the normal error curve. The numerical values of the error function lie between 0 and about 0.4 and must consequently be regarded as quantities of the 0 : th degree. Since Δn has already been defined as a first-degree quantity, it can be concluded that a and b must be of the same order of magnitude. This is a reasonable conclusion, standing in conformity with general experimental practice.

The angular off-axis position of the light source, q/p, will, as all other angles, be regarded as a first-degree quantity. The same assumption is made concerning the angular extension of the diffusion gradient as seen from the light source. Thus x/p is also a first-degree quantity, as well as b/p. Further, since a and b are of the same order of magnitude, the quantity a/p, if it appears, will be treated as a first-degree quantity, although it cannot be physically interpreted as an angle.

Finally, the second derivative, $n''(x)$, will appear in our approximations. Its order of magnitude must be the same as that of the first derivative, since it contains Δn as a factor, and since the first derivative of the error function is of the same order of magnitude as this function itself. It is to be noted, however, that the derivatives of n with respect to x are not dimension-less. They have to be multiplied by a distance in the same power as the order of the derivative under consideration before they can on the whole be compared to other quantities. The distance that appears in combination with the derivatives is the cell thickness, which, as already agreed upon, is regarded as being of the same order of magnitude as the thickness of the diffusion boundary.

To sum up, we can thus state that, on simplifying the different terms in equation (3) by mathematical approximations, we have to take care of all terms up to and including terms of the third degree in any combination of the above-mentioned variables of the first degree. In order to examplify this principle, we can start by inspecting the two aberration terms in equation (2). Since r is a dimension-less parameter of unity order of magnitude (0 : th degree), both these terms are found to be of the second degree (after division by a), since the first one contains δ_0 and $an'(x)$ and the second one $a^2n'^2(x)$. A δ_0^2 term would have to be included in (2) if it existed, but the mathematical analysis in the previous article showed that such an aberration does not exist. The fact that the two aberrations in (2) are of the second degree referring to the quantitative scale agreed upon here is of course the reason why the corresponding errors were called second-order aberrations.

In the third-order theory to be presented here, we thus have to take into account such terms as $a\,(n-m)\,\delta_0^2$, $a^3\,\delta_0^2\,n''(x)$, $a^5\,n'^2\,(x)\,n''(x)$, $a^4\,n'^2\,(x)/p$, to mention a few examples of terms that were neglected in the second-order theory.

The different variables are interconnected by the following equations, the validity of which is easily realized.

$$\tan\,\delta_0 = \frac{x_0 - q}{p - ra}, \tag{5}$$

$$m\,\sin\,\delta_0 = n\,(x_0)\,\sin\,\alpha_0, \tag{6}$$

$$n\,(x_a)\,\cos\,\alpha_a = n\,(x_0)\,\cos\,\alpha_0, \tag{7}$$

$$n\,(x_a)\,\sin\,\alpha_a = m\,\sin\,\delta_a, \tag{8}$$

$$x_{ra} = x_a + a\,(r-1)\,\tan\,\delta_a. \tag{9}$$

By squaring and adding equations (6) — (8), we get

$$m^2\,(\sin^2\,\delta_a - \sin^2\,\delta_0) = n^2\,(x_a) - n^2\,(x_0). \tag{10}$$

Along the trajectory, we have the following equations:

$$\frac{\mathrm{d}S}{\mathrm{d}z} = \frac{n\,(x)}{\cos\,\alpha}, \tag{11}$$

$$n\,(x)\,\cos\,\alpha = \text{a constant}, \tag{12}$$

$$\frac{\mathrm{d}x}{\mathrm{d}z} = \tan\,\alpha, \tag{13}$$

$$\frac{\mathrm{d}\alpha}{\mathrm{d}z} = \frac{n'\,(x)}{n\,(x)}. \tag{14}$$

Equation (14) is obtained by differentiation of (12) with respect to z.

III. **Second-order approximations of auxiliary variables.** — In order to carry out the computation of the third-order approximation of the path length difference, it is necessary first to derive the second-order approximations of some auxiliary variables. Thus, the only vertical coordinate that is known to the experimental worker is that on the photographic plate, and consequently all other coordinates such as x_0 and x_a, have to be eliminated from our equations in order to make them practically useful. The same thing can be said about the exit angles, δ_a and α_a, as well as the internal entrance angle α_0.

The exit coordinate, x_a. — In order to derive an approximate expression for this coordinate, we will so far regard x_0 as known, since the only thing that can be done at the start of the analysis is to establish a relation between the entrance and exit coordinates. Following the curved light path through the cell, we can regard x as a continuous function of z in the interval between $z = 0$ and $z = a$ and apply a MacLaurin series:

$$x_a = x_0 + \frac{a}{1}\left(\frac{\mathrm{d}x}{\mathrm{d}z}\right)_{z=0} + \frac{a^2}{2}\left(\frac{\mathrm{d}^2x}{\mathrm{d}z^2}\right)_{z=0} + \tag{15}$$

$$+ \frac{a^3}{6}\left(\frac{\mathrm{d}^3x}{\mathrm{d}z^3}\right)_{z=0} + \frac{a^4}{24}\left(\frac{\mathrm{d}^4x}{\mathrm{d}z^4}\right)_{z=0} + \frac{a^5}{120}\left(\frac{\mathrm{d}^5x}{\mathrm{d}z^5}\right)_{z=\theta a}$$

where the last term is the residual term with an unknown numerical figure θ lying between 0 and 1. It

is to be noted that the relation (15) holds whether the power series in a converges or not. Thus we need not worry about any convergence criteria for the power series, if only we can show that the residual term is of insignificant magnitude on our scale.

The first derivative in (15) is taken directly from (13), and the successive differentiation is easily carried out with the aid of (14). Thus we get the following second derivative

$$\frac{\mathrm{d}^2x}{\mathrm{d}z^2} = (1 + \tan^2 \alpha)\,\frac{n'}{n}\,, \tag{16}$$

where n' and n are abbreviated symbols for $n'(x)$ and $n(x)$, respectively. This abbreviated notation for n and its derivatives with respect to x will be used consistently in the following. In the above equation $\tan \alpha$ as well as n' (together with a, which appears as a factor in (15)) are of the first degree on our scale of orders of magnitude. Hence the second term, being of the third degree, can be omitted since we are looking for only the second-degree approximation of x_a. Thus, we have

$$\frac{\mathrm{d}^2x}{\mathrm{d}z^2} = \frac{n'}{n}\,. \tag{17}$$

Equation (17) can also be used in the computation of the higher derivatives, because the third-degree term in (16) does not give rise to any terms of lower degree on further differentiation.

The next differentiation of (17) gives, with the aid of (13),

$$\frac{\mathrm{d}^3x}{\mathrm{d}z^3} = \left(\frac{n''}{n} - \frac{n'^2}{n^2}\right)\tan \alpha, \tag{18}$$

without any approximations. Here again, we can discard the second term, since it is of the third degree, and we get

$$\frac{\mathrm{d}^3x}{\mathrm{d}z^3} = \frac{\alpha\, n''}{n} \tag{19}$$

because terms of the third and higher degrees in $\tan \alpha$ can also be disregarded. Differentiation of (19) once more gives only one term of the second degree

$$\frac{\mathrm{d}^4x}{\mathrm{d}z^4} = \frac{n'\, n''}{n^2}\,. \tag{20}$$

The fifth derivative contains, as is easily realized, only terms of the third and higher degrees. The residual term in (15) is thus too small to be considered and can be omitted. Consequently we get the following second order approximation of the exit coordinate :

$$x_a = x_0 + a\,\alpha_0 + \frac{a^2\, n_0'}{2\, n_0} + \frac{a^3\,\alpha_0\, n_0''}{6\, n_0} + \frac{a^4\, n_0'\, n_0''}{24\, n_0^2}\,. \tag{21}$$

The external entrance angle is known to an experimental worker, whereas the internal one is not. Thus we will eliminate α_0 in favour of δ_0 with the aid of the following relation, easily realized from equation (6) :

$$\alpha_0 = \frac{m\delta_0}{n_0} + \text{correction terms of the third and higher degrees.} \tag{22}$$

The correction terms can of course be omitted in a second order approximation, and we get

$$x_a = x_0 + \frac{ma\delta_0}{n_0} + \frac{a^2 n_0'}{2n_0} + \frac{ma^3\delta_0 n_0''}{6n_0^2} + \frac{a^4 n_0' n_0''}{24 n_0^2}\,. \tag{23}$$

It is, however, inconvenient to have the variable n_0 in the denominators. Therefore, it is advisable to make use of the following relation,

$$\frac{1}{n_0} = \frac{1}{m} - \left(\frac{1}{m} - \frac{1}{n_0}\right) = \frac{1}{m} - \frac{n_0 - m}{m n_0} = \frac{1}{m}\left(1 - \frac{n_0 - m}{n_0}\right). \tag{24}$$

Hence it is possible to replace $1/n_0$ by $1/m$ if a correction term of the next degree is added. (According to our assumptions regarding orders of magnitude, n_0-m is a quantity of the first degree). The same relation can, of course, be applied over and over again to the correction terms, which still contain n_0 in the denominator. If, now, relation (24) is applied to the two first-degree terms in (23), two additional, *i. e.* in all four, second-degree terms are obtained. All of them also contain n_0 in the denominators. The relation (24) can be applied to these terms also, which results in the formation of four terms of the third degree. We are, however, dealing with a second order approximation only, so the last-mentioned terms are omitted. Consequently, we are allowed simply to replace $1/n_0$ by $1/m$ in all terms of the second degree, and thus get the equation :

$$x_a = x_0 + a\delta_0 + \frac{a^2 n_0'}{2m} - \frac{a\delta_0(n_0 - m)}{m} - \frac{a^2 n_0'(n_0 - m)}{2m^2} + \frac{a^3\delta_0 n_0''}{6m} + \frac{a^4 n_0' n_0''}{24 m^2}\,. \tag{25}$$

The internal exit angle, α_a. — This angle will be derived in the same way, thus we put

$$\alpha_a = \alpha_0 + \frac{a}{1}\left(\frac{\mathrm{d}\alpha}{\mathrm{d}z}\right)_{z=0} + \frac{a^2}{2}\left(\frac{\mathrm{d}^2\alpha}{\mathrm{d}z^2}\right)_{z=0} + \frac{a^3}{6}\left(\frac{\mathrm{d}^3\alpha}{\mathrm{d}z^3}\right)_{z=0}$$

and start the successive differentiation from equation (14), which gives

$$\frac{d^2\alpha}{dz^2} = \frac{\alpha n''}{n}, \quad \frac{d^3\alpha}{dz^3} = \frac{n'n''}{n^2}.$$

Higher derivatives only contain terms of the third and higher degrees. Thus we get

$$(26) \quad \alpha_a = \alpha_0 + \frac{an_0'}{n_0} + \frac{a^2\alpha_0 n_0''}{2n_0} + \frac{a^3 n_0' n_0''}{6n_0^2}.$$

The external exit angle, δ_a. — It should be pointed out here that this angle is external with reference to figure 1, where $r>1$, but internal for $r<1$. Its value is, however, independent of r, and is calculated from equation (8). Since we are dealing with a second order approximation only, we can put the sines of this equation equal to their angles, and, further, by the use of a first order TAYLOR expansion of $n\ (x_a)$, we get

$$(27) \quad m\delta_a = \alpha_a \left[n(x_0) + (x_a - x_0) n'(x_0) \right].$$

The factor α_a is of the first degree. According to equation (25), that is also the case with $(x_a - x_0)$ after division by a, and $an'(x_0)$ is, according to our definitions, a first-degree quantity. Consequently, the second term in the above expression becomes of the third degree and has to be disregarded in our second order approximation. We thus arrive at the simple relation

$$(28) \quad \delta_a = \frac{n_0 \alpha_a}{m}.$$

With the aid of (26), (22), and (24), we get the following second order approximation for the external exit angle:

$$(29) \quad \delta_a = \delta_0 + \frac{an_0'}{m} + \frac{a^2\delta_0 n_0''}{2m} + \frac{a^3 n_0' n_0''}{6m^2}.$$

The coordinate in the Gaussian image plane of the plate, x_{ra}. — This coordinate is given by equation (9), in which $\tan \delta_a$ is approximated by δ_a, and in which we then introduce the expressions for x_a and δ_a just derived. The result is

$$(30) \quad x_{ra} = x_0 + ra\delta_0 + \frac{a^2 n_0' (2r-1)}{2m} - \frac{a\delta_0 (n_0 - m)}{m} - \frac{a^2 n_0' (n_0 - m)}{2m^2} + \frac{a^3 \delta_0 n_0'' (3r-2)}{6m} + \frac{a^4 n_0' n_0'' (4r-3)}{24m^2}.$$

The coordinate of the reference pencil in the middle of the cell. We have a considerable interest in this coordinate because of the conclusions drawn in the second order theory in reference 1. We will start this calculation from the exact equation:

$$(31) \quad \frac{x_{ra} - x_m}{a\,(r-1/2)} = \frac{x_{ra} - q}{p}.$$

By adding and subtracting x_0 in both numerators, and with the aid of (5), this equation can be written in the form

$$(32) \quad x_m - x_0 = x_{ra} - x_0 - \frac{a\delta_0\,(2r-1)}{2} - \frac{a(2r-1)\,(x_{ra} - x_0 - ra\delta_0)}{2p}.$$

The second order approximation of the first two terms above is given by (30). The third term is of the first degree and is added to the corresponding term in (30). The last term in (32) is of the second degree, since a/p is a first-degree quantity. In this term, it is consequently sufficient to introduce the first-degree terms of (30) exclusively. These substitutions give the result:

$$(33) \quad x_m - x_0 = \frac{a\delta_0}{2} + \frac{a^2 n_0' (2r-1)}{2m} - \frac{a\delta_0 (n_0 - m)}{m} - \frac{a^2 n_0' (n_0 - m)}{2m^2} + \frac{a^3 \delta_0 n_0'' (3r-2)}{6m} + \frac{a^4 n_0' n_0'' (4r-3)}{24m^2} - \frac{a^3 n_0' (2r-1)^2}{4mp}.$$

IV. **The third order approximation of the path length difference.** — We are now ready for attacking the different terms in the exact equation (3), and we will start this work by studying the path length within the cell.

The optical path length of the trajectory. — This length is easily obtained by a MACLAURIN approximation of the same kind as used earlier. We can write:

$$(34) \quad S_a = \int_0^a \frac{n(x)\,dz}{\cos\alpha} = \frac{a}{1}\left(\frac{dS}{dz}\right)_{z=0} + \frac{a^2}{2}\left(\frac{d^2S}{dz^2}\right)_{z=0} + \frac{a^3}{6}\left(\frac{d^3S}{dz^3}\right)_{z=0} + \frac{a^4}{24}\left(\frac{d^4S}{dz^4}\right)_{z=0} + \frac{a^5}{120}\left(\frac{d^5S}{dz^5}\right)_{z=0} + R_6$$

and omit the residual term R_6 if it can be shown to be of insignificant order of magnitude on our scale. The successive derivatives are obtained by differentiation of equation (11) with respect to z, making use of the relations (13) and (14). In each derivative, we are allowed to omit terms of the fourth and higher degrees. We then get

$$\frac{dS}{dz} = n(1+\alpha^2/2), \quad \frac{d^2S}{dz^2} = 2\alpha n', \quad \frac{d^3S}{dz^3} = \frac{2n'^2}{n} + 2\alpha^2 n'',$$

$$(35) \quad \frac{d^4S}{dz^4} = \frac{8\alpha n' n''}{n}, \quad \frac{d^5S}{dz^5} = \frac{8n'^2 n''}{n^2}.$$

The residual term contains the sixth derivative of S with respect to z, which is of the fourth degree in Δn and α, and need not be considered. Thus we get the

following third order approximation of the optical path length of the trajectory :

$$(36)\quad S_a = \int_0^{a} \frac{n(x)\,dz}{\cos\alpha} = an_0 + \frac{m^2 a\delta_0^2}{2n_0} + \frac{ma^2\delta_0 n_0'}{n_0} + \frac{a^3 n_0'^2}{3n_0} - \frac{m^2 a^3\delta_0^2 n_0''}{3n_0^2} + \frac{ma^4\delta_0 n_0' n_0''}{3n_0^2} - \frac{a^5 n_0'^2 n_0''}{15n_0^2}.$$

Before we proceed to the next term in equation (3), we will, however, eliminate the variable n_0 from all denominators by application of equation (24) to three terms of the second degree, and by putting $1/n_0 = 1/m$ in all terms of the third degree. We then get an equation with six terms of the third degree, which, however, is more convenient to use in the following treatment :

$$(37)\quad S_a = \int_0^{a} \frac{n(x)\,dz}{\cos\alpha} = an_0 + \frac{ma\delta_0^2}{2} + a^2\delta_0 n_0' + \frac{a^3 n_0'^2}{3m} - \frac{a\delta_0^2(n_0-m)}{2} - \frac{a^2\delta_0 n_0'(n_0-m)}{m} - \frac{a^3 n_0'^2(n_0-m)}{3m^2} + \frac{a^3\delta_0^2 n_0''}{3} + \frac{a^4\delta_0 n_0' n_0''}{3m} + \frac{a^5 n_0'^2 n_0''}{15m^2}.$$

The optical path length from the exit wall to the Gaussian image plane of the plate. This length is represented by the third term in equation (3), and is easily calculated, since we have already the second order approximation of the angle δ_a. We have

$$(38)\quad \frac{ma\,(r-1)}{\cos\delta_a} = ma\,(r-1)\,(1+\delta_a^2/2)$$

in which equation we have to introduce (29). If the latter equation is written in the abbreviated form

$$(39)\quad \delta_a = \delta_{a1} + \delta_{a2},$$

where the first term represents the first-degree part, and the second one the second-degree part of δ_a, then the third-degree approximation of its square can be written :

$$(40)\quad \delta_a^2 = \delta_{a1}^2 + 2\delta_{a1}\delta_{a2}.$$

Thus the computation of (38) is fairly easy, and the result is

$$(41)\quad \frac{ma\,(r-1)}{\cos\delta_a} = mra - ma + \frac{ma\delta_0^2(r-1)}{2} + a^2\delta_0 n_0'(r-1) + \frac{a^3 n_0'^2(r-1)}{2m} + \frac{a^3\delta_0^2 n_0''(r-1)}{2} + \frac{2a^4\delta_0 n_0' n_0''(r-1)}{3m} + \frac{a^5 n_0'^2 n_0''(r-1)}{6m^2}.$$

The optical path length from the light source to the entrance wall, and the total path length of the reference pencil. — These quantities, which are represented by the first and last terms of equation (3), respectively, are preferably treated together. We have

$$(42)\quad S_1 - S_4 = \frac{m\,(p-ra)}{\cos\delta_0} - \frac{mp}{\cos\delta_1} = \frac{mp\,(\cos\delta_1 - \cos\delta_0)}{\cos\delta_0\cos\delta_1} - \frac{mra}{\cos\delta_0}.$$

According to figure 1, we have, however, the relation :

$$(43)\quad x_{ra}-q = x_{ra}-x_0 + x_0-q = x_{ra}-x_0 + (p-ra)\tan\delta_0 = p\tan\delta_1,$$

from which we get, without any approximation,

$$(44)\quad p = \frac{x_{ra}-x_0 - ra\tan\delta_0}{\tan\delta_1 - \tan\delta_0}.$$

Introduction of this value of p into (42) gives

$$(45)\quad S_1 - S_4 = m\,(x_{ra}-x_0 - ra\tan\delta_0)\,\frac{\cos\delta_1 - \cos\delta_0}{\sin(\delta_1-\delta_0)} - \frac{mra}{\cos\delta_0}.$$

We know from equation (30) that $x_{ra}-x_0$ is of the first degree and conclude that the trigonometric function of the two entrance angles has to be computed to the second degree. Hence the first-degree approximation of the sine function and the second-degree approximation of the cosine function are adequate, which gives

$$(46)\quad S_1 - S_4 = -m\,(x_{ra}-x_0 - ra\delta_0)\,(\delta_1+\delta_0)/2 - mra\,(1+\delta_0^2/2).$$

Since the trigonometric function also appears to be of the first degree, it suffices to use the first-degree approximation of the tangent function in the first factor. It now remains to express the entrance angle of the reference pencil in terms of that of the pencil passing through the gradient. The accuracy required is that of the second degree and the desired relation becomes :

$$\delta_1 = \frac{x_{ra}-q}{p} = \frac{x_{ra}-x_0}{p} + \frac{x_0-q}{p} = \frac{x_{ra}-x_0}{p} + (1-ra/p)\tan\delta_0 = \delta_0 + \frac{x_{ra}-x_0-ra\delta_0}{p}.$$

Introduction of the first-degree terms of (30) further gives

$$(47)\quad \delta_1 = \delta_0 + \frac{a^2 n_0'(2r-1)}{2\,mp}.$$

After introduction of this value into (46), the latter equation can be written :

$$(48)\quad S_1 - S_4 = -m\left[\frac{a^2 n_0'(2r-1)}{2m} + (x_{ra}-x_0)_2\right]\left[\delta_0 + \frac{a^2 n_0'(2r-1)}{4mp}\right] - mra - \frac{mra\delta_0^2}{2},$$

where the subscript 2 is used to denote the second-degree terms of the function. On multiplying the two parentheses together, it is observed that the product of the two second-degree terms can be omitted, and the result is

$$(49)\quad S_1 - S_4 = -mra - \frac{mra\delta_0^2}{2} - \frac{a^2\delta_0 n_0'(2r-1)}{2} + a\delta_0^2(n_0-m) + \frac{a^2\delta_0 n_0'(n_0-m)}{2m} - \frac{a^3\delta_0^2 n_0''(3r-2)}{6} - \frac{a^4\delta_0 n_0' n_0''(4r-3)}{24m} - \frac{a^4 n_0'^2(2r-1)^2}{8mp}.$$

The total path length difference. — This is now easily obtained by adding equations (37), (41), and (49). The result is

$$(50)\quad \Delta S = a(n_0-m) + \frac{a^2\delta_0 n_0'}{2} + \frac{a^3 n_0'^2(3r-1)}{6m} + \frac{a\delta_0^2(n_0-m)}{2} - \frac{a^2\delta_0 n_0'(n_0-m)}{2m} - \frac{a^3 n_0'^2(n_0-m)}{3m^2} + \frac{a^3\delta_0^2 n_0''}{6} + \frac{a^4\delta_0 n_0' n_0''(12r-5)}{24m} + \frac{a^5 n_0'^2 n_0''(5r-3)}{30m^2} - \frac{a^4 n_0'^2(2r-1)^2}{8mp}.$$

This equation would be immediately useful for our purpose if x_0 were directly related to the vertical coordinate on the plate carrying the interferogram, but it is not. The reader is reminded about the fact that the symbols n_0, n_0', n_0'' are abbreviated forms of $n(x_0)$, $n'(x_0)$, and $n''(x_0)$, respectively, and that the entrance coordinate x_0 is not known to an experimental worker. No conclusions of interest can therefore be drawn from equation (50).

V. **The coordinate transformation.** — *Physical interpretation of coordinate transformation.* — After it had been shown in the second order theory that the skewness aberration could be brought to disappear by defocusing the middle of the cell 1/6 of its thickness in the direction towards the light source (by making $r = 2/3$), it was also found that the remaining second-order aberration, in the case of a light source without vertical extension, could be cancelled by experimental determination of the photographic enlargement factor using an object placed in the middle of cell in spite of the defocusing mentioned. When this is done, the cell should be filled with a medium of the refractive index m, and the light source system has to be the same as that used in the actual diffusion experiments (the same divergence parameter p, and the same off-axis position parameter, q/p). In practice, the diffusion cell is not at all used in this operation, but a transparent glass scale is placed on the cell stand at the same optical distance from the lens system as the middle of the cell in the actual experiments (correction for the cell wall and for half the thickness of the reference cell if the scale is not surrounded by a medium of refractivity m). The same procedure applies if the optical system is not free from distortion, that is, if the photographic magnification is not constant. The only difference is that one should talk about a calibration of the plate coordinate instead of a determination of an enlargement factor.

It is easily realized with reference to figure 1 that the procedure recommended makes the coordinate x_m, the coordinate of the reference pencil in the middle of the cell, directly related to the plate coordinate, since no refractive index gradient is used when the calibration is carried out. We thus conclude that it is impossible to interpret equation (50) without elimination of the coordinate x_0 in favour of x_m.

If we denote, by definition, the right-hand side of equation (33) by Δx, we thus have to introduce

$$(51)\qquad x_0 = x_m - \Delta x$$

in all terms of equation (50) where x_0 appears. This is the reason why it was advisable to get rid of $n(x_0)$ in all denominators. However, we now encounter another difficulty in the fact that Δx itself contains the variable x_0 which it shall serve to remove. Thus we have to start with removal of x_0 from the right-hand side of equation (33).

Removal of the entrance coordinate from the equation for the plate coordinate. — Equation (33) contains two terms of the first degree and five terms of the second degree on the right-hand side. If we take an arbitrary term of the last kind, *e. g.* the last term in equation (33), and introduce the new independent variable with the aid of (51), we get

$$\frac{a^3 n_0'(2r-1)^2}{4mp} = \frac{a^3(2r-1)^2}{4mp} n'(x_m-\Delta x) = \frac{a^3(2r-1)^2}{4mp}\left[n'(x_m) - \Delta x\, n''(x_m)\right].$$

The second term in the parenthesis is one order of magnitude smaller than the first. Since already the first term is of the second degree, the second one must be of the third degree and need not be included into a second order approximation. We conclude that x_0 can simply be replaced by x_m in all second-degree terms of (33), without impairing the exactitude of the equation. By the same reasoning, it can be concluded

that it is sufficient to apply the first order approximation of (33) :

$$(52) \qquad x_0 = x_m - \frac{a\delta_0}{2} - \frac{a^2 n_0' (2r-1)}{2m}$$

in the removal of x_0 from the two first-degree terms of the same equation. Now, the first of them does not contain x_0, so the substitution becomes in fact restricted to one single term :

$$(53) \qquad \frac{a^2 n_0' (2r-1)}{2m} = \frac{a^2 (2r-1)}{2m} \left[n'(x_m) - \right.$$
$$\left. - \frac{a\delta_0}{2} n''(x_m) - \frac{a^2 n_0' (2r-1)}{2m} n''(x_m) \right]$$
$$- \frac{a^2 n_m' (2r-1)}{2m} - \frac{a^3 \delta_0 n_m'' (2r-1)}{4m} - \frac{a^4 n_m' n_m'' (2r-1)^2}{4m^2} .$$

Here n_m' and n_m'' are abbreviated forms of $n'(x_m)$ and $n''(x_m)$. If (53) is introduced into (33), and if x_0 is changed to x_m in all second-degree terms, we get the following equation to be used in our coordinate transformation :

$$(54) \qquad x_0 = x_m - (\Delta x)_1 - (\Delta x)_2$$

where $(\Delta x)_1$ and $(\Delta x)_2$ represent the first-degree and second-degree terms, respectively, and are given by the equations :

$$(55) \qquad (\Delta x)_1 = \frac{a\delta_0}{2} + \frac{a^2 n_m' (2r-1)}{2m} ,$$

$$(56) \quad (\Delta x)_2 = - \frac{a\delta_0 (n_m - m)}{m} - \frac{a^2 n_m' (n_m - m)}{2m^2} -$$
$$- \frac{a^3 \delta_0 n_m''}{12m} - \frac{a^4 n_m' n_m'' (24r^2 - 28r + 9)}{24m^2} - \frac{a^3 n_m' (2r-1)^2}{4mp} .$$

Removal of the entrance coordinate from the expression for the total path difference. — We are now ready to attack equation (50) with the coordinate transformation (54). For reasons quite analogous to those presented in the foregoing section, it is superfluous to transform terms of the third degree ; in them, x_0 is simply replaced by x_m. In terms of the second degree, it is sufficient to use the simple relation :

$$(57) \qquad n'(x_0) = n'(x_m) - (\Delta x)_1 \, n''(x_m)$$

whereas in the only existing term of the first degree, we have to use the more complicated equation :

$$(58) \quad n(x_0) = n(x_m) - \left[(\Delta x)_1 + (\Delta x)_2 \right] n'(x_m) +$$
$$+ \frac{(\Delta x)_1^2}{2} n''(x_m).$$

The substitution involves no special difficulties, and one gets the following result :

$$(59) \quad \Delta S = a(n-m) \left[1 + \frac{\delta_0^2}{2} + \frac{a\delta_0 n'}{2m} + \frac{a^2 n'^2}{6m^2} \right] +$$
$$+ \frac{a^3 n'^2 (2-3r)}{6m} + \frac{a^3 \delta_0^2 n''}{24} + \frac{a^4 \delta_0 n' n''}{24m} +$$
$$+ \frac{a^5 n'^2 n'' (15r^2 - 20r + 7)}{30m^2} + \frac{a^4 n'^2 (2r-1)^2}{8mp} .$$

The effect of plano-parallel walls. — At the start of this analysis, two facilitating assumptions were made, first the assumption of infinitely thin cell walls, and second the assumption of an external refractivity equal to that of the reference cell. The first assumption is equivalent to the removal of two plano-parallel plates of a thickness equal to that of the walls, whereas the second one corresponds to the insertion of a plano-parallel plate of thickness $p - ra$ between the light source and the diffusion cell. These assumptions, which are thus of the same nature, facilitated the calculation greatly, since thereby the path of the reference pencil became rectilinear.

We are now going to free ourselves from these unrealistic assumptions simply by replacing δ_0, whereever it appears in (59), by δ_0/m, by replacing p by mp, and by redefining the distance p as the *optical distance* between the light source and the Gaussian image plane of the plate. This is the procedure generally adopted in elementary optics, and leads to the equation :

$$(60) \quad \Delta S = a(n-m) \left[1 + \frac{\delta_0^2}{2m^2} + \frac{a\delta_0 n'}{2m^2} + \frac{a^2 n'^2}{6m^2} \right] +$$
$$+ \frac{a^3 n'^2 (2-3r)}{6m} + \frac{a^3 \delta_0^2 n''}{24m^2} + \frac{a^4 \delta_0 n' n''}{24m^2} +$$
$$+ \frac{a^5 n'^2 n'' (15r^2 - 20r + 7)}{30m^2} + \frac{a^4 n'^2 (2r-1)^2}{8m^2 p} .$$

The correctness of the above procedure is of course not self-evident in a third-order approximation theory. It will be shown in Appendix 2, however, that the errors involved are negligible.

Equation (60) is thus our final equation for the optical path length difference. As is readily seen, it contains only one aberration term of the second degree. In the second order theory, two such terms were found as long as the independent variable was the coordinate x_{ra} in the Gaussian image plane of the plate. The term containing $a\delta_0 n'$ was then shown to disappear by a second coordinate transformation. In this treatment, we have transformed directly to the coordinate x_m of the reference pencil in the middle of the cell, so the absence of an $a\delta_0 n'$ term in (60) actually proves once more the correctness of the conclusions drawn in the previous paper. Since in the

following treatment we have no other vertical coordinate to deal with than x_m, the subscript has been dropped in equation (60).

The optimum position of the cell. — The obvious conclusion that the only remaining second-degree aberration disappears for $r = 2/3$ was drawn already in the previous article. There are only two more terms that depend on the longitudinal position of the cell, and among them the last one is present only in uncollimated light, which is comparatively seldom used. It is important to observe, however, that the a^5 term acquires a minimum value exactly for $r = 2/3$. Consequently the third order theory gives additional evidence in favour of the cell position recommended in the second order theory. We will consequently use this particular value of the parameter r in the following analysis, and equation (60) then takes the form:

$$(61) \qquad \Delta S = a\,[n\,(x)\text{—}m]\left[1 + \frac{\delta_0^2}{2m^2} + \frac{a\delta_0 n'}{2m^2} + \frac{a^2 n'^2}{6m^2}\right] + \frac{a^3\delta_0^2 n''}{24m^2} + \frac{a^4\delta_0 n' n''}{24m^2} + \frac{a^5 n'^2 n''}{90m^2} + \frac{a^4 n'^2}{72m^2 p}.$$

VI. **Physical interpretation of the third order approximation.** — If equation (61) is written in the form

$$(62) \qquad \Delta S = a\,[n(x)\text{—}m]\;[1 + R(x, t, \delta_0)] + A(x, t, \delta_0),$$

it is evident that we have to do with two different aberration functions, one absolute, $A\ (x,\ t,\ \delta_0)$, and one relative, $R\ (x,\ t,\ \delta_0)$. It is advantageous to treat these two functions separately.

1. *The absolute aberration function in collimated light.* — In collimated light, we have an infinitely large p value, and δ_0 is independent of x. The absolute aberration function reduces to three terms :

$$(63) \qquad A(x, t, \delta_0) = \frac{a^3\delta_0^2 n''}{24m^2\lambda} + \frac{a^4\delta_0 n' n''}{24m^2\lambda} + \frac{a^5 n'^2 n''}{90m^2\lambda}.$$

Here we have divided through by λ in order to get the aberration in terms of light waves.

Light source on the optical axis. In this case $\delta_0 = 0$, and the aberration function reduces to one single term. It is of great interest to investigate the magnitude of this term, since horizontal, collimated light is frequently used in practice.

The refractive index function prevailing in the cell has already been assumed to be that given by an ideally diffusing substance:

$$(64) \qquad n'(x) = \frac{\Delta n}{2\sqrt{\pi Dt}}\,e^{-x^2/4Dt} = \frac{\Delta n}{b}\,f(y),$$

where $f\ (y)$ is the error function and b half the distance between the two inflexion points of the curve $n'(x)$:

$$(65) \qquad f\,(y) = \frac{1}{\sqrt{2\pi}}\,e^{-y^2/2},\ b = \sqrt{2Dt}\,.$$

The quantity Δn will be regarded as positive. Hence the error function $f(y)$ has the same sign as $n'(x)$, which is negative in most practical applications. It follows further, since $x = by$ and $dx = b\ dy$, that the second derivative is given by the equation

$$(66) \qquad n''(x) = \frac{\Delta n}{b^2}\,f'(y) = -\frac{\Delta n}{b^2}\,y.f(y).$$

The last term in (63) now takes the form

$$(67) \qquad A\ (x,t,0) = \frac{a^5\,(\Delta n)^3 f^2 f'}{90m^2\ b^4\lambda}.$$

This quantity is at a maximum for $y = \pm\,1/\sqrt{3}$, in which point f^2f' has the value 0.022235. The precision that can be reached in interferometry without using photometry is of the order of $\lambda/50$. Consequently we must require that the maximum of the above expression be less than 0.02, which leads to the condition

$$(68) \qquad b^4 \geqslant 0.01235\ \frac{a^5\ (\Delta n)^3}{m^2\ \lambda}.$$

If we now introduce the total number of fringes in the interferogram

$$(69) \qquad N = a\ \Delta n/\lambda,$$

the condition can be put into the form

$$(70) \qquad b^2 \geqslant 0.1111\ \frac{\lambda a N^{3/2}}{m},\ b \geqslant 0.3334\ \frac{\sqrt{\lambda a}N^{3/4}}{\sqrt{m}}.$$

Since b^2 is proportional to the time, this condition can be regarded as a critical time condition, the aberration (67) being smaller than 1/50 of a light wave after the elapse of a time defined by (70).

Light source in an off-axis position. In this case, the entrance angle has a finite, but constant value. In order to facilitate the mathematical analysis of the aberration (63) as much as possible, the variable y is first introduced instead of x with the aid of the relations (64) and (66). Two new, dimension-less parameters B and C defined by the equations :

$$(71) \qquad b = B\,\frac{\sqrt{\lambda a}N^{3/4}}{\sqrt{m}},$$

$$(72) \qquad \delta_0 = C\,\frac{\sqrt{m\lambda}N^{1/4}}{\sqrt{a}}$$

are then used for elimination of b and δ_0. The exponents to the right in these equations have been chosen in accordance with equation (70) what concerns b, and for δ_0 in such a manner that the parameters m, λ, a, and N disappear altogether. Equation (63) consequently takes the form

$$(73) \qquad A\ (y, B, C) = \frac{C^2 f'}{24B^2} + \frac{C f f'}{24B^3} + \frac{f^2 f'}{90B^4}.$$

We will now investigate the conditions under which this aberration is smaller than 1/50 of a wave over the entire interferogram.

The aberration as a function of the entrance angle. The partial derivative of A with respect to C is

$$\frac{\partial A}{\partial C} = \frac{2Cf'}{24B^2} + \frac{ff'}{24B^3}. \tag{74}$$

This derative vanishes for

$$C = -f/2B \tag{75}$$

or, if we go back to the original variables, for

$$\delta_0 = -an'/2. \tag{76}$$

Since an' is the angular deflection in the cell, the conclusion can be drawn that this aberration is at a minimum when entrance and exit angles are equal but for the sign. This fact was revealed by Longsworth [4] several years ago by experimental tests with the *Schlieren*-scanning arrangement. It is also easily conceivable and plausible, since the x interval in the cell swept through by the ray must be at a minimum for a symmetrically passing ray. It is also interesting in this connection to compare the refractive index gradient in a plano-parallel cell with a prism of constant refractive index. The former gives a *maximum* deflection, whereas the latter gives a *minimum* deflection to the symmetrically passing ray.

It is also of interest to see how astonishingly small this minimum aberration is. If the value of C according to (75) is introduced into (73), the function A is found to assume the value

$$A_{\min.} = \frac{f^2f'}{1440\ B^4}. \tag{77}$$

This aberration is 16 times smaller than the corresponding aberration for horizontally entering light, given by (67). However, we have not very much use of this minimum aberration, because experimentally it is not very easy to make the entrance angle a function of the level in the cell such as to satisfy condition (76) in every point. Moreover, we have the time dependence of n' to take into a ccount.

The aberration as a function of time. Next we will consider the partial derivative with respect to B:

$$\frac{\partial A}{\partial B} = -\frac{C^2f'}{12B^3} - \frac{Cff'}{8B^4} - \frac{2f^2f'}{45B^5}. \tag{78}$$

If we put this derivative = 0, an equation of the second degree in B is obtained, the roots of which are

$$B_1 = -0.5792\ f/C,\ B_2 = -0.9208\ f/C. \tag{79}$$

Negative B values lack physical interpretation. Consequently the roots (79) have no physical meaning if C and f have the same sign. The function A is then monotonically decreasing when B increases from 0 to infinity. On the other hand, if C and f have opposite signs, the function first decreases to a minimum, then increases to a maximum, and finally falls off to 0. The values of this minimum and this maximum are

$$A_{\min.} = -0.008493\ C^4\ y/f,$$
$$A_{\max.} = -0.011229\ C^4 y/f. \tag{80}$$

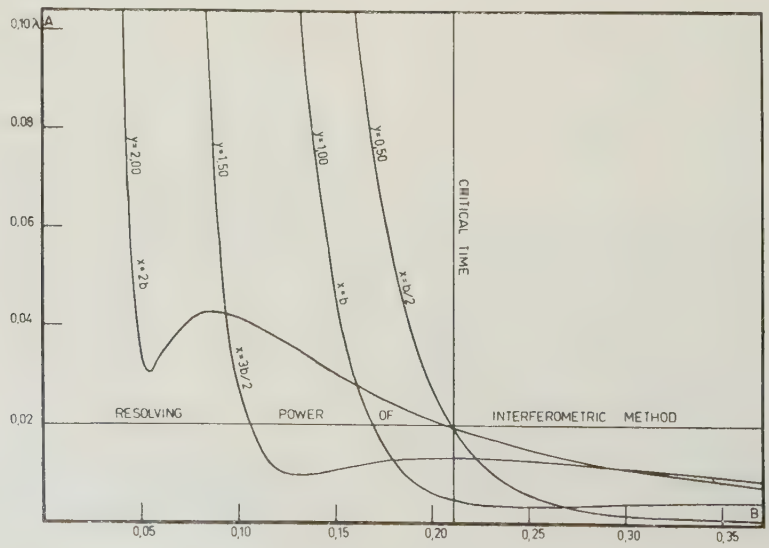

Fig. 2. — The absolute aberration A in collimated light as a function of time (B) at some different parts of the interferogram, and for $BC = -0.1195$. The values $x = b$ and $y = 1$ correspond to the inflexion point of the gradient curve. Each curve has a minimum and a maximum. In the central parts of the interferogram ($y < 1$), these extrema occur comparatively late and are not very pronounced. In the outer parts of the interferogram ($y > 1$), they take place at an early stage of the diffusion process, and the minimum, especially, is very sharp. After the critical time, represented by $B = 0.21$, the aberration is below the resolving power for all parts of the interferogram.

Consequently there is a constant ratio between these two extrema (1.322). The ratio is rather close to unity. This implies that the aberration, for fixed values of C and y, during its rapid decrease in the course of time, stays for a rather long period at the order of magnitude given by (80). It is interesting to note that the increase of the aberration from its minimum to its maximum occurs shortly after the minimum aberration corresponding to a variable entrance angle has been reached [compare equations (75) and (79)]. The decline of the absolute aberration in the course of time can be studied in figure 2 for some different parts of the interferogram.

The aberration as a function of the level in the cell. The time parameter B and the entrance angle parameter C will now be considered as constant, and y as variable. This function of y cannot be treated analytically, but instead we can study the family of curves presented in figure 3, showing the aberration function through half the diffusion boundary for some different values of the product BC. It is seen here that the aberration is always zero at the centre of the gradient, then rises to a maximum, falls to a minimum, rises to a second maximum, and finally falls off asymptotically to zero for large y values. For small negative values of BC, the first maximum is large and the second one small, and *vice versa* for large negative values of BC. Consequently, when it is required to find the most favourable conditions with regard to the whole interferogram, the two maxima should have the same value. This occurs for

$$BC = -0.1195 \tag{81}$$

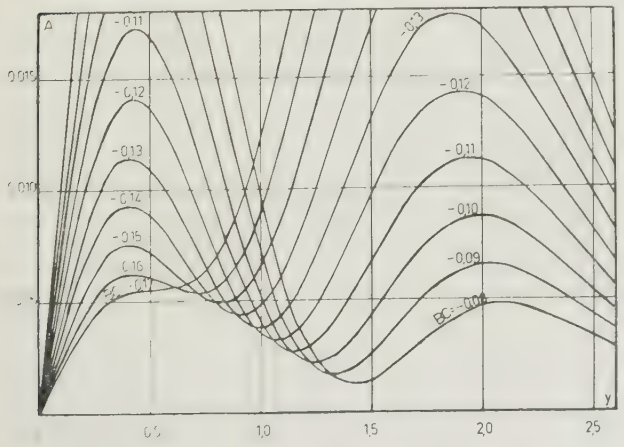

FIG. 3. — The absolute aberration A in collimated light as a function of the cell coordinate. The centre of the diffusion boundary is at $y = 0$ and the inflexion point of the gradient curve at $y = 1$. The function has, in each half portion of the interferogram, two maxima and one minimum. For a special relation between entrance angle and time, given by the equation $BC = -0.1195$, the two maxima have the same value. Using the critical time shown in figure 2, one thus arrives at an optimum entrance angle.

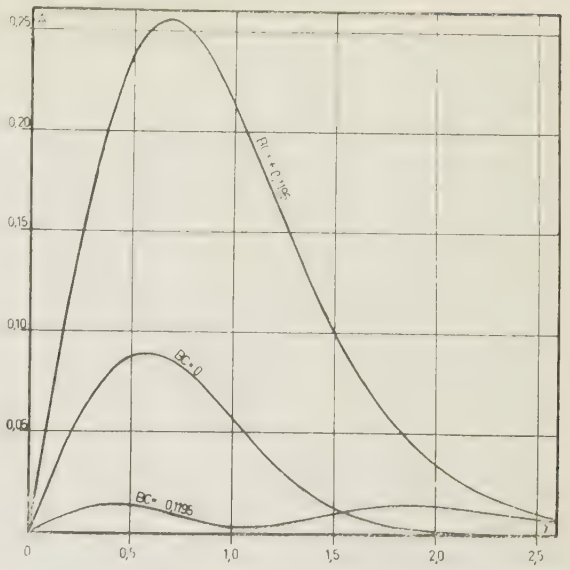

FIG. 4. The absolute aberration A in collimated light as a function of the cell coordinate. The centre of the diffusion boundary is at $y = 0$, and the inflexion point of the gradient curve at $y = 1$. The figure shows the aberration at the optimum entrance angle, $BC = -0.1195$, in comparison with the aberrations for horizontally entering light, $BC = 0$, and for the optimum entrance angle of the wrong sign, $BC = +0.1195$.

and the two equally large maxima then have the value

$$A_{\max.} = 0.01421/360\ B^4. \tag{82}$$

The curves in figure 3 all belong to negative values of BC. In order to give an idea of the magnitude of the aberration for non-negative values of BC, figure 4 has been constructed. Here the aberration curve for $BC = 0$ (horizontally entering light) can be compared to that for $BC = -0.1195$ and with that for $BC = +0.1195$. The aberration is 6 times greater for horizontally entering light and 18 times greater for light entering the cell under an entrance angle of the wrong sign.

Condition for aberration-free imagery with a variable entrance angle. If at any given time we choose an entrance angle satisfying condition (81), then we know that the function in figure 3 nowhere exceeds the value of 0.01421, and if we put down the condition

$$\frac{0.01421}{360B^4} \leqslant 0.02, \tag{83}$$

we get a critical time :

$$B^4 \geqslant 0.001974,\ B^2 \geqslant 0.04443,\ B \geqslant 0.2108 \tag{84}$$

after which the aberrations have certainly fallen below 1/50 of a light wave in the entire interferogram.

The condition (84) is thus a necessary condition for

an aberration-free imagery, and it would also be sufficient if the entrance angle were made to vary with time according to condition (81). It is of course not impossible to do this, but it is a little inconvenient to make such an adjustment before every exposure. We will therefore investigate the possibility of using a constant entrance angle throughout the diffusion experiment. It is then quite natural to choose that angle which satisfies condition (81) at the critical time defined by (84).

General condition for aberration-free imagery. Insertion of the value of B from (84) into condition (81) gives a numerical value of the entrance angle parameter:

$$C = -0.5669. \tag{85}$$

We know that this entrance angle gives an aberration-free interferogram at the time defined by (84). We now have to prove that the aberration does not increase beyond $\lambda/50$ in the course of time when C is kept at the constant value (85). There is apparently a risk for such an increase, since the aberration, regarded as a function of time only, was found to pass first a minimum, then a maximum, before it falls off to zero. The time period between this minimum and this maximum is evidently a period of increasing aberration and has to be investigated in more detail.

The time interval for an increasing aberration is given by equations (79), in which we now introduce the numerical value of C :

$$1.0217\ f \leqslant B \leqslant 1.6243\ f. \tag{86}$$

For $f = 0.1298$, $y = \pm 1.499$, we have the interval

$$0.1326 \leqslant B \leqslant 0.2108 \tag{87}$$

from which we can conclude that the aberrations will never exceed 1/50 of a light wave outside $y = \pm 1.499$ after the time defined by (84), if the entrance angle is kept constant at the value (85). It remains to be seen what happens inside $y = \pm 1.499$.

We then go to the second equation (80) in order to investigate the magnitude of the aberration maximum that occurs after the tentative critical time (84). After introduction of the numerical value of C, we can put down a requirement that this maximum be smaller than 1/50 of a light wave

$$y/f \leqslant 17.24. \tag{88}$$

The function y/f increases monotonically from 0 to infinity when y passes from 0 to infinity. It acquires the value of 17.24 for $y = \pm 1.679$, hence the condition (88) is satisfied in the region inside $y = \pm 1.679$. This region overlaps a little the regions outside $y = \pm 1.499$, which is to be regarded as a good luck, since we now can draw the following conclusion. At a constant entrance angle, defined by (85), the aberrations are bigger than 1/50 of a light wave at many points of the interferogram before the elapse of a diffusion time defined by equation (84). During this time, each point outside $y = \pm 1.499$ has a period of increasing aberrations, with maxima which may be greater than $\lambda/50$. After the critical time of diffusion given by (84), the aberrations lie below $\lambda/50$ in all parts of the interferogram. It is true that all points within $y = \pm 1.499$ have a short period of increasing aberrations, but these aberration maxima stay below $\lambda/50$. These relationships are also clearly illustrated in figure 2. Thus it has been proved that it is feasible to use the constant entrance angle given by (85) and that it is quite unnecessary to arrange for a variation in time according to equation (81), the optimum relation for a minimum aberration.

The Optimum Entrance Angle and the Critical Time of Diffusion. If we now go back to the original variables δ_0, b, and t with the aid of equations (65), (71), and (72), we get the following expression for the optimum entrance angle*:

$$\delta_0 = \pm\ 0.5669\ \frac{\sqrt{m\lambda}\ N^{1/4}}{\sqrt{a}} \tag{89}$$

and the critical time of diffusion, at which all aberrations have decreased to 1/50 of a light wave, is given by the equation

$$2Dt = b^2 = 0.04443\ \frac{\lambda a N^{3/2}}{m}. \tag{90}$$

With reasonable figures, $m = 4/3$, $\lambda = 5461$ Å, $a = 5$ cm, and $N = 25$, we get $\delta_0 = 0.0048$. This means that the light source should be situated about 5 mm below the optical axis in the focal plane of a lens with a focal distance of 1 meter. The result is quite reasonable.

In view of the fact that the aberration terms contain the cell thickness in up to the fifth power [*cf.* equation (37)], it is surprising indeed to find that the optimum entrance angle and the critical breadth of the diffusion boundary ($2b$) are inversely and directly proportional, respectively, to the square root of the cell thickness only, whereas the critical time becomes directly proportional to the cell thickness in the first power. Insertion of the reasonable figures suggested above also reveals that the critical time is surprisingly small. For cane sugar, with $D = 5.231 \cdot 10^{-6}$, one gets the figure 109 seconds. For water solutions investigated by the green light from a mercury lamp, equation (90) can be written :

$$a = 0.5280\ Dt \tag{91}$$

if the total number of fringes is 25, and if t is measured in minutes and D in units of the sixth decimal place. This leads to the simple diagram shown in figure 5.

It is also of interest to get an idea of the fringe density of the interferogram at the critical time. This is given by the equation

$$\frac{an'}{\lambda} = \frac{Nf}{b} = \frac{f\sqrt{m}\sqrt[4]{N}}{0.2108\sqrt{\lambda a}}. \tag{92}$$

* The sign of δ_0 is opposite that of $n'(x)$.

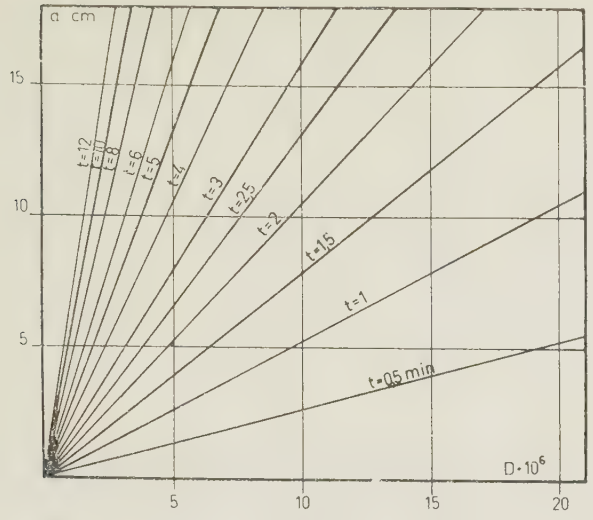

FIG. 5. — Graph showing the critical time of diffusion for different cell thicknesses and different diffusion coefficients. The graph is calculated for water solutions, for the wave-length of the green mercury line, and for a concentration of solute giving interferograms with 25 fringes. The critical time rises with the power 3/2 of the total number of fringes.

At the centre of the gradient, we have $f = 0.3989$, and if we give to the parameters the same values as earlier, we get a fringe density of 296 per cm at unit magnification, or a fringe separation of 34 μ. Thus one probably has to use a magnification factor of 2-3 and fine-grained plates in order to reach the resolution of 1/50 of a light wave, which was chosen as the basis of our numerical equations.

Vertically extended light source. It was found in the second order theory that a vertically extended light source must be expected to give rise to fringe blurring unless the Gaussian image plane of the plate coincides with the middle of the cell ($r = 1/2$). This conclusion was experimentally verified in reference 2.

Blurring of fringes arises from aberration terms containing δ_0 as a factor. This is natural, because light from the upper and lower ends of an extended light source must necessarily strike the entrance wall of the cell under different entrance angles. If δ_0 is retained to denote the entrance angle of light coming from the centre of a vertically extended light source, then every point of the cell will receive light pencils with all entrance angles lying between two limits, say $\delta_0 \pm \varepsilon$, where 2ε is the angular extension of the light source when viewed from the cell. It is then easily realized that aberration terms containing δ_0 in the first power will, in addition to the aberration they cause for a point source, give rise to a blurring which is symmetrical towards both sides of the fringe, that is, to a blurring not accompanied by any fringe displacement. On the other hand, terms containing the squared entrance angle must give rise to an asymmetric blurring and to a displacement of the centre of the fringe.

The most important blurring aberration is of course that already derived in the second order theory. This term is not present in equation (60) because of the direct transformation to the coordinate x_m, and because the equation was derived on the assumption of a point-shaped light source. In reference 1, however, the following equation was derived for the ε value corresponding to complete blurring :

$$\varepsilon\, a^2\, n'\, (1-2r) = m\lambda \tag{93}$$

Automatic guard against aberrations in interferograms. Half-blurred fringes are apparently obtained for the half of this ε value. After introduction of the variables y and B, we thus get the following condition for half-blurred fringes :

$$\varepsilon = \frac{3B\sqrt{\lambda m}}{2f\sqrt{a}\,N^{1/4}}\,. \tag{94}$$

The minimum permissible value of B is 0.2108, and the value of f at the centre of the boundary is 0.3989. Hence the fringes at the centre of the interferogram will be half-blurred at the critical time if the angular extension of the light source satisfies the equation

$$\varepsilon = 0.793\,\frac{\sqrt{m\lambda}}{\sqrt{a}\,N^{1/4}}\,. \tag{95}$$

Apparently it is a clever arrangement to use such an ε value since the blurring of the central fringes will then automatically prevent a meaningless evaluation of interferograms exposed before the critical time of diffusion has elapsed. In other words, by using a light source with the vertical extension given by (95), the fringes will grow sharp and well-defined at the same time as the aberrations are fading out to insignificance.

With the same numerical figures as used earlier in this article in order to exemplify applications, we get $2\varepsilon = 0.0047$, which means that a 4.7 mm long vertical slit should be used in the focal plane of a lens with a focal distance of 1 meter.

The additional blurring due to third-degree terms containing the entrance angle as a factor need not be considered.

2. *The absolute aberration function in uncollimated light.*

Additional aberration terms in the case of uncollimated light. Since the entrance angle δ_0 appears only in third-degree terms, it is permissible to use the value :

$$\delta_0 = \frac{x-q}{p} = \frac{x}{p} + \rho \tag{96}$$

instead of the exact value given by equation (5), because the quantities $(x_m-x_0)/p$ and ra/p are of the second and first degrees, respectively. In equation (96) p will then be regarded as a divergence para-

meter, while ρ is the off-axis parameter. The latter is identical with the entrance angle at the centre of the diffusion boundary and thus takes over the role hitherto played by δ_0.

On introduction of (96) into the absolute aberration function, given by the last four terms of equation (61), the terms containing ρ but not p become identical with the function (63) already treated, with ρ instead of δ_0. Then there remain four terms containing p:

$$(97)\quad Q(x,t,p,\rho) = \frac{a^2n''x^2}{24m^2p^2\lambda} + \frac{a^3xn''\rho}{12m^2p\lambda} + \frac{a^4xn'n''}{24m^2p\lambda} - \frac{a^4n'^2}{72m^2p\lambda}$$

After introduction of the variables y, B, and C with the aid of equations (64), (66), (71), and (72) (with ρ instead of δ_0), and after elimination of p in favour of the new dimension-less parameter P defined by the equation:

$$(98)\quad \frac{1}{p} = \frac{P\,m}{a\sqrt{N}}$$

the function (97) assumes the simpler form:

$$(99)\quad Q(y,B,C,P,) = -\frac{P^2y^3f}{24} - \frac{PCy^2f}{12B} - \frac{Pf^2(1-3y^2)}{72B^2}$$

or with the numerical values of B and C according to equations (84) and (85):

$$(100)\quad Q(P,y) = -0.0417\,P^2y^3f + 0.2241\,Py^2f + 0.3126\,Pf^2(1-3y^2)$$

The permissible divergence or convergence of a light beam. The course of the divergence aberration (100) through a diffusion boundary is given in figure 6 for $P = 0.4$, which is the numerical value of the divergence parameter that gives rise to aberrations touching our tolerable limit, 1/50 of a light wave. The same negative value, which corresponds to convergent light through the cell, is also useful. As a matter of fact, $P = -0.4$ gives a curve centrosymmetric with respect to that in the figure, since a sign reversal of both P and y in (100) changes the sign of each term.

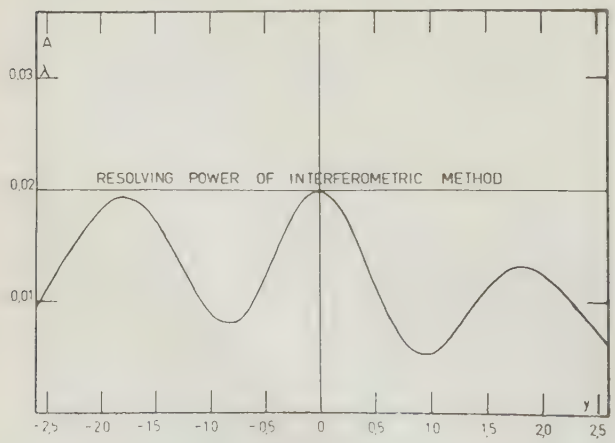

Fig. 6. — The contribution to the absolute aberration A which is due to non-parallel light, for a divergence parameter $P = 0.4$. The figure shows this divergence to be the maximum permissible.

We can thus formulate the following condition for the divergence parameter in the case of uncollimated light:

$$(101)\quad P = \frac{a\sqrt{N}}{mp} \leqslant 0.4$$

which can also be written in the form

$$(102)\quad \frac{a}{p} \leqslant \frac{0.4\,m}{\sqrt{N}}.$$

With the same numerical figures as applied earlier, one finds that a/p should be smaller than 0.11, which is also a reasonable figure.

3. *The relative aberration function in collimated light.*

This function is given by the equation

$$(103)\quad R(x,t,\delta_0) = \frac{\delta_0^2}{2m^2} + \frac{a\delta_0n'}{2m^2} + \frac{a^2n'^2}{6m^2}.$$

After introduction of the variables y, B, and C, it takes the form

$$(104)\quad R(y,B,C) = \frac{\lambda\sqrt{N}}{2ma}\left[C^2 + \frac{Cf}{B} + \frac{f^2}{3B^2}\right].$$

With a fixed value of C, this relative aberration can be regarded as a function of one single variable, f/B. This function has a minimum and increases in both directions therefrom. Consequently the highest value this function can acquire is either at the lower or at the upper limit of the interval within which f/B can vary. These limits are 0 and $0.3989/0.2108 = 1.8923$, respectively, and the latter limit gives the higher value of R. Hence this aberration satisfies the inequality (for $C = -0.5669$):

$$(105)\quad R(y,B,C) \leqslant \frac{0.2211\lambda\sqrt{N}}{ma}.$$

With the very unfavourable figures of $N = 100$ and $a = 1$ cm, this gives $R = 0.9\cdot10^{-4}$, which is a relative error without importance. It may be concluded that the relative aberration never requires consideration under conditions making the absolute aberration insignificant.

It should be noted that negative C values (if f positive) have the same favourable effect on this error as it was shown to have on the absolute aberration. If C were allowed to change sign, all three terms of R would get the same sign.

4. *The relative aberration function in uncollimated light.*

Introduction of (96) into (103) gives the following three terms containing the divergence parameter p :

$$(106) \qquad R\,(x,\,t,\,p) = \frac{x^2}{2m^2p^2} + \frac{\rho x}{2m^2p} + \frac{axn'}{2m^2p}\,.$$

The first two terms have their origin in the cosine error due to obliquely incoming light. This is the only aberration that actually *increases* in the course of time. This is evident from the fact that the x interval covered by the diffusion boundary grows larger and larger indefinitely as the diffusion process progresses. Thus the first term in the above equation, especially, increases with time rather rapidly and without limit.

An upper bound to this aberration can best be obtained by insertion of plausible figures in each term separately. There is no reason for making a diffusion cell longer than 6 cm, thus x is always smaller than 3 cm. Likewise, one can say that a plausible lower limit for p is 50 cm (*cf.* equation 102). With $m = 4/3$, one then finds that the first term of (106) stays below 10^{-3}, which is at the border of a tolerable error in precise measurements.

In the second term, we will assume ρ to be smaller than 0.01, and make the same assumptions regarding x and p as above. We then find that the numerical value of this term never exceeds $1.7 \cdot 10^{-4}$.

The third term actually contains the second derivative, since it can be written in the form

$$(107) \qquad \frac{axn'}{2m^2p} = \frac{ab^2n''}{2m^2p} = \frac{a\,(\Delta n)\,f'}{2m^2p} = \frac{a\,(\Delta n)\,yf}{2m^2p}\,.$$

The maximum value of $f' = -yf$ is $1/\sqrt{2\pi e} = 0.242$. With the same numerical values as earlier for m and p, we thus find this term always to be smaller than $4 \cdot 10^{-5}$, if Δn is smaller than 0.01.

VII. **Discussion.** — *Mathematical considerations.* — Although only elementary mathematics is involved in this treatment, the problem must be said to be unusually complex. The analysis is connected with an extensive algebraic labour. The risks of making algebraic mistakes are numerous, and the computations have to be carried out with a scrupulous care. It should be sufficient for the interested reader, however, to get a clear understanding of the principles of the mathematical methods. The correctness of the equations is granted by the fact that the same results have been gained by independent mathematical methods. It would lead too far to describe in detail other possible ways of computing the third order aberrations, but one hint will be given. The second order approximations for the exit coordinate and the exit angle can be derived by the method of undetermined coefficients. It one puts, tentatively,

$$(108) \qquad x_a = x_0 + A\alpha_0 + B\,(\Delta n) + C\alpha_0^2 + D\alpha_0(\Delta n) + \\ + E\,(\Delta n)^2$$

it follows because of equation (13) that the exit angle is obtained by differentiation with respect to a :

$$(109) \qquad \alpha_a = \frac{\mathrm{d}A}{\mathrm{d}a}\,\alpha_0 + \frac{\mathrm{d}B}{\mathrm{d}a}\,(\Delta n) + \frac{\mathrm{d}C}{\mathrm{d}a}\,\alpha_0^2 + \\ + \frac{\mathrm{d}D}{\mathrm{d}a}\,\alpha_0\,(\Delta n) + \frac{\mathrm{d}E}{\mathrm{d}a}\,(\Delta n)^2.$$

If these expressions are introduced into equation (7), and if $n(x_a)$ and the cosine functions are developed into their second order approximations, an identity is obtained which in turn gives rise to a series of differential equations. These can easily be solved for the coefficients A, B, C, D, and E. The result thus obtained is identical with equations (21) and (26).

It is also possible to check the correctness of the equations by insertion of the different variables into the exact equations (6) — (10). The third degree approximations of these equations then must reduce to identities $0 = 0$. One such check will be demonstrated in Appendix 1.

The author has attacked the theory of the light path through a diffusion boundary on two earlier occasions [5, 6]. The first trial was made in 1940 using very simple mathematical means, while the later one was more elaborate. Both these works pertained to the *Schlieren* method, so the results of the present theory have to be differentiated with respect to x before a comparison can be made. They are open to criticism from both mathematical and optical points of view, but, nevertheless, it is interesting to observe that many of the results now reached on firm and sound mathematical and optical bases were actually anticipated already in the 1940 article. Thus it was concluded already there that the WIENER skewness aberration could be removed, although a wrong numerical value of the cell defocusing was reported. The flattening of the top of the gradient curve, the correct value of which is obtained by differentiation of equation (63) with respect to x and by putting $x = 0$ $(n'' = 0)$:

$$(110) \qquad \frac{\mathrm{d}A(0,t,\,\delta_0)}{\mathrm{d}x} = \frac{a^3\delta_0^2 n'''(0)}{24m^2} + \\ - \frac{a^4\delta_0 n'(0)n'''(0)}{24m^2} - \frac{a^5 n'^2(0)n'''(0)}{90m^2}$$

was reported in the 1940 article to have the figure 72 instead of 90 in the denominator of the last term (only the case of horizontally entering light, $\delta_0 = 0$, was investigated). This figure was the result of a guess between two limits, 48 and 96, given by the mathematical analysis. In the paper of 1946, the correct value of this term was found (p. 79, equation 79). As we have seen in this article, the WIENER skewness and the aberration (110) are the two most important aberrations. A critical time condition was also given in reference 6 (p. 80, equation 103), according to which this time appears to be proportional

to the square of the cell thickness. This discrepancy relative to the result reported here is, however, only apparent, since our parameter N includes the cell thickness in the first power.

The fact that a defocused cell is most favourable even in the cases of finite entrance angles and uncollimated light was not revealed in these earlier works.

The fact that different aberration terms of the third degree have been found to counterbalance each other to a great extent is very valuable, since it makes it possible to bring down the aberrations quite appreciably. However, it also involves a risk that fourth-degree terms, if they do not balance each other in the same favourable way, are not appreciably smaller than the algebraic sum of the third-degree terms. The theory retains its essential validity, however, even if the fourth-degree terms rise to the same order of magnitude as the minimized sum of the third-degree terms. The results gained cannot be questioned unless one assumes the fourth-degree terms appreciably to surpass the third-degree terms in magnitude. Such an assumption appears to the author as highly improbable, if not impossible. Anyhow, experimental proofs of the validity of these results must be regarded as highly desirable.

Optical considerations. — The author has been criticized regarding the work in reference 6 on this topic for the reason that the *Schlieren* method cannot on the whole be treated by ray-optical means. This criticism was justified, and it was also shown through the excellent works of Kegeles and Gosting [7], Longsworth [8], Coulson *et al.* [9], Adler and Blanchard [10], and Gosting and Onsager [11] published shortly after reference 6 that the various modifications of the *Schlieren* method, the scale method, and the Gouy interference method are afflicted with an aberration at the top of the gradient curve that could only be accounted for by a wave-optical theory. The objects of the present theory are interferometric methods characterized by optical imagery of the cell, and the difficulty discussed above does not enter the picture. It should be pointed out in this connection that interferometric methods for recording the gradient curve are available [12, 13, 14, 15], and that these methods are also free from the wave-optical aberration discussed above.

The analysis presented here has been guided by experimental-optical considerations, whereby care has been taken to avoid unnecessary assumptions based on conventional habits and preconceived opinions regarding optical adjustments. This principle has resulted in the introduction of a number of parameters, the numerical values of which are open to free choice, each parameter having an experimental-optical counter-part. These parameters are the cell position parameter, the entrance angle parameter, the divergence parameter, the parameter related to the vertical extension of the light source, and the parameter pertaining to the plane in which the object is placed in the calibration of the plate coordinate in terms of the cell coordinate. The last parameter was never introduced, because its optimum value was already known from the second order theory. That was the case with the cell position parameter too, but this parameter was introduced here again in order to show that its optimum value, $r = 2/3$, also minimizes the third-degree aberrations.

The introduction of so many parameters of course contribute to make the handling of the mathematics extremely complex, but only in this way has it been possible to reach a number of valuable conclusions. Only in this way could it be revealed that a certain defocusing of the middle of the cell has a very pronounced and favourable effect in that it completely removes the important aberration corresponding to the well-known Wiener skewness of the gradient curve. Likewise, the far from self-evident recommendation of measuring the photographic enlargement from the middle of the cell, in spite of the defocusing mentioned, could not have been found by a less elaborate procedure.

The entrance angle has hitherto been regarded as more or less arbitrary, and horizontal, collimated light is in general used. It has now been shown, however, that a certain entrance angle of a sign opposite to that of the refractive index gradient gives much smaller aberrations than horizontal light, and appreciably reduces the time required for the aberrations to fade out to insignificance. The equation given for this optimum entrance angle is easily applicable to experimental work since it only contains known apparatus constants and data available from the preparation of the experiment (the total number of fringes — proportionnal to the concentration and to the cell thickness).

The dimensions of the light source have also been regarded as more or less arbitrary hitherto, provided that they satisfy the requirements of the interferometric optical system without regard to the diffusion cell. As is well known, some such systems require a point source, others can be operated with a slit-shaped source, while others again may be run with a circular or rectangular source. In the latter two cases, the stop at the light source has been used merely in order to regulate the light intensity to a proper value. In the previously published second-order theory, it was found that a vertically extended light source must give rise to fringe blurring as soon as the middle of the cell is defocused. Thus the defocusing necessary for abolishing the Wiener aberration has to be accompanied by a suitable reduction in the vertical extension of the light source. It has now been shown in the third order theory that this fringe blurring actually can be used to advantage. By a proper adjustment of the vertical extension of the light source, it is possible purposely to produce blurring of the central fringes during an initial time period while the interferograms are not yet aberration-free.

The necessary light intensity can be obtained by a proper choice of lamp and by selecting an interferometric set-up that allows the use of a horizontally extended light source.

The realization of such an automatic guard against a meaningless evaluation of interferograms not yet free from aberrations necessitates exact equations for the fringe blurring and for the time required for aberration-free imagery. Both these equations are given. They are also combined into an explicit and easily applicable equation for the optimum vertical extension of the light source.

The critical time period, *i. e.* the time required for the aberrations to decrease below the resolving power of the optical system, has been found to be surprisingly short if the tricks recommended in the optical adjustment are applied. The diagram in figure 5 gives an idea of the order of magnitude of this critical time for different diffusion coefficients and cell thicknesses.

It has also been shown that precise measurements can very well be carried out using uncollimated light. There is no optimum value of the divergence or convergence parameter, because the additional aberrations caused by uncollimated light have the same sign through the whole diffusion boundary, while the aberrations in collimated light have opposite signs on both sides of the starting boundary. An equation for the maximum allowable divergence or convergence of the light is given.

Physico-chemical considerations. — Experimental workers in diffusion are familiar with two different deviations of refractivity gradient curves from the shape of the Gaussian error function, which is obtained in the case of ideal diffusion. One deviation is a skewness, and its physico-chemical background is a concentration-dependent diffusion coefficient. The other deviation consists in an abnormal height of the curve. This deviation is the result of polydispersity or of impure preparations. The study of these deviations from the normal error curve is of great importance, since they involve possibilities of measuring concentration dependence and polydispersity if and when reliable theories of these phenomena become available.

It is interesting to note that the second and third order aberration theories have revealed the presence of two optical aberrations of the same nature as those mentioned above with physico-chemical origin. It is quite natural, then, that it is impossible to make correct physico-chemical interpretations of non-ideal diffusion curves unless they are optically aberration-free, or corrections can be applied.

The possibility of removing the optical skewness aberration completely is consequently a matter of great physico-chemical interest. Thus it has been found recently by Thompson [16] that the skewness in early exposures differs from that in later exposures for material with a concentration-dependent diffusion coefficient, a variation that could be explained by taking the Wiener skewness into account.

The absolute aberration function (63) results in a flattening of the gradient curve, that is, to an effect opposite to that of polydispersity. This depression of the $n'(x)$ maximum is given by equation (110). An interferogram photographed before the aberration (63) has decreased enough may therefore give rise to an erroneous interpretation of the polydispersity of the material. The direction of this misinterpretation is such as to indicate too small a heterogeneity.

In case of a pronounced concentration dependence, it is customary to measure the diffusion coefficient at a series of different absolute concentrations, using a small and constant concentration difference between top and bottom solutions in the diffusion cell. In order to retain a high accuracy in such measurements, it is desirable to increase the cell thickness in order to keep the total number of fringes at a suitable value (25-50). In this connection it is of great interest to note from the present theory that the critical time period rises with the first power of the cell thickness only, although the aberration terms themselves contain the cell thickness in the fifth and lower powers. This fact, together with the favourable indications regarding the critical time period shown in figure 5, promises very good conditions for measuring diffusion coefficients at extremely low concentration differences. Its lower limit depends probably more on the temperature regulation device than on the accuracy of the optical recording system. The lower the concentration difference, the greater the sensitivity of the boundary to liquid circulation below and on top of it.

Appendix I. — Here we will demonstrate in detail a cross-control of the correctness of two equations of the theory. We choose the equations (25) and (29), and the check will be made using equation (10).

It is necessary during such a computation always to be clear about the degrees of the different terms. Otherwise much work in vain is carried out in carrying along terms of the fourth and higher degrees, with which we are not concerned in this theory. Thus, the square of the external exit angle is found to be :

$$(111) \qquad \delta_a^2 = \left(\delta_0 + \frac{an_0'}{m}\right)^2 + 2\left(\delta_0 + \frac{an_0'}{m}\right)\left(\frac{a^2\delta_0 n_0''}{2m} + \frac{a^3 n_0' n_0''}{6m^2}\right) =$$

$$= \delta_0^2 + \frac{2a\delta_0 n_0'}{m} + \frac{a^2 n_0'^2}{m^2} + \frac{a^2\delta_0 n_0''}{m} + \frac{4a^3\delta_0 n_0' n_0''}{3m^2} + \frac{a^4 n_0' n_0''}{3m^3}.$$

On the left-hand side of equation (10), it is sufficient to use the first order approximations of the sine

functions, that is, to put the sines equal to their angles, because the third degree terms on squaring give rise to terms of at least the fourth degree. Thus we get, with the aid of (111),

$$(112) \qquad m^2(\sin^2\delta_a - \sin^2\delta_0) = m^2(\delta_a^2 - \delta_0^2) = 2ma\delta_0 n_0' + a^2 n_0'^2 + ma^2\delta_0^2 n_0'' + \frac{4a^3\delta_0 n_0' n_0''}{3} + \frac{a^4 n_0'^2 n_0''}{3m}.$$

This is the third order approximation of the left-hand side of equation (10).

If we now turn to the right-hand side and use equation (25), it is again advantageous to distinguish sharply between first-and second-degree terms. If we denote them by subscripts 1 and 2, respectively, we can write

$$(113) \qquad n(x_a) = n(x_0) + (x_a - x_0)_1\, n'(x_0) + (x_a - x_0)_2\, n'(x_0) + \frac{1}{2}(x_a - x_0)_1^2\, n''(x_0).$$

Here the first term on the right hand side is of the 0 : th degree, the second is of the second degree, and the third and fourth terms are of the third degree. Hence first-degree terms are not present. When we now have to square this equation, and want to retain only terms of up to the third degree, there only remain the square of the first term and the double products of this term and each of the other three terms :

$$(114) \qquad n^2(x_a) - n^2(x_0) = 2n_0 n_0' \left[a\delta_0 + \frac{a^2 n_0'}{2m} - \frac{a\delta_0(n_0 - m)}{m} - \frac{a^2 n_0'(n_0 - m)}{2m^2} + \frac{a^3\delta_0 n_0''}{6m} + \frac{a^4 n_0' n_0''}{24m^2} \right] + n_0 n_0'' \left(a\delta_0 + \frac{a^2 n_0'}{2m} \right)^2.$$

In this equation we put $n_0 = m + (n_0 - m)$, develop the square, and discard the terms containing the square of $(n_0 - m)$ since they are of the fourth degree. We then obtain

$$(115) \qquad n^2(x_a) - n^2(x_0) = 2ma\delta_0 n_0' + a^2 n'^2 + ma^2\delta_0^2 n_0'' + \frac{4a^3\delta_0 n_0' n_0''}{3} + \frac{a^4 n_0'^2 n_0''}{3m}.$$

Comparison with equation (112) shows that equation (10) is in complete agreement with the second order approximations (25) and (29).

Appendix II. *The aberrations caused by plano-parallel plates.* — In figure 7 there is a plano-parallel plate of thickness t and refractive index m, situated between the planes $z = -t(1 - 1/m)$ and $z = t/m$. The plane through the x axis perpendicular to the plane of the paper is then to be regarded as the Gaussian image plane of the left-hand plane surface of the plate. We will regard a light pencil entering the plate under the entrance angle δ on the z axis. Within the plate, it makes the angle φ with the axis. At B the pencil leaves the plate, and when traced rectilinearly backwards from the exit point we arrive at the point

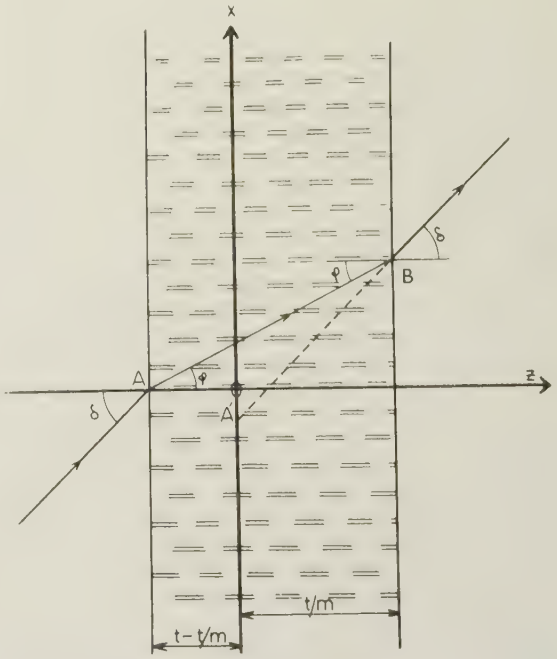

Fig. 7. — Optic effect of a plano-parallel plate. The x axis is the Gaussian image plane of the left-hand surface of the plate of thickness t. The origin, O, is thus the optical image of the point A, and the aberration OA' is calculated in the text, as well as the optical path length between A and A'.

A' in the Gaussian image plane of A. In the first order approximation, the distance $OA' = \Delta x$ is equal to zero, but we will now calculate the third order approximation as a function of δ, m, and t. We will also compute the optical path length between the object A and its image A' as a function of the same variables. This will give us a quantitative measure of the deviations from true Gaussian imagery through plano-parallel plates.

The vertical shift of the Gaussian image. The magnitude of Δx can be taken directly from the figure

$$(116) \qquad \Delta x = t\tan\varphi - \frac{t}{m}\tan\delta$$

and the third-order approximation of Snell's law of refraction is

$$(117) \qquad \varphi = \frac{\delta}{m} - \frac{m^2 - 1}{6m^3}\delta^3.$$

After the tangent functions in (116) have also been developed into their third order approximations,

equation (117) is introduced into it, which gives the following equation :

$$\Delta x = -\frac{m^2-1}{2m^3}\, t\, \delta^3. \tag{118}$$

The step from equation (59) to (60) in the present analysis consisted in the removal of a planoparallel plate of thickness p and refractive index m on the assumption that the imagery through this plate were strictly Gaussian. Equation (118) now gives us the possibility of investigating the order of magnitude of the deviation from Gaussian imagery through such a plate. Since p varies between, say, 50 cm and infinity, this deviation appears, at the first sight, to increase indefinitely on passing over from uncollimated to collimated light. This is incorrect, however, because the two coherent pencils have nearly the same direction. The error that comes into play is thus only the difference in (118) for the two angles δ_0 and δ_1, and we get with the aid of equation (47) (r is put $= 2/3$) :

$$\Delta^2 x = \frac{(m^2-1)\ \delta_0^5 a^2 n'}{4m^4}\ . \tag{119}$$

With the aid of relations given earlier, this can be brought into the form

$$\Delta^2 x = \frac{(m^2-1)\ C^2\ f N^{3/4} \lambda^{3/2}}{4Ba^{1/2}m^{5/2}} \tag{120}$$

and the error has its highest possible value at the critical time, $B = 0.2108$, with $C = -0.5669$, and with $f = 0.3989$. With $N = 25$, $a = 5$ cm, $m = 4/3$, and $\lambda = 5461$ Å, the numerical value of this error is found to be as low as 11.6 Ångström units.

On the camera side of the cell, we have to take into account the second cell wall and, possibly, a thermostat window and a certain thickness of thermostat water. The optical imagery through these plano-parallel plates has also been assumed to be Gaussian. We can assume the added thickness to be less than 10 cm of water, and the two angles we have to deal with are δ_1 for the one and $\delta_0 + an'$ for the other pencil. One easily finds that this error is of the same order of magnitude as that on the light source side of the cell.

The error in optical path length. The optical path length from A to A′ in figure 7 is given by the equation

$$S = \frac{m\, t}{\cos \varphi} - \frac{t}{m \cos \delta}\ . \tag{121}$$

The cosine functions here have to be approximated to the fourth degree :

$$1/\cos x = 1 + x^2/2 + 5\, x^4/24.$$

We then obtain, with the aid of (118),

$$S = \frac{t\,(m^2-1)}{m}\left(1 - \frac{3\delta^4}{8m^2}\right). \tag{122}$$

Here again, we are only concerned with the difference in path length for the two pencils. Hence we have, on the light source side of the cell, with $t = p$, and the angles equal to δ_0 and δ_1 :

$$\Delta S = \frac{(m^2-1)\ \delta_0^3 a^2 n'}{4m^4}\ . \tag{123}$$

Comparison with equation (119) reveals that this error is still one order of magnitude smaller, consequently far below the measurable range.

REFERENCES

[1] H. Svensson, *Opt. Acta*, **1**, 1954, p. 25.
[2] O. Wiener, *Ann. Phys. Chem.*, N. F., **49**, 1893, p. 105.
[3] R. Forsberg and H. Svensson, *Opt. Acta*, **1**, 1954, p. 90.
[4] L. G. Longsworth, personal communication (1945).
[5] H. Svensson, *Kolloid-Z.*, **90**, 1940, p. 141.
[6] H. Svensson, *Ark. Kem. Mineral. Geol.*, **22A**, 1946, No. 10.
[7] G. Kegeles and L. J. Gosting, *J. Am. Chem. Soc.*, **69**, 1947, p. 2516.
[8] L. G. Longsworth, *J. Am. Chem. Soc.*, **69**, 1947, p. 2510.
[9] C. A. Coulson *et al.*, *Proc. Roy. Soc.* **A 192**, 1948, p. 382.
[10] F. T. Adler and C. H. Blanchard, *J. Phys. Coll. Chem.*, **53**, 1949, p. 803.
[11] L. J. Gosting and L. Onsager, *J. Am. Chem. Soc.*, **74**, 1952, p. 6066.
[12] G. Vallet, *Mém. Serv. chim. de l'Etat*, **33**, 1947, p. 247.
[13] H. Svensson, *Acta Chem. Scand.*, **4**, 1950, p. 1329.
[14] H. Svensson, R. Forsberg, and L. A. Lindström, *Acta Chem. Scand.*, **7**, 1953, p. 159.
[15] E. Ingelstam, *Arkiv Fysik*, **9**, 1955, p. 197.
[16] Th. E. Thompson, personal communication (1955).

Manuscrit reçu le 5 juin 1956.

The determination of the absorption coefficient of luminescent microcrystals

Gy. Gergely
Research Institute for Telecommunication, Budapest, Hungary.

Summary. — *The absorption and luminescence emission of single Zn-type microcrystals was investigated. A photoelectric microscope photometer was built which consists of a* Zeiss *microscope and a* 931 *A multiplier phototube. Evaluating the results of absorption measurements, neither a plane-parallel, nor a spherical crystal model furnished reliable results for the absorption coefficient. The application of an empirical model, based on the non-absorbed radiation (*5 770 Å*) made possible the determination of the ultraviolet absorption coefficient by comparing the transmission of single microcrystals for different wavelengths. The method was experimentally checked on* $K_2Cr_2O_7$ *crystals. The ultraviolet absorption coefficient of luminescent microcrystals may also be determined from the dependence of the light emission on the particle size.*

Sommaire. — *On étudie ici l'absorption et l'émission luminescente d'un microcristal simple de Zn-type. Un microphotomètre photoélectrique a été construit dans ce but, à partir d'un microscope* Zeiss *et d'une cellule photomultiplicatrice* 931 *A. L'interprétation des mesures d'absorption n'a donné de résultats valables ni pour un cristal plan parallèle ni pour un cristal sphérique. L'utilisation d'un modèle empirique, basé sur la radiation non absorbée* (5 770 Å) *a rendu possible la détermination de coefficient d'absorption de l'ultraviolet, par comparaison avec la transmission de quelques microcristaux pour différentes longueurs d'onde. La méthode a été appliquée expérimentalement pour des cristaux de* $K_2Cr_2O_7$. *Le coefficient d'absorption de l'ultraviolet de microcristaux luminescents peut aussi être déterminé en relation avec l'émission lumineuse de la particule.*

Zusammenfassung. — *Die Absorption und Lumineszenzstrahlung eines einzelnen Mikrokristalls vom Zn-Typ wurde untersucht. Hierzu wurde ein elektrisches Mikrophotometer aus einem* Zeiss-*Mikroskop und einem Multiplier* 931 *A zusammengestellt. Bei der Auswertung der Absorptionsmessungen ergeben sich aber weder für eine planparallele Platte noch für einen sphärischen Modellkristall zuverlässige Werte des Absorptionskoeffizienten. Erst die Verwendung eines empirischen Modelles, das von der nicht absorbierten Strahlung* (5 770 Å) *ausgeht, machte es möglich, den Absorptionskoeffizienten im Ultraviolett zu bestimmen, indem man die Durchlässigkeit einzelner Mikrokristalle für verschiedene Wellenlängen vergleicht. Die Methode wurde experimentell an* $K_2Cr_2O_7$*-Kristallen erprobt. Der Absorptionskoeffizient im Ultraviolett kann bei einem lumineszierenden Mikrokristall auch aus der Abhängigkeit der Lichtemission von der Teilchengrösse ermittelt werden.*

A considerable proportion of luminescent materials are microcrystals of 1-30-100 micron particle size. In view of this, the absorption coefficient cannot be determined by the simple method as in the case of macroscopic crystals. Although the problem is a classical one, its solution has only recently been achieved. The coefficient of absorption is sometimes determined by statistical methods, from the coefficient of diffuse reflection, as it was described by Bodo [1], Johnson [2] and Antonov-Romanovsky [3], or by the microscopic method, developed by Brumberg and Pekerman [4].

We do not wish to give a detailed discussion of the different methods, but some difficulties of the statistical method must be mentioned. Everybody using statistical methods has employed models essentially simpler than reality (plane-parallel crystals). The absorption coefficient has been expressed in involved formulae, and the formulae — excepted Bodo's — had an unknown parameter, i. e., the refractive index. The formulae also had a term, μl, product of the absorption coefficient μ and the light path l. The latter corresponds to the particle size only in exceptional cases. For the most part, the light rays are repeatedly totally reflected within the crystal [3]. For this reason, statistical methods give a smaller value for μ than the real one.

Besides the theoretical difficulties, there is a practical difficulty, too : the measurements of the diffuse reflectance must be carried out on samples having homogeneous particle size. In practice, the homogeneous fractions are produced by sedimentation [1] and a considerable quantity of material (50-100 g) is necessary for this purpose. A further difficulty lies in the fact that repeated sedimentations cause surface deterioration, and darken the ZnS type crystals. The darkening strongly affects the diffuse reflection.

The advantage of the statistical methods lies in the simplicity of the reflection measurements. Although the microscopic method is experimentally more difficult, its use is justified by its advantages. The microscopic method was first employed by Brumberg and Pekerman [4]. They used a quartz microscope spectrograph for the determination of absorption spectra of microcrystals. They photographed the light transmitted by selected plane-parallel crystal samples. The original Brumberg-Pekerman method offers some difficulties. It can only be applied for strictly plane-parallel crystals, whereas, the ZnS type microcrystals have approximately spherical or ellipsoidal shape. Brumberg and Pekerman measured the absorption spectra only up to 4 000-4 500 Å. Otherwise, the photographic procedure is not possible.

To eliminate the difficulties of the original Brumberg-Pekerman method, a photoelectric microscope photometer and a new evaluation of the experimental results was developed.

Experimental arrangement. — Figure 1 shows the experimental arrangement. The radiation of a high pressure 125 W mercury lamp is projected on the microcrystal to be examined by means of a mirror and

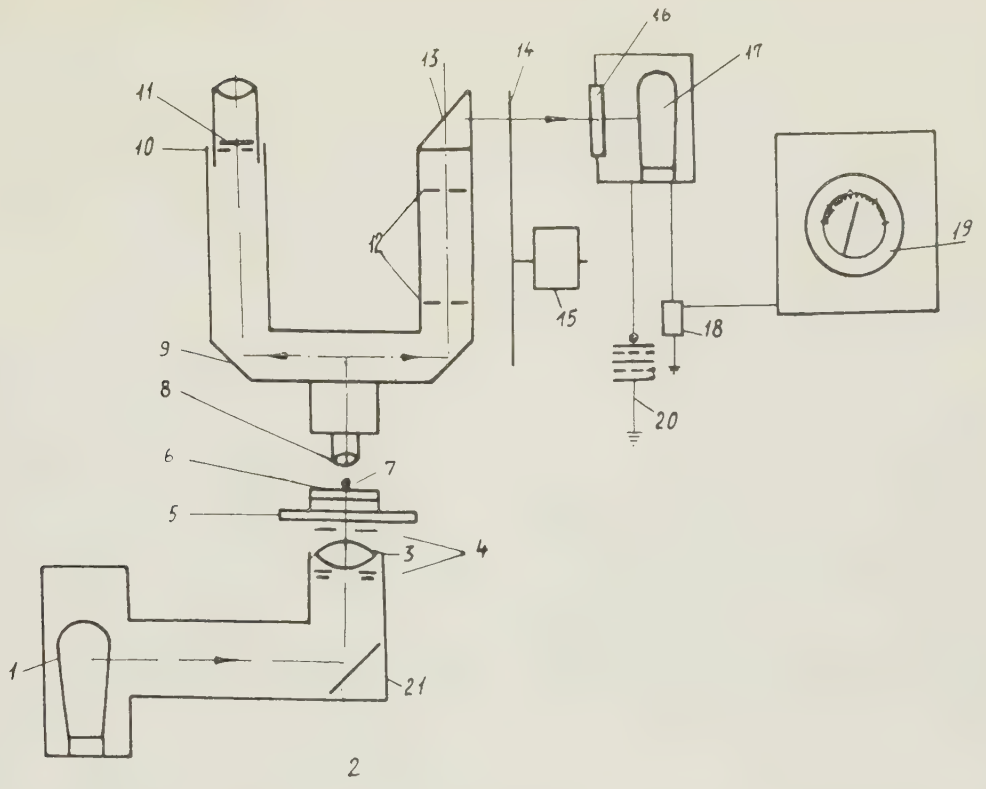

FIG. 1. — Experimental arrangement. Notation on the figure : 1, mercury lamp ; 2, mirror ; 3, condenser lens ; 4, diaphragms ; 5, microscope stage ; 6, slide ; 7, microcrystal ; 8, objective ; 9, binocular attachment ; 10, eyepiece ; 11, eyepiece micrometer ; 12, diaphragms ; 13, prism ; 14, light modulating sector ; 15, motor ; 16, filter ; 17, multiplier phototube ; 18, load resistance ; 19, electronic voltmeter ; 20, high voltage supply.

a condenser. The light rays are limited by suitable diaphragms. The microcrystals are sedimented on a glass slide and immersed in vaseline oil.

Light leaving the crystal is collected by the objective. The microscope has a binocular attachment, dividing the light into two separate beams ; the image of the crystal is observed by the left eyepiece provided with an ocular micrometer, in order to determine the particle size and to adjust the object on the optical axis.

A real image of the object is produced on the cathode of a multiplier phototube by the right-hand beam, diaphragms being provided to eliminate stray light. The upper diaphragm selects a 4.5 micron diameter part of the microcrystal on the image, so that light from a small area only of a larger (10-40 micron) crystal reaches the photocathode.

The multiplier phototube was a selected sample of type 931 A. The light entering the photocell was modulated by a rotating sector. The photocurrent produced an alternating voltage on the load resistance, measured by an electronic voltmeter. The photocell was combined with suitable optical filters (SHOTT interference, SCHOTT Glass, Jena).

The total magnification of the optical system was 160.

Since a quartz microscope was not available, measurements were carried out only up to 3 650 Å.

The measurements were performed as follows : the individual microcrystals were introduced onto the optical axis. Using different optical filters, the radiation escaping both from the single crystals and from the " background " was measured. The intensity of the " background " radiation is equal to the radiation reaching the crystals. The measurements were carried out with many single crystals of different sizes.

The evaluation of the experimental results. — The photoelectric microscope photometer furnishes the following data : the particle size of the individual crystals, the intensity of radiation leaving the crystal and the intensity of the " background " radiation. The 3 650, 4 046-78, 4 358, 5 460 and 5 770-90 Å mercury lines were sufficiently intense to be detected despite of the very strong attenuation in the optical system.

To evaluate the experimental data, three different models have been considered.

a) *The plane-parallel model.* — The plane-parallel crystal model was first used by BODO in his statistical method. Although good results were obtained by the statistical method, the plane-parallel model cannot be

used in case of individual crystals, because their shape differs considerably from this form and absorption measurements on single crystals an incompatible with the plane-parallel model. ZnS microcrystals have negligible absorption of the 5 460 and 5 770 Å mercury lines [7]. In the case of non-absorbed radiation, the transmission of a single crystal would be given by :

$$T = \frac{1-\alpha}{1+\alpha}, \quad \alpha = \left(\frac{n-1}{n+1}\right)^2$$

where n is the refractive index. For ZnS crystals immersed in vaseline oil, $n \cong 1.5$, giving

$$T \cong 0.92$$

independently of the particle size. The experiments disproved this supposition.

b) *The spherical model.* — Antonov-Romanovsky used the spherical crystal model in his statistical method. Examining ZnS type microcrystals by the microscope, their shape was found to be approximately spherical or ellipsoidal. When parallel radiation reaches a spherical crystal, the particle acts as a spherical lens. Mecke [5], Blumer [6] and others discussed the optical properties of spherical particles. Their problems, in some aspects, differed of those presented by our work. Using the optical system of figure 1, the rays leaving an area of 4.5 micron diameter of the object reach the photocathode. Figure 2 shows the ray traces within the spherical crystal. The radiation transmitted by a spherical crystal was calculated by integrating the Fresnel-formulae on the surface of the sphere. The calculations are of interest for non-absorbed radiation, because they can be checked experimentally. It was found that the transmission of a spherical particle is given by :

$$T = G(l)\, l^2$$

denoting by l the diameter of the sphere. $G(l)$ is a complicated integral based on the Fresnel-formulae.

The results of experiments did not agree with the theoretical calculations. The light collecting effect of a spherical crystal predicted by calculations was found to exist qualitatively, but its magnitude was less than the calculated values. No pronounced correlation was found between l^2 and the transmission of the crystals. The discrepancies between theory and experiment may be explained by small deviations from the ideal spherical shape and by the sub-microscopic roughness of the crystal surfaces. The calculations are valid only for optically polished spherical surfaces.

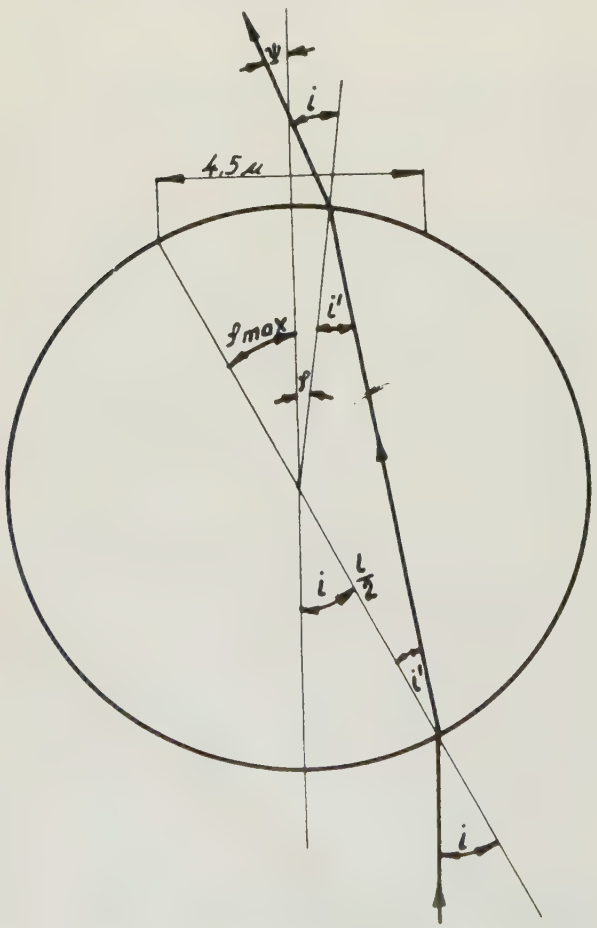

Fig. 2. — Ray tracing in a spherical crystal.

c) *The empirical model.* — The use of non-absorbed radiation makes possible the determination of the ultraviolet absorption coefficient in the following manner. When a crystal was irradiated by non-absorbed radiation, it either collected the light rays because of its spherical lens properties, or else scattered them because of its irregular shape. Denoting by I_0 the intensity of the background radiation, and by I the intensity escaping from the crystal, the quantity f_s is the empirically determined shape factor of the particle :

$$f_s = I/I_0 \ .$$

The quantity f_s may be supposed to depend on the shape, size and surface of the crystal. It may be assumed that it does not vary with the wavelength ; this is only an approximation, since f_s depends on the refractive index and consequently on the wavelength. The small size of the particle (10-40 microns) permits the approximation.

In the case of absorbed radiation, the intensity leaving the crystal and reaching the photocell, is given by

$$I_\lambda = I_{0\lambda}\, f_s\, \mathrm{e}^{-\mu l}$$

l is the light path in the crystal. Because of the approximate spherical shape, l was taken equal to the diameter. In the case of particles of ellipsoidal form, l was taken equal to the smaller diameter of the crystal. Crystals deviating strongly from spherical or ellipsoidal shape were excluded from the measurements.

Table I shows the experimental results for a 90 ZnS-10 CdS-Cu phosphor. It may be seen that the absorption coefficients determined on different crystals have the same magnitudes. Table I contains f_s for two wave

TABLE I

l	f_0 5770-90 Å	f_0 5460 Å	μ (3650)	μ (4060)	μ (4358)
13.5	1.31	1.17	627	137	107
13.5	1.55	1.58	583	334	178
14.9	1.19	1.28	678	235	114
14.9	1.32	1.44	*277*	124	124
14.9	0.97	0.94	624	218	168
15.6	1.33	1.27	640	250	157
15.6	1.17	1.09	782	286	308
16.9	0.885	0.885	438	*93*	77
16.9	0.72	0.735	418	172	77
17.6	1.64	1.88	765	762	131
18.2	0.815	0.790	335	256	*49*
20.3	1.56	1.78	582	221	160
20.3	1.41	1.68	*313*	191	*40*
21.6	2.11	2.41	540	192	88
21.6	0.483	0.500	304	172	*40*
22.3	1.3	1.12	502	238	73
23.6	0.548	0.585	*242*	*89*	*54*
23.6	1.39	1.13	402	191	144
25	0.94	1.0	496	214	69
27	1.96	1.78	395	158	121
30.4	0.84	0.77	*291*	*95*	84
33.8	0.736	0.743	328	*58*	*43*
$\overline{\mu}$			478	195	110
μ			292	84	45

lengths (5 460-5 470 Å), showing good agreement. The differences in the values of μ may be caused by several factors. The uncertainty in the l-determination (the thickness of the crystals has been supposed to be equal to the horizontal diameter) ; neglecting the change of refractive index with the wavelength may also cause an error ; the interference effects, too, are neglected ; they are dependent on the wavelength. The most important factor is the real path of light within the crystal. This problem was mentioned also by [ANTONOV-ROMANOVSKY [3] who distinguished the perfectly regular shaped crystals from the irregular ones. Through a perfectly regular-shaped crystal, e.g., a sphere or a cube, the light passes without internal total reflection, while in an irregular shaped crystal rays passing through are repeatedly totally reflected. The true value of the absorption coefficient is not the average value calculated from the measurements, $\overline{\mu}$, but their minimum value. It may be assumed that the minimum values are those found for crystals through which the radiation passes only once. This corresponds to the perfectly regular-shaped particles. The true value of μ cannot be furnished by any statistical method. Single microcrystals examined for brightness justify this supposition.

The microscope photometer and the empirical model of evaluation were experimentally checked on $K_2Cr_2O_7$

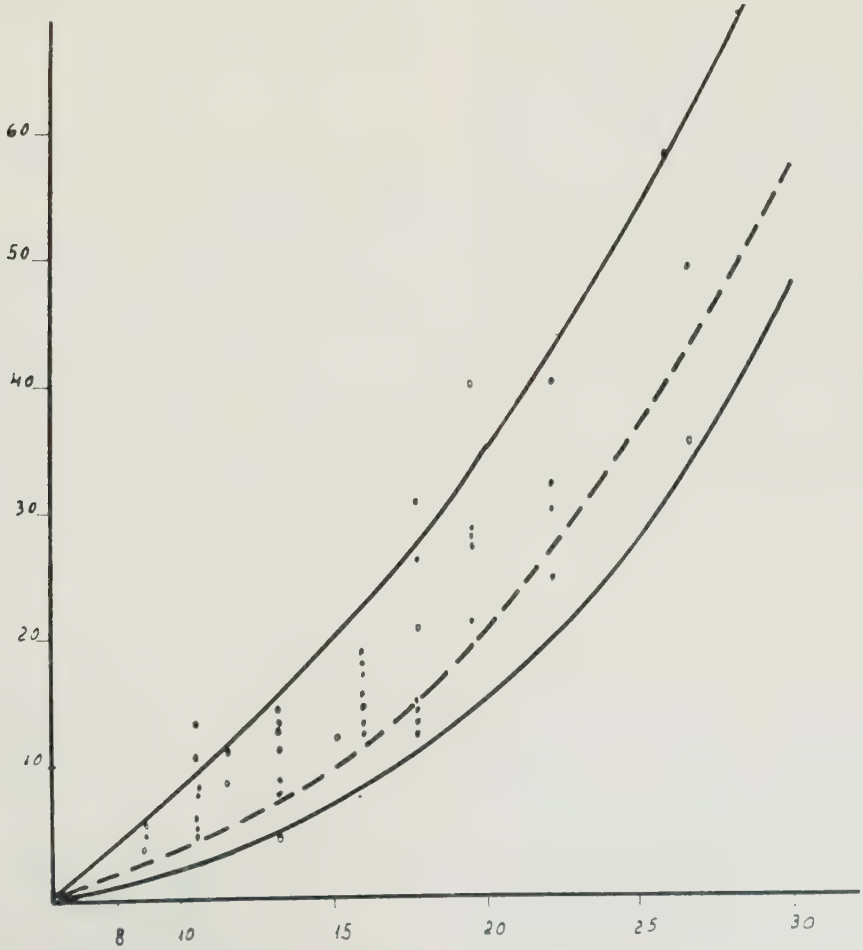

FIG. 3. — The light emission of microcrystals of different particle size.

crystals. A very good agreement was found for the 5 460 Å absorption coefficient determined for microcrystals and large crystals.

Relation between light emission and absorption of luminescent microcrystals. — In 1950, BODO [1] examined the surface brightness of halophosphate microcrystals under 2 537 Å excitation by a visual method. He found a relation between the average surface brightness and the ultraviolet absorption of the crystals.

A slight modification of the experimental arrangement of figure 1 makes possible the measurement of the light emission of single crystals. Figure 3 shows the results of measurements with the 90 ZnS-10 CdS-Cu sample. The light emission increases with increasing particle size, but no continuous curve has been found ; the experimental points are situated in an area limited by two curves. The upper limiting curve may be described by the equation :

$$I = kl^2$$

k being a constant. The lower curve is :

$$I = k(l^2/l - \mathbf{e}^{-\mu l})$$

In this equation μ is equal to the minimum value of the 3 650 Å absorption coefficient, determined by the microscope-photometer. The upper limiting curve corresponds to the irregular shaped crystals. The light emission is proportional to the absorbed ultraviolet energy. Ultraviolet radiation is practically perfectly absorbed in consequence of multiple internal total reflections. The absorbed energy is proportional to the crystal surface, l^2. The lower limiting curve on figure 3 represents the case of perfectly regular shaped crystals. In practice, the majority of the crystals fall between the two limiting cases. Using $\bar{\mu}$ in the formula gives the dotted line in figure 3, corresponding to the average absorption.

Experimental results. — Table II contains the absorption coefficients for some ZnS-type materials. The crystals examined were prepared by I. HANGOS and Mrs K. TOTH.

TABLE II

Specimen	3650 Å		4060 Å		4358 Å	
	$\bar{\mu}$	μ	$\bar{\mu}$	μ	$\bar{\mu}$	μ
hex. ZnS-Ag sample 1 ...	372	120				
hex. ZnS-Ag sample 2 ...	538	148				
hex. ZnS-Ag sample 3 ...	397	124				
hex. ZnS sample 3 without Ag	340	57.3				
cub. ZnS-Ag	364	139				
hex. ZnS Cu	423	220	144	77	65	13
hex. 90 ZnS-10CdS-Cu...	478	292	195	84	110	45
hex. 50 ZnS-50CdS-Ag ...	843	636	740	555	131	80

Reflectivity of microcrystals. — A modification of the optical arrangement of figure 1 (vertical illumination) made reflectivity measurements on single microcrystals possible. From the reflectivity data, the refractive index could be estimated.

A full description of the apparatus, the experimental methods, the optical properties of spherical microcrystal and detailed data on ZnS-type microcrystals will be given in the *Acta Phys. Hung.*

Acknowledgement. — The author wishes to express his thanks to his co-workers, J. ADAM, I. HANGOS and Mrs K. TOTH.

REFERENCES

[1] Z. BODO, *Acta Phys. Hung.*, **1**, 1951, p. 135.
[2] P. P. JOHNSON, *J. O. S. A.*, **42**, 1952, p. 978.
[3] V. V. ANTONOV-ROMANOVSKY, *J. Exp. i. Teor. Phys*, **26**, 1954, p. 459.
[4] E. M. BRUMBERG, F. M. PEKERMAN, *Dokl. Akad. Nauk.*, **61**, 1948, p. 43 ; *Izv. Akad. Nauk. Ser. Phys.*, **13**, 1949, p. 218.
[5] R. MECKE, *Ann. Phys.*, Leipzig, **61**, 1920, p. 623.
[6] H. BLUMER, *Z. f. Phys.*, **38**, 1926, p. 920.
[7] S. J. CZYZAK, D. C. REYNOLDS, R. C. ALLEN, C. C. REYNOLDS, *J. O. S. A.*, **44**, 1954, p. 864.

Manuscrit reçu le 18 mai 1956.

The dependence of the human electroretinogram on the shape of the stimulus as a function of time *

Lucia RONCHI and Silvano GRAZI
Istituto Nazionale di Ottica, Arcetri, Firenze (Italie).

SUMMARY. — *The human electroretinogram has been studied for various time-gradients of illumination of the retina, using an intense white stimulus, for both a light and dark adapted eye. In general the cone response appears to be masked by rod activity. By varying the time of rise of the stimulus between 1 and 70 msec no remarkable variations in the ERG are evident. On the other hand, when the time of rise ranges from 70 to 600 msec remarkable changes in both shape and size occur, and the latency time increases.*

SOMMAIRE. — *L'électrorétinogramme (ERG) a été étudié pour différents gradients temporels d'éclairement sur la rétine de l'œil humain, éclairé par une lumière blanche intense, adapté à l'obscurité ou non. La variation du temps d'établissement du stimulus entre 1 et 70 msec, n'a pas apporté de changement notable dans l'ERG.*

D'autre part, quand ce temps passe de 70 à 600 msec, des changements remarquables se produisent dans la forme et la grandeur de l'ERG, et la latence augmente.

ZUSAMMENFASSUNG. — *Das Elecktro-Retinogramm wurde für das menschliche Auge bei Hell- und Dunkeladaptation untersucht, wenn bei einem starken weissen Reiz verschieden schnelle zeitliche Anderungen der Beleuchtungsstärke auf der Netzhaut benutzt*

(*) This research has been made possible through the support and sponsorship of the Air Research and Development Command, United States Air Force, between its European Office and the Istituto Nazionale di Ottica under contract N° AF61 (514)-634 C.

werden. Bei zeitlichen Änderungen der Reizzunahme zwischen 1 und 70 msec. ist kein Unterschied in den Elektro-retinogramm zu bemerken. Wenn aber die Zeit für das Anwachsen des Reizes zwischen 70 und 600 msec. liegt, so ergeben sich beträtliche Abweichungen in Form und Grösse und die Latenzzeit wächst an.

Introduction. — The electroretinogram (ERG), represents the only measurable objective index of what takes place in the retina in response to change in illumination [1]. The " changes in illumination " are usually realized by means of a light stimulus the form of which is a very complicated function of time. In a simple case, the curve presents four angular points, A, B, C, D, as represented in figure 1.

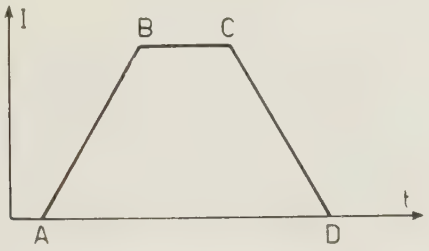

FIG. 1. — A simple light stimulus (intensity as a function of time).

It is conceivable that if the duration of the stimulus is sufficient, we may obtain two well-separated responses both at the beginning and at the end of the light stimulus (the so called on-effect and off-effect respectively). Also it is conceivable that the on-effect is a response depending on the variation A only, provided the slope of the segment AB is suitable.

These problems involve the study of two factors influencing the ERG : the total duration of illumination and the shape of the light stimulus. The former was taken into account for the first time by DE HAAS in 1903 [2], and until WIRTH [3] few authors have attempted a similar investigation. On the other hand, the shape of the stimulus as a factor has never been examined, so far as we know.

We have undertaken a program of research beginning with very simple light stimuli, containing only the first two variations A, B represented in figure 1, i.e., we used time gradients of illumination (fig. 2) and our aim was to examine how the ERG is influenced by varying the slope of the gradient.

Our research originated at the suggestion of Professor TORALDO who pointed out similarities in the

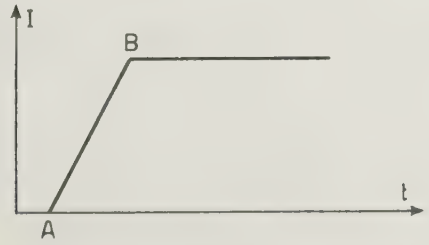

FIG. 2. — Time gradient of illumination (intensity as a function of time).

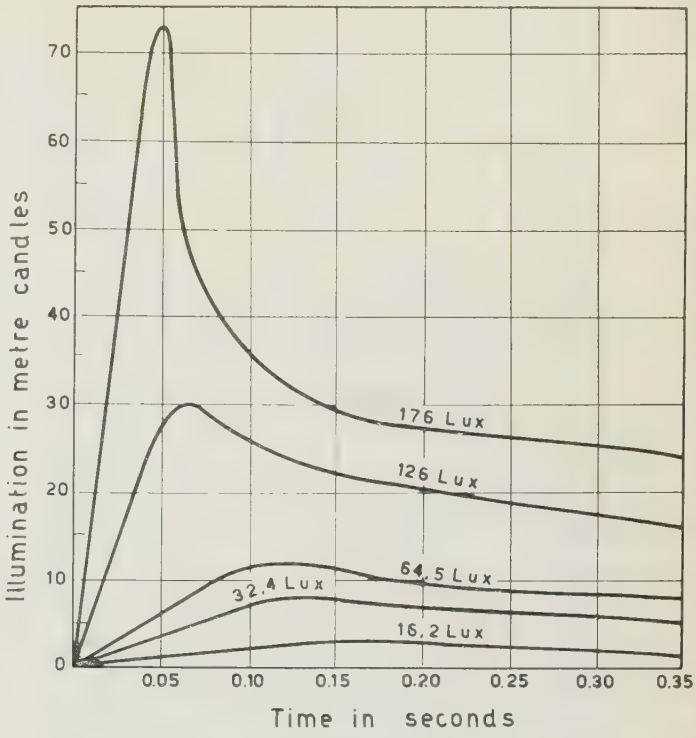

FIG. 3. — The development of the visual response during stimulation with white light (BROCA and SULZER).

results of widely different experiments, observed by some authors. For instance, in 1945, WRIGHT [4] said that " the general similarity between the curves representing the BROCA-SULZER phenomenon (fig. 3) and the early part of the ERG should be noted ". On the other hand, TORALDO (personal communication) notes the similarity between the early part of the ERG and the behaviour of the differential threshold in a field with a spatial gradient of illumination [5] (see fig. 4). The connecting link between the spatial and temporal phenomena is assumed to be in the small involuntary movements of the eye.

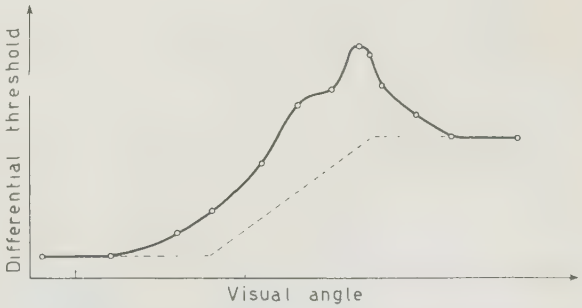

FIG. 4. — The differential threshold (full line) measured on a field with a gradient of luminance (broken line); the abscissae are the visual angles measured from the centre point of the field (FIORENTINI).

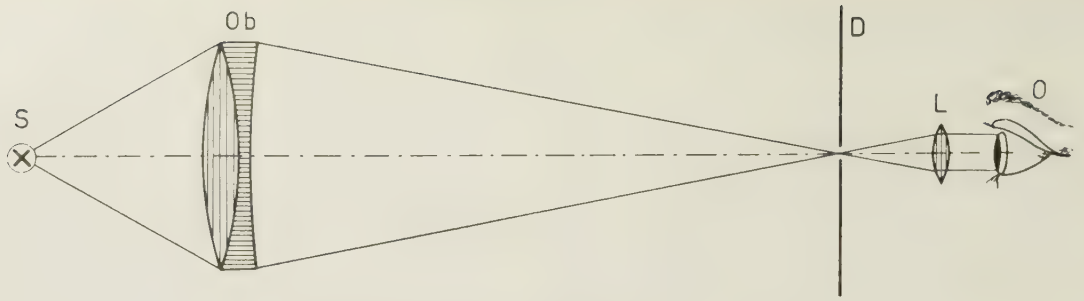

Fig. 5. — Stimulating system (for significance of symbols see text).

The crucial point is the comparison between the subjective response and the objective response (ERG). A more specific connection might be derived by considering the relation between the b-wave and the rise in frequency of the optic nerve discharge. (Such an analysis would necessarily assume a similarity in behaviour of the nerve fibres of cold- and warm-blooded animals). This rise in frequency is similar to the rise in the sensation of brightness in man (Broca and Sulzer effect) [6]. We hope that the research which we have begun will be a contribution to the question " how is the form of the stimulus connected with the form of the ERG ? " ; in other words, our purpose consists in clarifying under what conditions the eye gives an electrical response which is independent of the energy-time distribution of the light stimulus, and under what conditions, on the other hand, the ERG is influenced by the energy-time distribution.

1. **Apparatus.** — The apparatus used in the study of the electroretinograms consists of two main parts ; one of these, a stimulating system, is used to deliver time gradients of illumination to the eye and the other, a recording system, is used to trace the electrical response.

Stimulating system. — Figure 5 provides a view of the principal elements of this system ; an objective Ob forms at D the image of a 6 amp., 6 volts ribbon filament lamp, and the lens L, placed close to the eye, projects the image to infinity, and images the aperture of Ob at the eye pupil.

The observer's eye views the filament through L ; the diameter of the light beam entering the eye pupil does not exceed three millimeters. Great care is therefore required in order to assure immobility of the observer's position. Fixing the head is by the usual dental impression method. The observer is further helped in avoiding voluntary eye movements by a dim red fixation point placed at the centre of the screen D.

The stimulus has the form shown in figure 2 ; as can be seen, the exposure time is not limited. A slotted plate guided by vertical rails falls under gravity from a given height and allows a linear time gradient of illumination to be realised. The time of rise t_0 of the light stimulus depends on the drop-height ; the rising of illumination is linear if the aperture of Ob has a particular form, which depends also on the drop-height.

This method has been adopted for t_0 ranging from 1 to 60 msec. For obtaining values of t_0 greater than 60 msec., the aperture of Ob is made rectangular and its size is independent of t_0 ; the falling plate is driven by a synchronous motor, whose speed may be varied.

Recording system. — A block diagram of the recording system is shown in figure 6. Electrical potentials are recorded between an active electrode mounted in the corneal bulge of a contact lens and an indifferent electrode worn on the forehead. Signals picked up by these electrodes are taken to a capacitance-coupled amplifier, the output of which is connected to a cathode ray oscilloscope. Permanent records are made by pho-

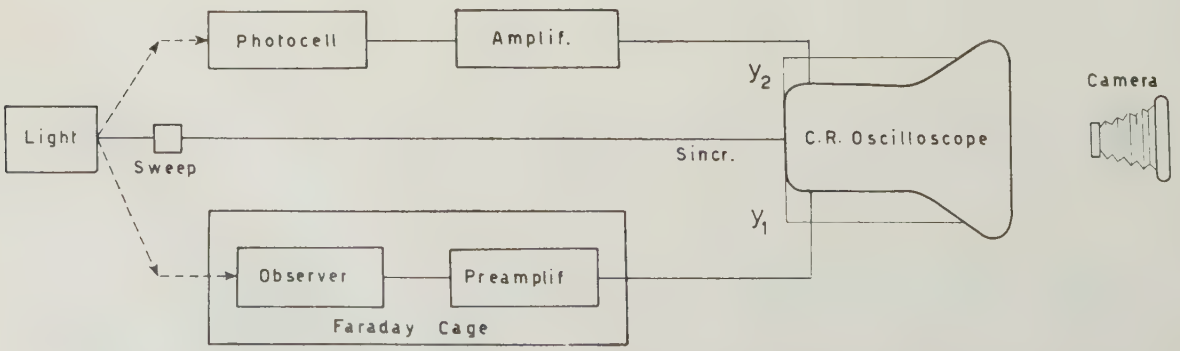

Fig. 6. — Block diagram of the recording system.

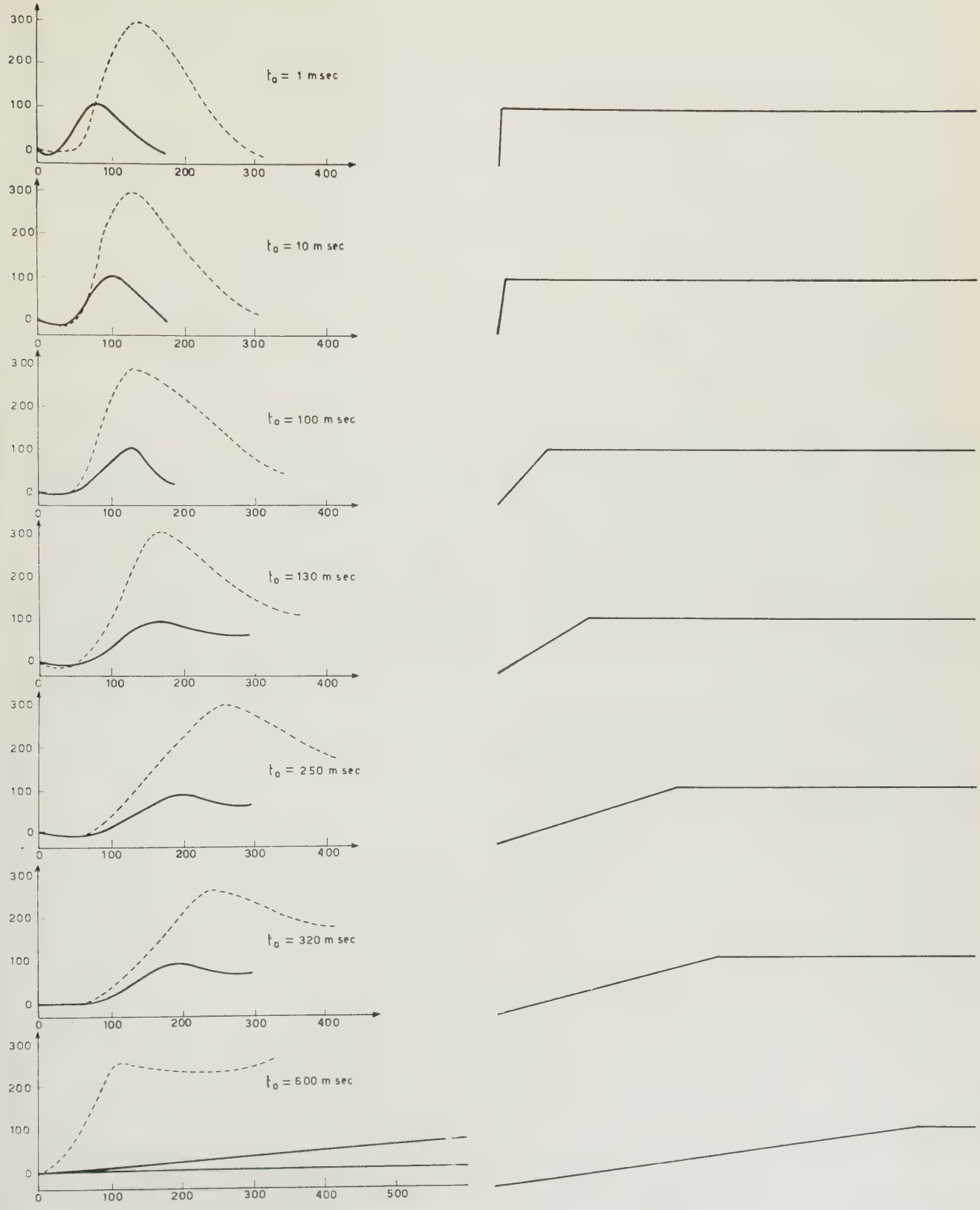

FIG. 7. — Left : average records obtained by one observer (S. G.) ; the full line refers to light adaptation, the broken line to dark adaptation. The time of rise t_0 of the stimulus is indicated in each figure. Right : the form of the light stimuli.

tographing the trace on the oscilloscope. The gain of the amplifier may be varied from 600 to 1 000.

The sweep is provided externally ; it consists of a microswitch placed conveniently on the vertical rails ; the falling plate acting on the microswitch provides the current necessary for the displacement of the spot along the time axis.

Besides the channel providing a complete record of all activity appearing between the electrodes, another channel has been used in order to provide a complete record of the form of the light stimulus. This channel is also capacitance coupled and is fed from a photocell which receives a part of the light stimulus by reflection from a mirror placed on the screen D shown in figure 5.

2. **Procedure.** — During an experimental session, the subject sits in a Faraday cage and first dark or light-adapts for fifteen minutes. When dark-adaptation is required, no light passes through the walls of the screened cage, but when light adaptation is required, the walls are diffusely illuminated at a given level.

A few seconds before a test-stimulus is to be administered, the experimenter signals the observer, who moves his eye to the central fixation point, the other eye being covered. After the stimulation, the eye is again light or dark-adapted as required. The stimuli are administered at five minute intervals.

The angular aperture of the beam entering the eye pupil is nearly one degree. The illumination at the eye is 100 lux during stimulation, 15 lux during light-adaptation. Two normal observers took part in these experiments. The contact lenses were produced by Firm " Opticon " in Milan.

3. **Results.** — The experimental results given by observer S. G. are represented in figures 7 to 11. The total number of responses examined was 834. Figure 7 shows the average of the responses obtained for the times of rise of the stimulus, t_0, indicated for each curve. The broken line refers to dark-adaptation (d.a.), the full line to light adaptation (l.a.) corresponding to an illumination at the eye of 15 lux. The form of each light stimulus is represented at the right of the corresponding response.

From the figures we see that when the rate of rise of the stimulus decreases, the rate of rise of the response (b-wave) decreases also. After the peak, when t_0 is large, there is no return to the base line, and we could suggest, perhaps, the presence of another component of the b-wave.

In addition, a curious effect has been noticed ; for a given value of t_0 greater than 150 msec., we obtained many unfamiliar responses, consisting for instance of two or more subsequent b-waves. In the last curve of figure 7 we see for instance that, in light adaptation, the response may consist either of a slow rise of potential, or in a line parallel to the time axis.

In figure 8 the height of the b-wave is plotted against t_0. In figure 9 the rate of rise s_b of the b-wave is plotted against t_0, and figure 10 represents the behaviour of s_b as a function of log $1/t_0$. It is evident that $1/t_0$ represents the rate of rise of the light stimulus, if l expresses the luminous level in arbitrary units. In figure 11 the latency time of the b-wave is plotted against t_0.

Let us consider now the other observer L. R., from whom about 100 records have been obtained in the light adapted state. These results seem in general agreement with those of S. G. However we may note the following differences : the heights of the b-wave are nearly 40 % greater, and the latency times nearly 50 % less than in the records of the first observer. Besides, for L. R., a number of small waves are detected superimposed on the b-wave. Figure 12 shows three records each referred to the value of t_0 indicated on the right.

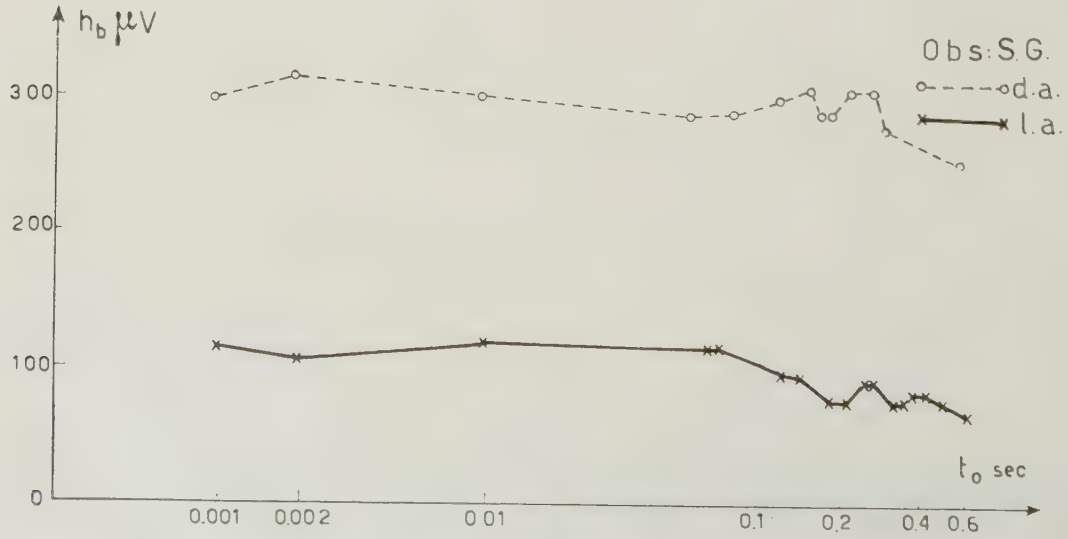

Fig. 8. — The height of the b-wave, in μV, is plotted against t_0, the time of rise of the stimulus, expressed in seconds. Observer S. G. (d. a., dark adaptation ; l. a., light adaptation).

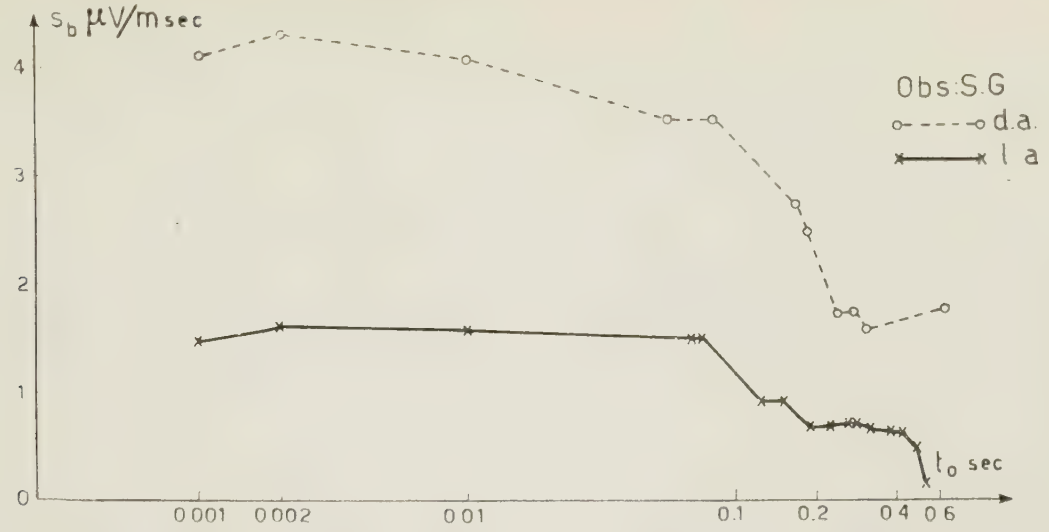

FIG. 9. — The slope of the b-wave is plotted against t_0, the time of rise of the stimulus, expressed in seconds.

4. **Discussion.** — We may attribute the above mentioned differences in the form of the response to a given light stimulus to disturbances such as fatigue due to prolonged fixation. However, we read in GRANIT [7] : " ... Sometimes much to the experimenter's surprise, two quite different responses to the same stimulus may alternate, or even appear or disappear, according to no obvious rule... The eye seems to remain in excellent condition during the experiment and shows no sign of fatigue ". In his opinion, the erratic behaviour of the component PII (responsible for the b-wave) must account for a phenomenon similar to the rotation activity among the elements participating in the nerve discharge. In other words, these experiments suggest that the retinal elements which respond to light with the reaction PII do not all behave alike ; PII therefore shows a certain degree of complexity. Although these effects are very frequent at low intensities, they cannot be excluded at high intensities. Analogously we consider that in our case the above effect is very frequent for large values of t_0, but sometimes it has been observed also for small values of t_0.

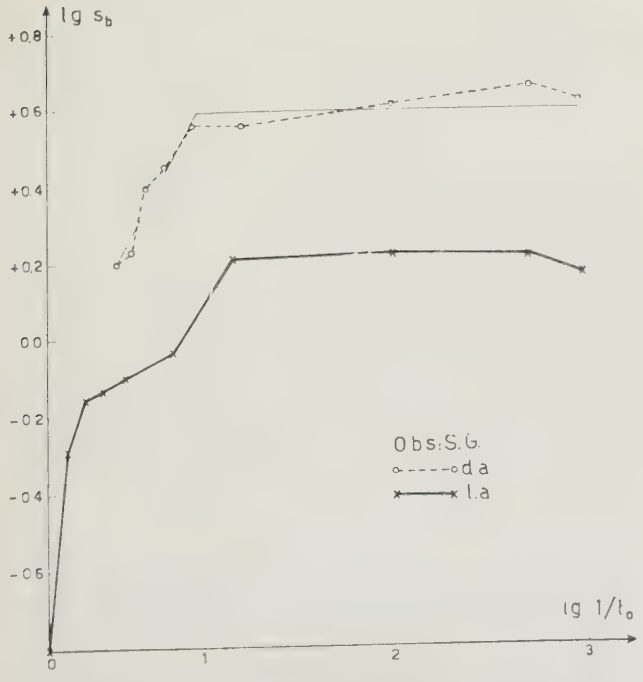

FIG. 10. — The decimal logarithm of the slope of the b-wave is plotted against the logarithm of the slope of the light stimulus.

By examining our records, we notice that for t_0 less than 70 msec., the b-wave starts before the " plateau " in the light stimulus is reached. On the other hand, for t_0 greater than 70 msec., the response seems to be due to both variations of illumination A and B (fig. 2) occurring in the stimulus. For times of rise of the stimulus ranging between 1 and 70 msec., the response of the eye seems not to be influenced by variations of t_0 ; on the other hand, when t_0 is greater than 70 msec., the height and the rate of rise of the b-wave decrease, and the latency time increases ; but the decrease of the rate of rise is more pronounced than that of the height.

Let us consider now figure 10 ; the curve obtained in dark adaptation may be divided into two main parts ; one of these is independent of t_0 ; the other one may be considered as a straight line, the slope of which is unity. This means that the rate of rise of the b-wave is a linear function of the rate of rise of the light stimulus. The behaviour of the curve referred to light adaptation seems to be more complicated.

Further, we may add that in the dark adapted state, component PII is dominant with respect to light adaptation. It seems reasonable to ask what has happened to the cone response in the records given by observer

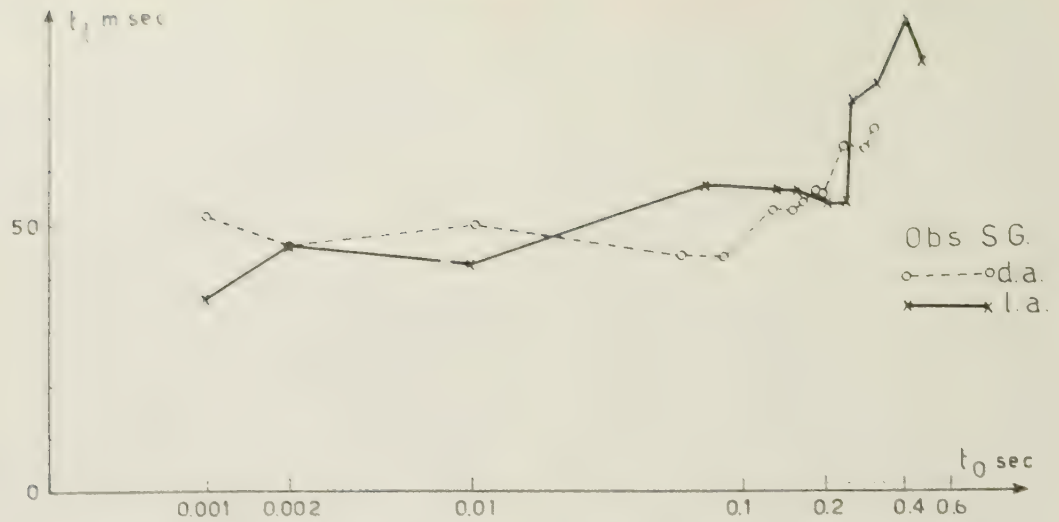

Fig. 11. — The latency time of the b-wave is plotted againts the time of rise of the stimulus.

S. G. For t_0 ranging from 1 to 10 msec., the a-wave is very small (10 to 20 V) and for t_0 greater than 10 msec. the a-wave is not detected.

For t_0 less than 10 msec., a very small wave is sometimes indicated, suggesting a reduced form of Motokawa and Mita's X-wave [8]. But as the curve is of the same order of magnitude as the noise level, no definite statement can be made at this stage.

The intensity of our stimuli may be considered high, and in light-adaptation the cone response should be

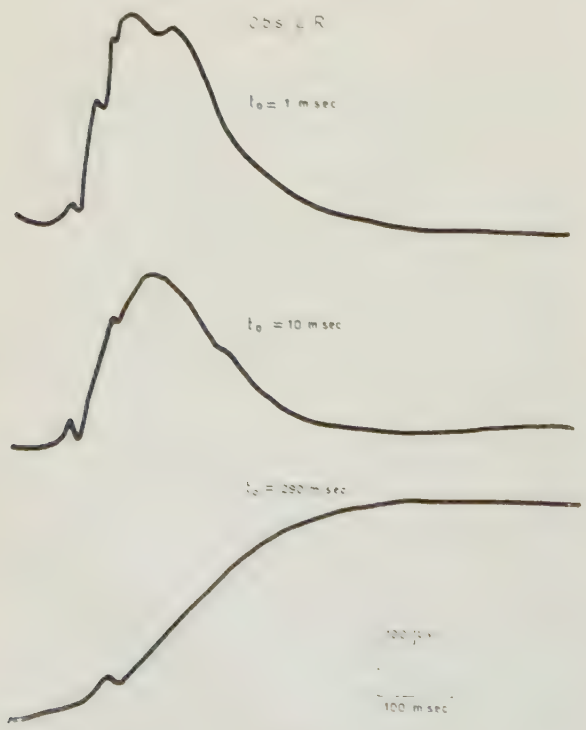

Fig. 12. — Some records obtained by observer L. R.

" uncovered ", according to Granit [9] [10]. The suppression of cone activity by the rods might depend on the length of time of illumination. According to Wirth [3], the cone response in light adaptation when strong stimuli are used is elicited when the exposure time is less than 20 msec. The same limit holds also in dark-adaptation. In our case, by using time gradients of illumination, the exposure time is not limited ; the lack of cone activity in the responses given by S. G. therefore agrees with Wirth's results.

In the responses given by L. R., the a-wave is very small, but the cone response does not seem to be completely suppressed. A small wave near the beginning of the b-wave is present in all the responses obtained for t_0 ranging between 1 and 300 msec. The X-wave seems to appears for $t_0 = 10$ msec., while, for $t_0 = 1$ msec., the b-wave has a composite nature. The behaviour of L. R. is not in disagreement with Wirth's results. We suggest that if the light stimulus is very short and rises rapidly, then only the cone system is able to react.

If the light stimulus is long and rises slowly (within limits), the rods response may be recorded. If the stimulus is rising rapidly and of long duration, the responses of both systems may coexist, or as in the case of S. G., the rod response being dominant suppresses cone activity. It should depend on the relation between the time-constants of both cone and rod systems in the retina of each observer.

Conclusion. — In the present study we examined the influence on the human electroretinogram of intense light stimuli, having time gradients of illumination.

By varying the rate of rise of the stimulus, both the shape and size of the electroretinogram undergo modifications if the time of rise is greater than 100 msec.

When the stimulus rises slowly, the response is of the low-intensity type. When it rises rapidly, the responses of one observer probably show signs of cone activity ; on the other hand, in the corresponding responses of the other observer, the cone activity seems to be completely masked by that of the rods.

Acknowledgements. — The authors gratefully acknowledge the part played by Prof. G. Toraldo in initiating this study. They wish to express their thanks to Prof. A. Wirth for his advice ; to Prof. A. Manfredi and Dr T. Fazzini for their help in the construction of the apparatus ; in addition they are indebted to Dr C. Calamandrei for fitting the contact lenses.

REFERENCES

[1] R. Granit, *Sensory mechanisms of the retina*, Oxford University Press, London, 1947, p. 22.
[2] R. Granit, *Ibid.*, p. 175.
[3] A. Wirth, *Arch. Soc. Biol.*, **40**, 1956, p. 163.
[4] W. D. Wright, *Researches in normal and defective color vision*, Kimpton, London, 1946, p. 39.
[5] A. Fiorentini, Atti della Fond. G. Ronchi, **21**, 1956, p. 66.
[6] R. Granit, *Ibid.*, p. 169.
[7] R. Granit, *Ibid.*, p. 81.
[8] K. Motokawa, T. Mita, *Tohoku J. Exp. Med.*, **42**, 1942, p. 114.
[9] R. Granit, *Ibid.*, p. 146.
[10] R. Granit, *Receptors and sensory perception*, Yale University Press, New Haven, 1955, p. 164.

Manuscrit reçu le 13 juillet 1956.

Lettres à l'éditeur

The effect of defocusing and third order spherical aberration on the transfer function of a two dimensional optical system

G. B. Parrent and C. J. Drane
Air Force Cambridge Research Center. Bedford, Mass., U. S. A.

The effect of defocusing and third order spherical aberration on the transfer function of a two-dimensional optical system is the subject of a study now reaching completion at this Laboratory. Some results of general interest are already apparent and form the subject of this communication.

The recent emphasis on the optical transfer function as an analytic tool precludes the need for presenting an extensive mathematical development. It is readily shown that for incoherent illumination the transfer function $\tau(\mu, \nu)$ is the convolution of the aperture illumination $\tilde{\tau}(\mu, \nu)$ with its complex conjugate (Duffieux) [1].

$$(1) \quad \tau(\mu, \nu) = \iint_{-\infty}^{+\infty} \tilde{\tau}(\mu', \nu')\, \tilde{\tau}(\mu' - \mu, \nu' - \nu)\, d\mu'\, d\nu'.$$

where (μ, ν) are the aperture variables.
With uniform transmission over the aperture

$$(2) \quad \tilde{\tau}(\mu, \nu) = e^{ik\Delta(\mu, \nu)} \quad \mu, \nu \subset \text{aperture}$$
$$= 0 \quad \mu, \nu \subset \text{aperture}$$

where Δ describes the deviation of the actual wavefront from a reference sphere. For third order spherical aberration and defocusing

$$(3) \quad \Delta = a(\mu^2 + \nu^2)^2 + b(\mu^2 + \nu^2)$$

where a and b are the coefficients of spherical aberration and defocusing, respectively. After a suitable change of variables equation (1) becomes

$$(4) \quad \tau(\beta) = 4 \int_0^{\sqrt{1-\beta^2}} \int_0^{\sqrt{1-\nu'^2}} \beta \cos 4ka \times$$
$$\times [2\beta\mu'^3 + 2\beta\mu'\nu'^2 + 2\beta^3\mu' + c\beta\mu'] \, d\mu'\, d\nu'$$

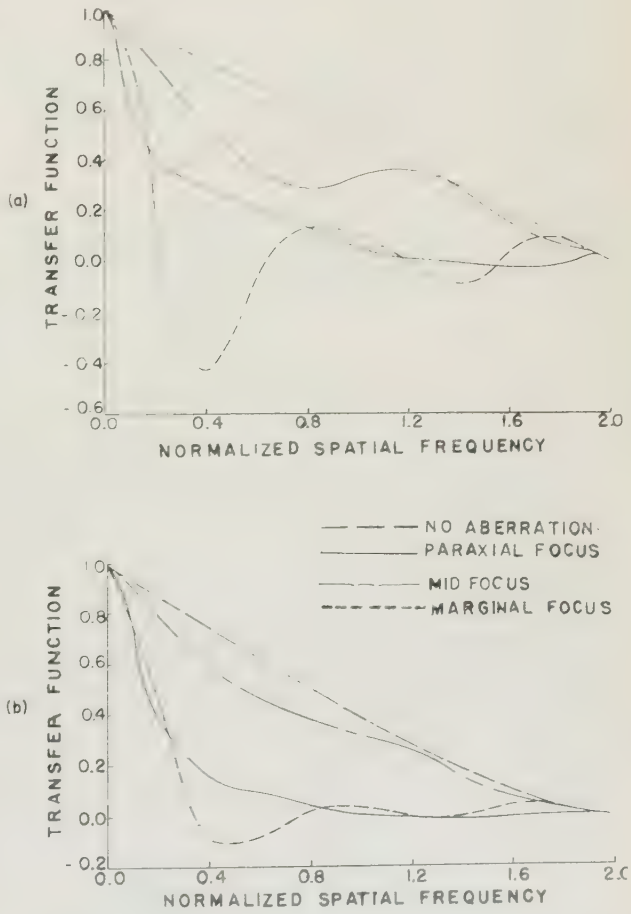

Fig. 1. — Comparison of one (a) and two (b) dimensional transfer function for one wavelength of spherical aberration.

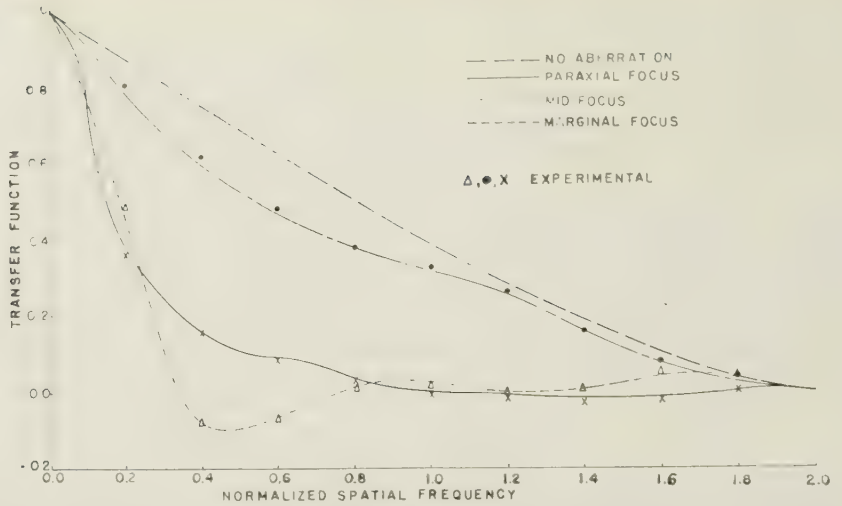

Fig. 2. — Comparison of theoretical and experimental transfer functions for one wavelength of spherical aberration in two dimensions.

$$\text{where } c = \frac{b}{a} = \frac{-2 \text{ focal shift}}{\text{total longitudinal aberration}} = \text{focal setting.}$$

The inner integral will be recognized as Airy's Incomplete Integral. However, existing tables were inadequate and the integrals were evaluated numerically. Simple generative relationships are readily obtained which make possible the extension to larger aberrations.

Since the convolution integral represents a smoothing action, it might be expected that the chief difference between the one and the two-dimensional function would be the extra smoothing effect in the two-dimensional case, that is, changes in the one-dimensional functions (Parrent) [2] would be more pronounced than corresponding changes in the two-dimensional functions. That this is indeed the case is seen from figure 1. The excellent quantitative agreement between our calculated results and those obtained on the Analog Interferometer at Boston University* is shown in figure 2.

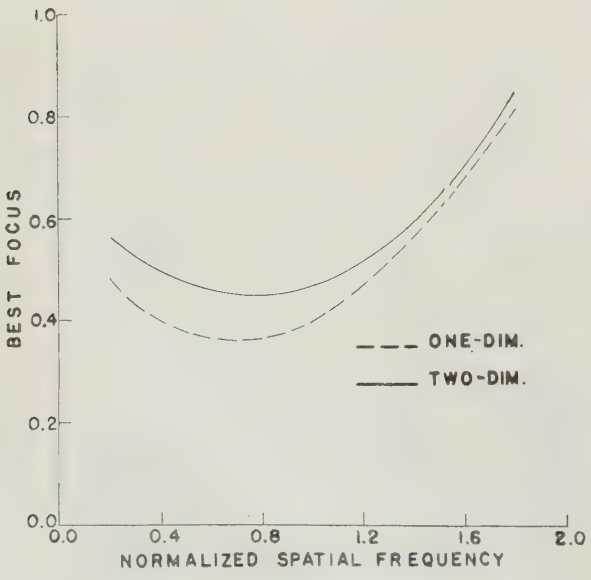

Fig. 3. — Best focus between paraxial (O) and marginal (1) in the presence of one wavelength of spherical aberration.

As would be expected from geometric optics, a much better system is indicated by the midfocus curves in figures 1 and 2 than by the paraxial or marginal focus curves, since the extremes show reduced contrast and considerable amounts of spurious resolution. A detailed analysis, however, demonstrates that no single focal setting is best for all spatial frequencies. If, therefore, the best focus for periodic detail were to be defined as that focal setting at which the transfer function is maximum for the desired frequency, it would be possible to plot best focus versus frequency as in figure 3. As would be expected from the « smoothing » integral, the shift in the two-dimensional case is less pronounced than that observed in the one dimensional case. This curve is in good qualitative agreement with the experimental results reported independently by Kingslake [3], MacDonald [4], and Schack and Ball [5].

In most applications of optical systems, one observes random distributions, not sine wave targets. A pertinent question therefore is where lies the best focus for random detail. Since the root mean square fluctuation in the image is related to the square of the transfer function, a reasonable criterion (in the absence of spatial phase shift) is the area under the squared transfer function (Schade's equivalent bandpass) [6] :

* A device which simulates a shearing interferometer by making use of Moire fringes.

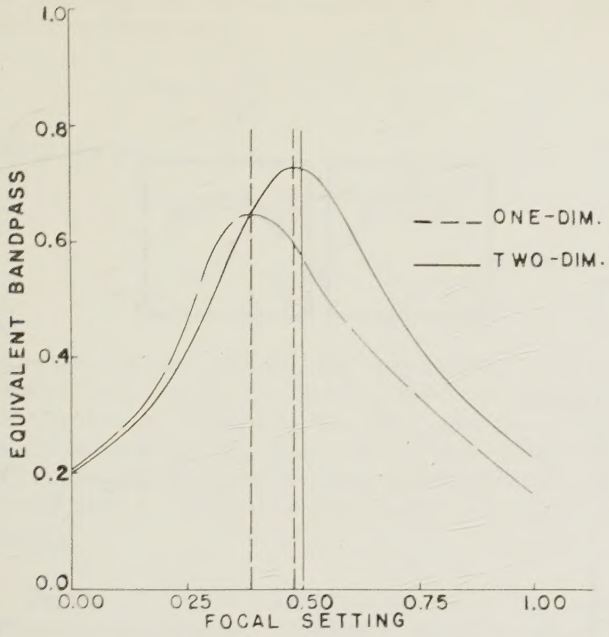

FIG. 4. — Equivalent band pass vs. focal setting between paraxial (0) and marginal (1) for one wavelenght of spherical aberration in one and two dimensions.

$$(5) \qquad \Omega e = \int_{-\infty}^{+\infty} \left| \tau(\mu, \nu) \right|^2 d\mu \, d\nu.$$

Since spherical aberration does not involve a spatial phase shift, it is reasonable to define best focus for random detail as that focal setting for which the bandpass is a maximum. In figure 4 the equivalent bandpass versus focal setting for one wavelength of spherical aberration is plotted for a one dimensional and a two-dimensional optical system. It should be noted that the maxima of these curves are shifted toward the paraxial focus, which is in qualitative agreement with the results of LANSRAUX [7]. Further, it is significant that the shift is more pronounced for the one-dimensional than for the two-dimensional system.

REFERENCES

[1] P. M. DUFFIEUX, *L'intégrale de Fourier et ses applications à l'optique*, Société Anonyme des Imprimeries Oberthur, Rennes, 1946.
[2] G. B. PARRENT, Jr., *The Effect of Spherical Aberration on the Optical Transfer Function*, M. A. Thesis, Boston University, 1955.
[3] R. KINGSLAKE, 1951 *Symposium « Optical Image Evaluation »*, U. S. Bureau of Standards, Circular 526, 1954.
[4] D. E. MACDONALD, 1951 *Symposium « Optical Image Evaluation »*, U. S. Bureau of Standards, Circular 526, 1954, p. 62.
[5] R. V. SCHACK and J. BALL, U. S. Bureau of Standards Report No. 2396, 1953, pp. 3-15.
[6] O. H. SCHADE, *R. C. A. Review*, **9**, 1948.
[7] G. LANSRAUX, *Rev. Opt.*, **34**, 1955, pp. 65-91.

Manuscrit reçu le 18 juillet 1956.

The calorimetric determination of the diffuse reflectance of magnesium oxide.

Gy. GERGELY,
Research Institute for Telecommunication, Budapest.

The diffuse reflectance of magnesium oxide has been studied by many authors. Recently BENFORD, Knowles MIDDLETON, SCHWARZ, LLOYD [1-4], TELLEX and WALDRON [5] described the results of highly precise measurements. All of them used some modification of the integrating sphere method. The results of the different measurements agreed well. Here we do not wish to mention more than two aspects of the problem. The above mentioned authors found that the diffuse reflection of magnesium oxide is affected by the conditions of preparing the coatings, further it varies with irradiation, age, etc. of the coating — as described by JACQUEZ and co-workers [6]. The changes of the reflectance especially in the ultraviolet part of the spectrum cannot be neglected. Last year TELLEX, WALDRON and HAMMOND [7] drew attention to the importance of the thickness of the coating.

In order to reduce the errors in the determination of the reflection spectra of diffuse powders, e. g., luminescent powders, a comparison standard was used in our laboratory. Our standard diffuse reflectance surface was a layer of magnesium oxide powder 1 mm thick, in order to avoid the uncertainties of the magnesium oxide coating. An 1 mm thick layer is an optically infinite thick layer. It can easily be prepared and changed.

The preparation of the magnesium oxide layer. — The preparation of thick magnesium oxide coatings, especially the coating of an integrating sphere having thick layer, can be a very difficult task. TELLEX and WALDRON described a procedure, but their method is a difficult one. A thick magnesium oxide layer can be easily produced by spraying magnesium oxide powder on a sample holder plate. We used pure magnesium oxide powder for this purpose. The powder was dehydrated at 1 000°C as described by R. RAZOUK and MIKHAIL [12].

The calorimetric determination of the diffuse reflection coefficient. — The diffuse reflectance of thick magnesium oxide powder layers cannot be determined

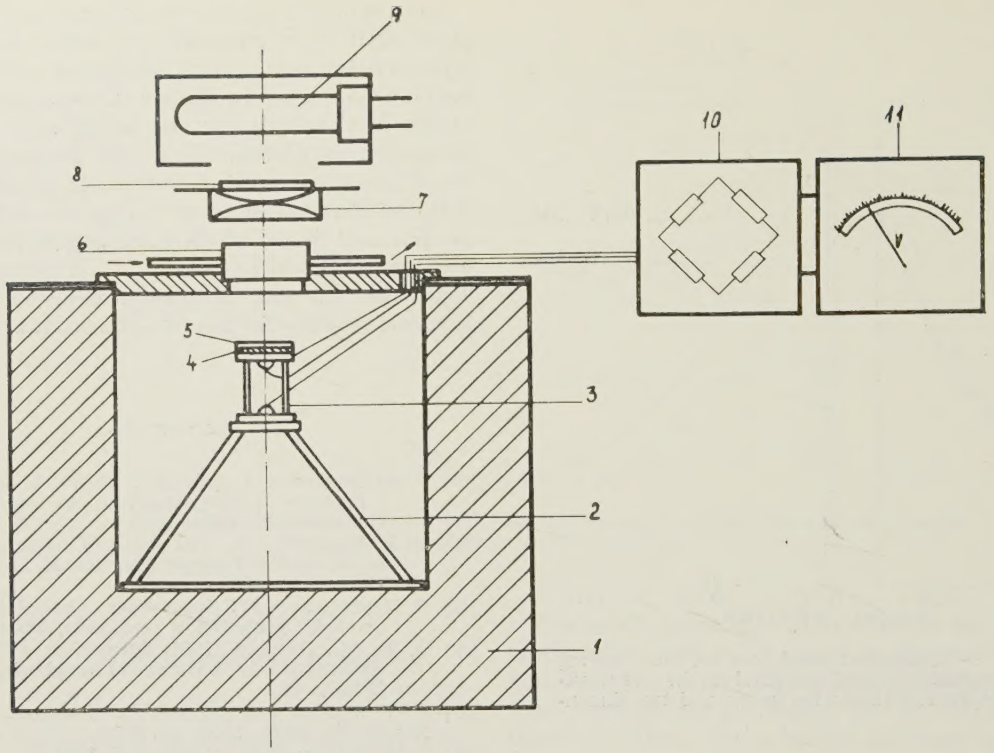

FIG. 1. — Experimental arrangement. 1 : ultra-thermostat ; 2 : thermal insulator frame ; 3 : disc thermistors ; 4 : magnesium oxide sample ; 5 : blackened plate ; 6 : quartz absorption cell; 7 : condenser lens ; 8 : interference filter (SCHOTT) ; 9 : high pressure mercury lamp ; 10 : electricon thermistor bridge ; 11 : electronic voltmeter.

by the integrating sphere method used by the above quoted authors [1-5]. The reflectance of a non-luminescent powder can be easily determined by a calorimetric method. ALENCEV [8] and BODO [9] used a microcalorimeter for the determination of luminescence efficiency. We improved ALENCEV's and BODÓ's experimental technique. Instead of thermocouples, thermistors were used, as it was done by HUTCHINSON and WHITE [10].

Figure 1 shows the sketch of our apparatus. The magnesium oxide sample to be examined was placed on a sample holder plate, within an ultrathermostat of the HOEPPLER type. Following BODÓ's method, another sample holder plate, blackened with carbon black, was used for the determination of the intensity of radiation. Both sample holder plates were placed upon the copper plate of a disc thermistor connected with another thermistor by a thin copper rod. The two thermistors formed the arms of a bridge.

The magnesium oxide sample and the carbon black surface were irradiated by a high pressure mercury lamp. The strong spectral lines of the lamp were selected by SCHOTT interference filters. The radiation entered the thermostat through a quartz absorption cell, through which the distilled water of the thermostat was circulated.

Irradiating the magnesium oxide and the carbon black samples raised their temperature. The temperature rise was detected by the thermistors by means of an electronic bridge developed by Gy. ALMÁSSY. This apparatus will be described in another paper [11]. The method of measurement was similar to that of BODÓ, used for luminescence efficiency determination. The formulae derived by BODÓ will be employed also in this paper.

Irradiating the magnesium oxide sample, its temperature rise is given by the differential equation :

$$(1) \quad K\mathrm{d}T = I_{0\lambda}(1 - r_{m\lambda})\,\mathrm{d}t - B_1(T - T_0)\mathrm{d}t\,.$$

where

T is the temperature of the sample,
T_0 is the ambient temperature,
K is the heat capacity of the system,
t is the time,
$I_{0\lambda}$ is the intensity of radiation at the wavelength λ,
r_m is the reflectance of MgO,
B_1 is the heat transfer coefficient.

Solving equation (1) gives

$$(2) \quad T_1 - T_0 = \frac{I_{0\lambda}(1 - r_{m\lambda})}{B_1}\left(1 - \exp - \frac{B_1}{K}\,t\right).$$

A similar equation gives the temperature rise of the carbon black sample. Using a similar notation, where r_c is the reflectance of the carbon black, gives

$$(3) \quad T_2 - T_0 = \frac{I_{0\lambda}(1 - r_c)}{B_2}\left[1 - \exp - \frac{B_2}{K}\,t\right].$$

Reaching the thermal equilibrium at approximately $t = 10$ minutes :

$$\exp -\frac{B_1}{K} t = \exp \varepsilon_1 t \cong 0 .$$

Thus, we get

$$r_{m\lambda} = 1 - (1 - r_0) \frac{M_1 \varepsilon_1}{M_2 \varepsilon_2} ,$$

$$M_1 = \frac{I_0(1 - r_{m\lambda})}{B_2} , \qquad \varepsilon_1 = \frac{B_1}{K} , \tag{4}$$

denoting by M_1, and M_2 the assymptotic value of temperature rise, by $1/\varepsilon_1$ and $1/\varepsilon_2$ the time constants of the system, irradiating the MgO, and the carbon black respectively. M_1, M_2, ε_1 and ε_2 were determined by measuring the rate of heating of the system. It was found that $r_c \cong 0{,}015$ independently of the wavelength.

Results. — Table I contains the result for some intense mercury lines. The 2 537 Å radiation was produced by means of a low pressure mercury discharge lamp. For the purpose of comparison, Table I contains the results of Benford and co-workers. It may be seen that agreement was found with the result published in [1-6]. In the ultraviolet part of the spectrum, the reflectance of our sample was less than that found by Benford and co-workers. This difference may be explained by the small traces of iron impurity of our MgO powder.

Acknowledgment. — The author wishes to express his thanks for the preparation of the thermistors to Mr F. Csapó, for the development of the electronic thermistor bridge, to Mr Gy. Almássy, for the help in the measurements, to Mr J. Adám, for building the electronic device, to Mr P. Nagy, and, for building the microcalorimeter, to Mr E. Németh.

Table I

Wavelength Å	Diffuse reflectance of magnesium oxide	
	calorimetric determination	Benford's and co-workers' results
2 537	83 %	94.5 %
3 650	91.2 %	94.5 %
4 060	97.1 %	97 %
4 358	96.4 %	98 %
5 460	99 %	99 %

REFERENCES

[1] F. Benford, G. P. Lloyd, S. Schwarz, *J. O. S. A.*, **38**, 1948, p. 445.
[2] F. Benford, S. Schwarz, G. P. Lloyd, *J. O. S. A.*, **38**, 1948, p. 964.
[3] W. E. Knowles Middleton, C. L. Sanders, *J. O. S. A.*, **41**, 1951, p. 419.
[4] C. L. Sanders, W. E. Knowles Middleton, *J. O. S. A.*, **43**, 1953, p. 58.
[5] P. A. Tellex, J. R. Waldron, *J. O. S. A.*, **45**, 1955, p. 19.
[6] J. A. Jacquez, W. McKeehan, J. M. Dimitroff, H. F. Kuppenheim, *J. O. S. A.*, **45**, 1955, p. 971.
[7] H. K. Hammond, *J. O. S. A.*, **45**, 1955, p. 904.
[8] M. M. Alencev, *J. Exp. Theor. Phys.*, **21**, 1955, p. 133.
[9] Z. Bodó, *Acta Phys. Hung.*, **3**, 1953, p. 23.
[10] W. P. Hutchinson, A. G. White, *J. scient. Instr.*, **32**, 1955, p. 309.
[11] Gy. Gergely, Gy. Almássy, J. Adam, *Acta Phys. Hung.* (to be published).
[12] R. J. Razouk, R. S. Mikhail, *J. Phys. Chem.*, **59**, 1955, p. 636.

Manuscrit reçu le 18 mai 1956.

INFORMATION

Colloque international sur les Problèmes physiques de la télévision en couleurs

(Paris, juillet 1957)

Sous le patronage de l'Union Internationale de Physique Pure et Appliquée, un Colloque consacré à l'Etude des Problèmes Physiques que pose la Télévision en Couleurs sera organisé à Paris du 2 au 6 juillet 1957. Les séances de travail auront lieu au Conservatoire National des Arts et Métiers, 292 rue Saint-Martin à Paris.

Programme provisoire. — Au cours de l'Assemblée plénière du Comité Consultatif International des Radiocommunications tenue à Varsovie en août-septembre 1956, la Commission XI (Télévision) a recommandé la recherche de méthodes et de résultats quantitatifs relatifs à l'évaluation des qualités des images de Télévision et approuvé la constitution d'un groupe de travail à cette fin. Les physiciens, les ingénieurs électroniciens et opticiens, les spécialistes de la télévision trouveront ainsi l'occasion de se réunir et d'étudier les points suivants :

A. Comportement de l'œil,

B. Prise de vues et restitution de l'image,

C. Mesure des résultats obtenus dans la restitution d'une image colorée,

D. Système de codage utilisés pour la transmission des signaux de Télévision en Couleurs.

Communications.— Les communications à présenter au Colloque devront être annoncées très prochainement et en tous cas avant le 1er mai 1957 pour permettre l'impression et la distribution d'une liste de titres et de résumés en temps utile.

Les communications pourront être présentées et commentées dans la langue choisie par l'auteur ; toutefois l'usage du français et de l'anglais sont recommandés.

Démonstrations, visites, excursions. — Enfin des démonstrations, visites et excusions seront organisées.

La cotisation du Colloque sera de l'ordre de 1 500 Francs Français pour chaque participant. Etant donné l'affluence des touristes à Paris en juillet, le Comité d'organisation sera reconnaissant à tous ceux qui envisagent de participer au Colloque de le faire savoir dès que possible à l'adresse ci-dessous :

Colloque International sur les Problèmes Physiques de la Télévision en Couleurs, Conservatoire National des Arts & Métiers, 292, rue Saint-Martin, Paris, 3e. France.

ERRATA

« The defocused image of sinusoidal gratings » by W. H. Steel, *Optica Acta*, **2**, 1956, 65.

Page 68 :

Right hand line below Table 1 — for $(2\ \xi\ \xi')^{-\frac{3}{2}}$, read $(2\ \omega\ \xi')^{-\frac{3}{2}}$.

Ordinate scales, Figure 2 — for " 0.5 ", read " — 0.5 ".
for " 0.05 ", read " — 0.05 ".

Page 69 :

Top line, equation (14) — for $= S' \int_{\omega} \cos \ldots$, read $= \int_{\omega} \cos \ldots$.

Pages 70 :

Penultimate expression — for $\frac{\omega^2 - 1}{2\ \omega\sigma}$, read $\frac{\omega^2 - 1 + \sigma^2}{2\ \omega\sigma}$.

Pages 73 :

Second line of Appendix — for " « The frequency of a... ".
read " « The frequency response of a... ".

Pages 74 :

Reference [12] — for " 1954 " read " 1953 ".

Throughout (pp. 65, 66, 68, 69, 70 and 73) — for " spacial " read " spatial '.

ADDENDUM

J. Focke. Wellenoptische Untersuchungen zum Öffnungsfehlers, *Optica Acta*, **3,** 1956, 126.
Literaturhinweise : Siehe auch Picht, J., *Optische Abbildung*, Braunschweig, 1931.

N° d'éditeur 129. — *Revue d'optique.* — *Le Directeur :* Emile Perrin.
Commission paritaire des papiers de Presse n° 29754

3385. — Imprimerie JOUVE, 15, rue Racine, Paris. — 2-57